

MAGNETOM Flash

Issue Number 77 · 2/2020

RSNA Edition

[siemens.com/magnetom-world](https://www.siemens.com/magnetom-world)

Page 4

Compressed Sensing in Metal Hip Imaging

Mustafa M. Almuqbel, et al.

Page 14

MR Fingerprinting for Precision Imaging in Neuro-Oncology

Domenico Zacà and

Guido Buonincontri

Page 23

Personalized Treatment for Patients with Prostate Cancer Using MRI-guided Transurethral Ultrasound Ablation

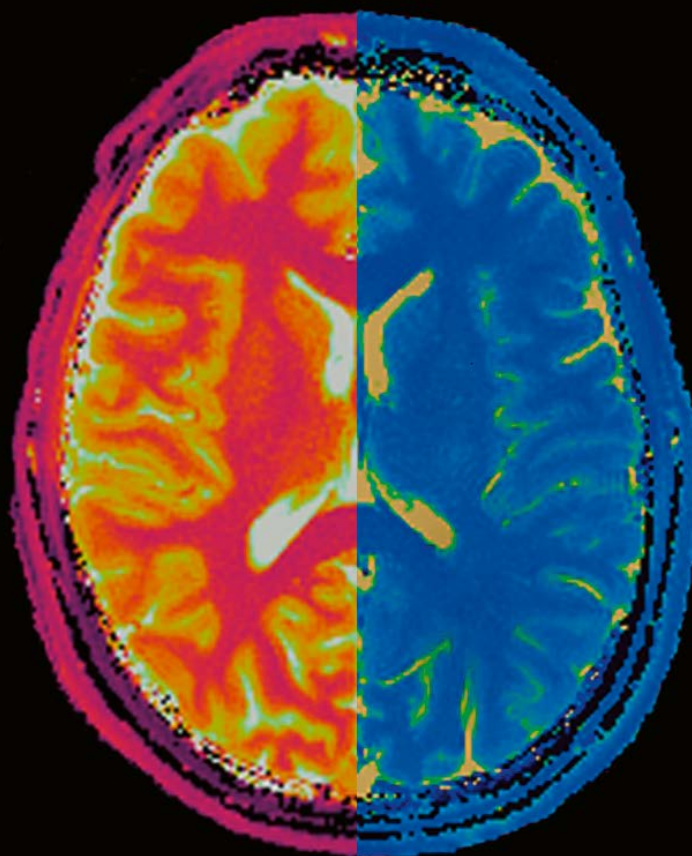
Jurgen Fütterer, et al.

Page 62

Improving Productivity in MRI – Clinical Experience in a Multisite Outpatient Practice Setting

Mike Notohamiprodjo and

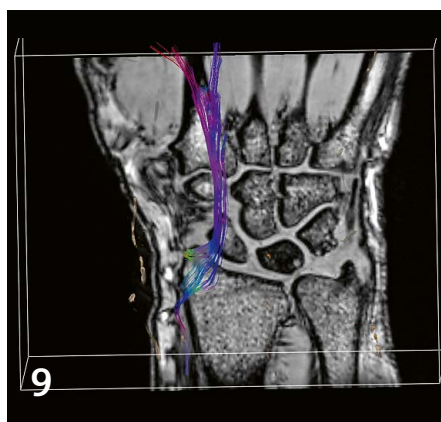
Gerwin Schmidt



MR Fingerprinting T1 and T2 maps



Compressed Sensing
in metal hip imaging¹



SMS-RESOLVE tractography
for surgical management



Breast MRI on MAGNETOM Sola

Musculoskeletal Imaging

4 Compressed Sensing in Metal¹ Hip Imaging: Our Experience

Mustafa M. Almuqbel, Ross J. Keenan, et al.
Pacific Radiology Group, Christchurch, New Zealand

Neurologic Imaging

9 SMS-RESOLVE Tractography for Surgical Management of Brachial Plexus Trauma

Thomas Lloyd, et al.
Princess Alexandra Hospital, Brisbane QLD, Australia

14 Magnetic Resonance Fingerprinting² for Precision Imaging in Neuro-Oncology

Domenico Zacà and Guido Buonincontri
Siemens Healthineers, Italy

Oncological Imaging

20 Breast MRI on 1.5T MAGNETOM Sola

Sindre Øverstad
Radiumhospitalet, Oslo University Hospital, Oslo, Norway

23 Personalized Treatment for Patients with Prostate Cancer Using MRI-guided Transurethral Ultrasound Ablation (TULSA)

Jurgen Fütterer, et al.
Radboud University Nijmegen Medical Centre, Nijmegen, The Netherlands

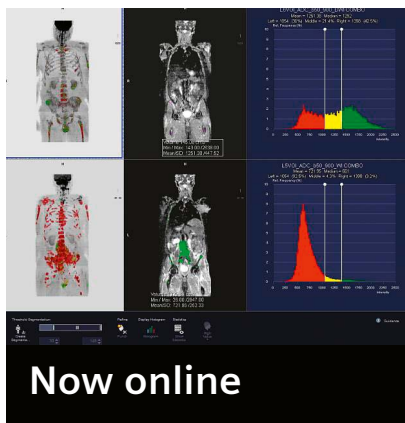
Abdominal Imaging

28 New Advances in Radiomics of Liver Imaging

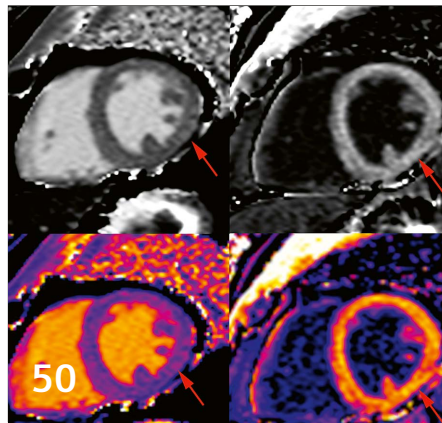
Roberto Cannella and Tommaso V. Bartolotta
University Hospital "Paolo Giaccone", Palermo, Italy

¹The MRI restrictions (if any) of the metal implant must be considered prior to patient undergoing MRI exam. MR imaging of patients with metallic implants brings specific risks. However, certain implants are approved by the governing regulatory bodies to be MR conditionally safe. For such implants, the previously mentioned warning may not be applicable. Please contact the implant manufacturer for the specific conditional information. The conditions for MR safety are the responsibility of the implant manufacturer, not of Siemens Healthineers.

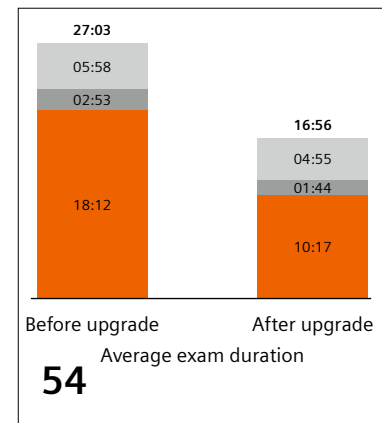
²Work in progress. MR Fingerprinting is not commercially available in some countries. Due to regulatory reasons its future availability cannot be ensured. Please contact your local Siemens Healthineers organization for further details.



Upgrading syngo.via VB30 to VB40



CMR of myocardial inflammation regression in convalescence of acute myocarditis caused by SARS-CoV-2



New clinical possibilities and increased productivity after upgrading to MAGNETOM Sola Fit

How-I-do-it

35 Reduced Stress and Consistent Contrast-enhanced MRI Scans with Precisely Timed, Automated Injection Enabled by MR-Injector Coupling

Gregor Thoermer, Sri Shriram, et al.
Siemens Healthineers, Germany

39 Revisiting 3T: Pearls and Pitfalls Compared with 1.5T

Corentin Mauris, et al.
IRM74 Economic Interest Group, Annecy, France

48 **Now online:** Upgrading syngo.via VB30 to VB40 – What's New in MRI?

Corentin Mauris, et al.
IRM74 Economic Interest Group, Annecy, France

Business

54 New Clinical Possibilities and Increased Productivity after Upgrading from MAGNETOM Aera to MAGNETOM Sola Fit

Philip Chappel
ZNA Jan Palfijn Hospital, Merksem, Belgium

62 Improving Productivity in MRI – Clinical Experience in a Multisite Outpatient Practice Setting

Mike Notohamiprodjo and Gerwin Schmidt
DIE RADIOLOGIE, Munich, Germany

68 Utilizing Blended Learning for Customer Support During the COVID-19 Pandemic: An Experience from the UK and Ireland

Chris Kasap and Karen Hackling-Searle
Siemens Healthineers & Cobalt Health, UK

Cardiology

50 Case Report: CMR of Myocardial Inflammation Regression in Convalescence of Acute Myocarditis Caused by SARS-CoV-2

Carlos Eduardo Rochitte
Hospital do Coração, Sao Paulo, Brazil

Compressed Sensing in Metal Hip Imaging: Our Experience

Mustafa M. Almuqbel, RT, (MR), ARRT, Ph.D.^{1,2,3}; Tracy R. Melzer, Ph.D.^{2,3};
Byron J. Oram, MBChB, FRANZCR^{1,4}; Ross J. Keenan, MBChB, FRANZCR^{1,2,4}

¹Pacific Radiology Group, Christchurch, New Zealand

²New Zealand Brain Research Institute, Christchurch, New Zealand

³Department of Medicine, University of Otago, Christchurch, New Zealand

⁴Department of Radiology, Christchurch Hospital, Christchurch, New Zealand

Introduction

For end stage hip disease, total hip arthroplasty (THA) has become an attractive management option for many patients [1, 2]. While THA offers excellent pain relief and helps a majority of patients to regain some portion of day to day mobility, it is not without complications. About 40% of patients who undergo THA report groin and thigh pain [3, 4]. Despite the development in implant design, fixation approaches, and bearing materials, most prostheses eventually fail [5]. Given this, there is an increasing demand for more accurate diagnosis and visualization prior to hip revision.

Recently, magnetic resonance imaging (MRI) has become the imaging modality of choice for most clinicians to image potential THA-related complications¹ [6, 7]. In one imaging session, MRI can provide useful information about periprosthetic fractures, and osteolysis, postoperative hematoma, disruption of the pseudocapsule, synovitis caused by polyethylene wear and adverse local tissue reactions, periprosthetic masses, bursitis, tendinopathy, and neurovascular compromise [8]. However, MRI near metal comes with a well-known challenge, the susceptibility induced blooming artifact. This artifact hinders image quality and consequently diagnostic accuracy.

Magnetic susceptibility refers to the extent by which a substance is magnetised when exposed to the magnetic field. Different substances exhibit various degrees of magnetic susceptibility when exposed to a static magnetic field [9, 10]. Metallic objects have higher magnetic susceptibility than biological tissues. This induces severe spin dephasing (incoherence) around metallic implants and causes signal drop out and a form of image distortion [11].

In practice, using high bandwidth (BW), thinner slices, smaller field of view, finer matrix and imaging at lower

magnetic fields are all helpful protocol adaptations to reduce the metal-induced artifact. However, these changes to the MR sequence lead to reduced signal to noise ratio (SNR) and often increased specific absorption rate (SAR). Therefore, practitioners tend to scan for longer times to mitigate the adverse effects associated with reducing the metal-induced artifact.

syngo WARP is a Siemens Healthineers solution that offers techniques to reduce susceptibility-related distortions. *syngo* WARP comprises

- Turbo Spin Echo (TSE) sequence optimized for imaging in the presence of metal implants
- “View Angle Tilting” or VAT and
- “Slice Encoding for Metal Artifact Correction” or SEMAC².

When VAT is added to a turbo spin echo pulse sequence, an additional gradient is applied in the data readout step to correct the in-plane distortion. However, only correcting for the in-plane distortion is not enough. Hence, the SEMAC option has been introduced. SEMAC offers through-plane distortion correction, similar to 3D imaging, where additional phase-encoding steps are added in the third dimension. This provides information on how the slice profile is distorted, which is used later to correct the distortion during the image reconstruction stage. Therefore, the more additional phase-encoding steps, the richer the slice profile, which enhances the distortion correction process. However, while adding additional phase-encoding steps helps in improving the image quality, it requires longer scanning time and additional postprocessing [12, 13].

What is promising is that one can use VAT and SEMAC simultaneously. That is, concurrently correcting

¹The MRI restrictions (if any) of the metal implant must be considered prior to patient undergoing MRI exam. MR imaging of patients with metallic implants brings specific risks. However, certain implants are approved by the governing regulatory bodies to be MR conditionally safe. For such implants, the previously mentioned warning may not be applicable. Please contact the implant manufacturer for the specific conditional information. The conditions for MR safety are the responsibility of the implant manufacturer, not of Siemens Healthineers.

²SEMAC is part of the Advanced WARP package

for in-plane and through-plane metal-induced distortions. However, unlike VAT, SEMAC impacts the scan time dramatically, making the addition of SEMAC to every sequence impractical in clinical settings. However, publications have shown a clear diagnostic benefit of SEMAC protocols for hip and knee joint replacements [14–16]. As a solution to this problem, we present our experience with a “Compressed Sensing” technique for metal hip imaging and its added benefit in improving image quality and reducing scan times.

Although it is beyond the scope of this work to discuss the technical aspects of the Compressed Sensing (CS) technique, briefly CS refers to the ability to reconstruct the image-forming signals with fewer measurements (or samples) than what was classically thought necessary. Therefore, Compressed Sensing is a method to accelerate the MRI procedure by collecting less data (i.e., undersampling k -space) while maintaining image quality [17, 18].

³Work in progress; the application is currently under development and is not for sale in the U.S. and in other countries. Its future availability cannot be ensured.

Methods

43 patients with total hip arthroplasty (THA) were scanned on a 48-channel 1.5T MAGNETOM Aera system (Siemens Healthcare, Erlangen, Germany). In addition to their clinical imaging protocol (which includes “VAT only” WARP), we acquired additional SEMAC and Compressed Sensing-SEMAC (CS-SEMAC)³ sequences. The latter being a prototype provided by Siemens Healthineers. All imaging was performed using the 18-channel body coil. Table 1 shows the imaging parameters of these three implemented sequences.

Aim

Combining VAT and SEMAC to achieve both in-plane and through-plane distortion correction is an attractive option; however, adopting such an approach is limited due to the long scan times. Leveraging Compressed Sensing (CS), we aim to explore whether CS-SEMAC³ can offer improved image quality at reasonable imaging times.

Sequence	VAT only (default protocol)	VAT+SEMAC (12 PES)	VAT+CS-SEMAC (12 PES)	VAT+CS-SEMAC (20 PES)
Imaging plane	Coronal oblique	Coronal oblique	Coronal oblique	Coronal oblique
Image weight	Proton density	Proton density	Proton density	Proton density
Repetition time	2800 ms	2640 ms	3880 ms	3880 ms
Echo time	38 ms	32 ms	32 ms	32 ms
Field of view	240 mm	240 mm	240 mm	240 mm
Slice thickness	3.5 mm	3.5 mm	3.5 mm	3.5 mm
Matrix	320×256	320×256	320×256	320×256
Bandwidth	600 Hz	650 Hz	650 Hz	650 Hz
Flip angle	140	150	135	135
Averages	4	1	1	1
Turbo factor	15	14	21	21
GRAPPA	2	2	Off	Off
Compressed Sensing	Off	Off	On	On
VAT	50%	100%	100%	100%
SEMAC additional phase-encoding steps (PES)	Off	12	12	20
Echo spacing	7.56 ms	8.06 ms	8.06 ms	8.06 ms
Bandwidth	600 Hz/Px	650 Hz/Px	650 Hz/Px	650 Hz/Px
Scan time (minutes)	03:20	06:50	02:50	04:25

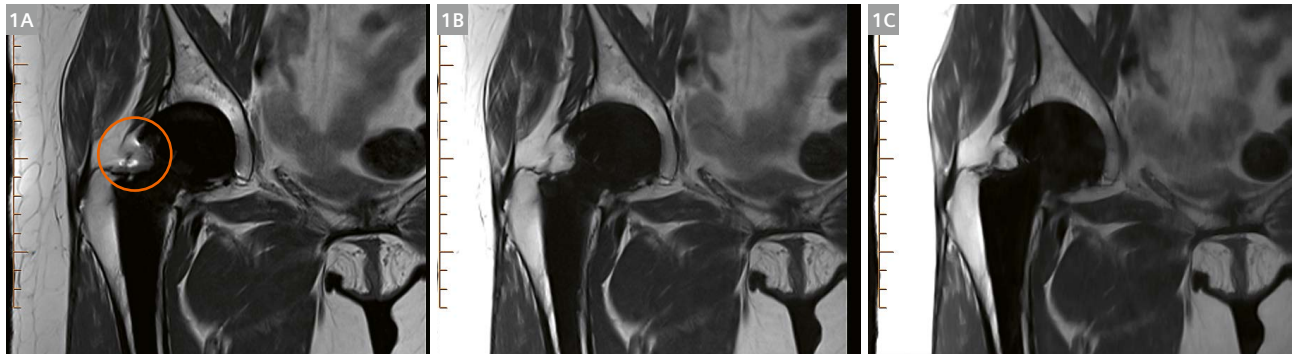
Table 1: Imaging parameters

VAT = View Angle Tilting; SEMAC = Slice Encoding for Metal Artifact Correction;

PES = Phase-encoding steps; GRAPPA = GeneRalized Autocalibrating Partially Parallel Acquisitions

Findings and discussion

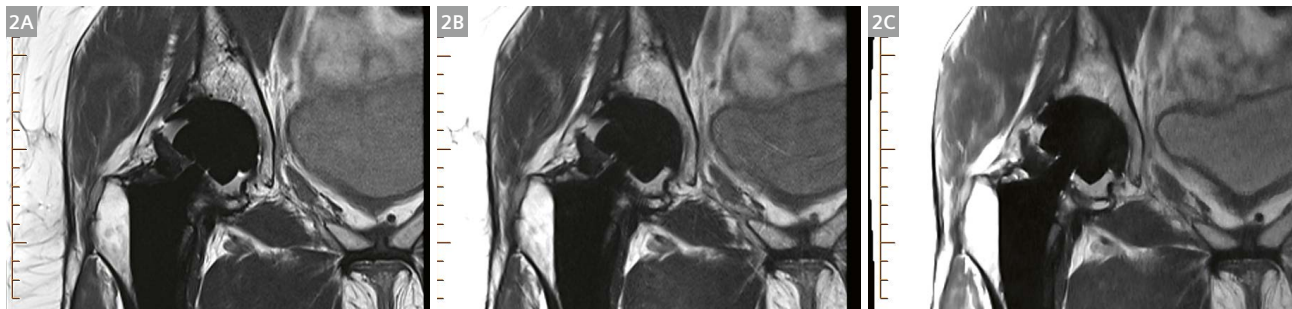
VAT-only versus SEMAC:



Sequence	Cor PD VAT-only (product)	Cor PD VAT+SEMAC (product)	Cor PD VAT+CS-WARP (WIP)
Quality	Image quality degraded by pile-up artifact (circled in orange).	Artifact reduced.	Artifact markedly reduced.
Time	03:20 min	06:50 min	02:50 min
Overall rating	Still suffers an artifact.	Good artifact reduction, but infeasibly long.	Reduced artifact and short scan time.

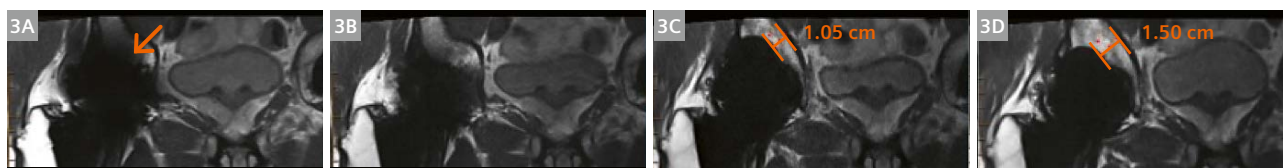
1 A 61-year-old female with right total hip arthroplasty (THA). The implant-associated artifact is relatively benign (i.e., relatively subtle susceptibility artifact). However, the VAT-only image (1A) shows signal “pile up” caused by the signal aggregation (circled in orange). While the use of the SEMAC sequence (1B) was helpful in reducing the “pile up” artifact significantly, the imaging time was unacceptably long in a busy clinical setting. The application of Compressed Sensing (1C) resulted in reduced artifact, excellent image quality, and shorter scan time.

SEMAC “with motion” versus CS-SEMAC:



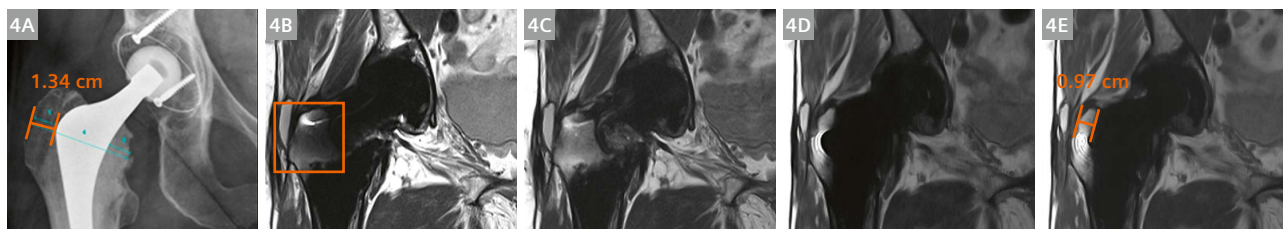
Sequence	Cor PD VAT-only (product)	Cor PD VAT+SEMAC (product)	Cor PD VAT+CS-WARP (WIP)
Quality	Image quality degraded by susceptibility artifact.	Susceptibility artifact with image blurring (due to patient movement).	Mild susceptibility artifact, without patient movement.
Time	03:20 min	06:50 min	02:50 min
Overall rating	Still suffers an artifact.	Patient was in pain and moved during this long scan. We decided not to repeat this scan.	Relative to the VAT-only scan, not only did we achieve better artifact reduction, but we saved 4 minutes by avoiding repeating the long VAT+SEMAC blurry scan.

2 40-year-old female with right total hip arthroplasty (THA). The patient was referred to MRI with right hip pain. The VAT-only image (2A) shows a minimal amount of metal-induced artifact in relation to the case in Figure 1. Image (2B), took nearly 7 minutes to acquire. Unfortunately the patient moved during this long scan, resulting in motion-degraded images. The Compressed Sensing VAT+SEMAC scan (2C) took just 02:50 minutes to collect and was better tolerated by the patient. This case shows the advantage of using Compressed Sensing in accelerating the scan while maintaining and improving image quality. This is especially important in cases where patients are uncomfortable and cannot remain still.

SEMAC versus CS-SEMAC:

Sequence	Cor PD VAT-only (product)	Cor PD VAT+SEMAC (product)	Cor PD VAT+CS-WARP-12 (WIP)	Cor PD VAT+CS-WARP -20 (WIP)
Quality	Severe susceptibility artifact.	Susceptibility artifact reduced.	Susceptibility artifact reduced, with recovery of pubic bone detail.	Susceptibility artifact reduced, with excellent pubic bone recovery.
Time	03:20 min	06:50 min	02:50 min	04:25 min
Overall rating	Still suffers an artifact.	Despite the artifact reduction, it is still infeasibly long.	Reduced artifact and short scan time.	The gain in near-metal visibility outweighs the 1.75 min extra time added, in our opinion.

3 59-year-old male with right cementless metal-on-metal total hip arthroplasty (THA). The patient enjoyed 8 years of excellent functional outcome after the THA. He was referred to MRI with right groin pain and clunking sensation. The implant-associated artifact is severe. Using the pubic bone as a reference (orange arrow), on the VAT-only image (3A), it is difficult to visualize the pubic bone due to the artifact impact on the image. On the VAT+SEMAC image (3B), despite the long scan time, only a slight improvement has taken place and the bone detail suffers significant distortion. Implementing CS-SEMAC with 12 phase-encoding steps (3C), the bone morphology normalises. Finally, using the CS-SEMAC sequence, we increased phase-encoding steps from 12 to 20 (3D); this resulted in a marked improvement in visualisation of the anatomy. When we compared CS-SEMAC-12 to CS-SEMAC-20 images, we achieved 70% morphology recovery (1.05 cm to 1.50 cm). In our opinion, the gain in image quality afforded by the CS-SEMAC-20 sequence outweighs the additional scan time (02:50 min to 04:25 min).

SEMAC versus CS-SEMAC:

Sequence	Hip Radiograph	Cor PD VAT-only (product)	Cor PD SEMAC (product)	Cor PD VAT+CS-WARP -12 (WIP)	Cor PD VAT+CS-WARP-20 (WIP)
Quality	The greater trochanter measures 1.34 cm.	Severe distortion of the greater trochanter (orange square).	Susceptibility artifact reduced, but the image still suffers an artificial bone distortion similar to the image in 4B.	Greater trochanter image quality improved, it measured 0.86 cm.	Further image quality improvement, with reduced artifact. The greater trochanter measured 0.97 cm.
Time		03:20 min	06:50 min	02:50 min	04:25 min
Overall rating		Still suffers an artifact with misleading greater trochanter measurement – induced by the artifact.	Still suffers an artifact with misleading greater trochanter measurement – induced by the artifact.	The addition of CS-SEMAC allowed for better artifact reduction and more realistic structural measurement around the implant.	Artifact reduction is shown to be directly associated with the number of phase encoding steps in the Compressed Sensing technique.

4 67-year-old female with right total hip arthroplasty (THA). The patient had two dislocations and was referred to MRI to rule out abductor dysfunction. While both the VAT-only and VAT+SEMAC scans (4B & 4C) were degraded by geometric distortion and susceptibility artifact, the Compressed Sensing scans (4D & 4E) demonstrated a great ability to reduce these artifacts. This resulted in marked improvement in periprosthetic image quality, with mild residual inherent artifact. In the CS-SEMAC scan, despite the increase in the scan time after increasing the number of phase encoding steps from 12 to 20, the gain in the image quality was clinically significant.

Conclusion

Imaging near metals is largely “implant” dependant – some implants induce significantly detrimental artifacts while others result in relatively minor distortion. The recent improvement in imaging techniques such as VAT and SEMAC allowed imaging professionals to correct for both in-plane and through-plane metal-induced artifacts, with a corresponding improvement in diagnostic accuracy. However, acquiring images with VAT and SEMAC combined prolongs the imaging time, which is impractical in many clinical settings.

In this work, we demonstrated the utility of Compressed Sensing (CS) SEMAC technique not only in reducing the scan time, but also in improving image quality. Artifact severity was inversely associated with the number of the phase-encoding steps performed in the Compressed Sensing approach – that is, increasing phase encoding steps reduced artifact severity, but at the expense of increased scan time.

The only challenge we have experienced during our usage of the CS WIP package was the image reconstruction time. While data acquisition is remarkably short, it took a few minutes for the images to reconstruct (on our scanner at least). The reconstruction time is proportional to the number of phase-encoding steps. This has changed completely with the product implementation, where optimized algorithms are exploiting the power of a reconstruction system specifically designed for CS calculations. In conclusion, we are impressed with the image quality and scan times achievable with the CS-SEMAC technique.

Contact

Dr Mustafa Almuqbel
Pacific Radiology Group
151 Leinster road, Strowan
Christchurch, 8014
New Zealand
Tel: +64 3 379 0770
mustafa.almuqbel@pacificradiology.com



References

- 1 Mancuso CA, Salvati EA, Johanson NA, Peterson MG, Charlson ME. Patients' expectations and satisfaction with total hip arthroplasty. *The Journal of arthroplasty*. 1997;12(4):387-96.
- 2 Krushell R, Bhowmik-Stoker M, Kison C, O'Connor M, Cherian JJ, Mont MA. Characterization of patient expectations and satisfaction after total hip arthroplasty. *J Long Term Effects Med Implants*. 2016;26(2).
- 3 Sharkey PF, Hozack WJ, Rothman RH, Shastri S, Jacoby SM. Why are total knee arthroplasties failing today? *Clinical Orthopaedics and Related Research®*. 2002;404:7-13.
- 4 Ulrich SD, Seyler TM, Bennett D, Delanois RE, Saleh KJ, Thongtrangan I, et al. Total hip arthroplasties: what are the reasons for revision? *International orthopaedics*. 2008;32(5):597-604.
- 5 Brown TE, Larson B, Shen F, Moskal JT. Thigh pain after cementless total hip arthroplasty: evaluation and management. *JAAOS-Journal of the American Academy of Orthopaedic Surgeons*. 2002;10(6):385-92.
- 6 Siegel MJ. Magnetic resonance imaging of musculoskeletal soft tissue masses. *Radiologic Clinics Of North America*. 2001;39(4):701-20.
- 7 Bitar R, Leung G, Perng R, Tadros S, Moody AR, Sarrazin J, et al. MR pulse sequences: what every radiologist wants to know but is afraid to ask. *Radiographics*. 2006;26(2):513-37.
- 8 Fritz J, Lurie B, Miller TT, Potter HG. MR imaging of hip arthroplasty implants. *Radiographics*. 2014;34(4):E106-E32.
- 9 Le Bihan D, Poupon C, Amadon A, Lethimonnier F. Artifacts and pitfalls in diffusion MRI. *Journal of Magnetic Resonance Imaging: An Official Journal of the International Society for Magnetic Resonance in Medicine*. 2006;24(3):478-88.
- 10 Dietrich O, Reiser MF, Schoenberg SO. Artifacts in 3-T MRI: physical background and reduction strategies. *European journal of radiology*. 2008;65(1):29-35.
- 11 Smith MR, Artz NS, Wiens C, Hernando D, Reeder SB. Characterizing the limits of MRI near metallic prostheses. *Magn Reson Med*. 2015;74(6):1564-73.
- 12 Bachschmidt T, Lipps F, Nittka M. syngo WARP: Metal Artifact Reduction Techniques in Magnetic Resonance Imaging. *Magnetom Flash*. 2012;2:24-5.
- 13 Jungmann PM, Ganter C, Schaeffeler CJ, Bauer JS, Baum T, Meier R, et al. View-angle tilting and slice-encoding metal artifact correction for artifact reduction in MRI: experimental sequence optimization for orthopaedic tumor endoprostheses and clinical application. *PLoS one*. 2015;10(4):e0124922.
- 14 Sutter R, Ulbrich EJ, Jellus V, Nittka M, Pfirrmann C. Reduction of metal artifacts in patients with total hip arthroplasty with slice-encoding metal artifact correction and view-angle tilting MR imaging. *Radiology*. 2012;265(1).
- 15 Gupta A, Subhas N, Primak AN, Nittka M, Liu K. Metal artifact reduction standard and advanced magnetic resonance and computed tomography techniques. *Radiol Clin N Am* 53 (2015) 531–547.
- 16 Fritz J, Fritz B, Thawait GK, Rathel E, Gilson WD, Nittka M, Mont MA. Advanced metal artifact reduction MRI of metal-on-metal hip resurfacing arthroplasty implants: compressed sensing acceleration enables the time-neutral use of SEMAC. *Skeletal Radiol*. 2016;45(10):1345-56.
- 17 Lustig M, Donoho D, Pauly JM. Sparse MRI: The application of compressed sensing for rapid MR imaging. *Magnetic Resonance in Medicine: An Official Journal of the International Society for Magnetic Resonance in Medicine*. 2007;58(6):1182-95.
- 18 Jaspan ON, Fleysher R, Lipton ML. Compressed sensing MRI: a review of the clinical literature. *The British journal of radiology*. 2015;88(1056):20150487.

SMS-RESOLVE Tractography for Surgical Management of Brachial Plexus Trauma

Dr Thomas Lloyd¹; Andrew Whittering²; Dr Michael Wagels³; Dr Wei Liu⁴; Dr Jin Jin⁵

¹Department of Radiology, Princess Alexandra Hospital, Brisbane QLD, Australia

²University of Queensland and Department of Radiology, Princess Alexandra Hospital, Brisbane QLD, Australia

³Department of Plastic and Reconstructive Surgery, Princess Alexandra Hospital and Herston Biofabrication Unit, Royal Brisbane and Women's Hospital, Herston QLD, Australia

⁴Siemens Shenzhen Magnetic Resonance Ltd., Application Department, Shenzhen, China

⁵Siemens Healthcare Pty Ltd, MR Research Collaborations and MR R&D, Bowen Hills QLD, Australia

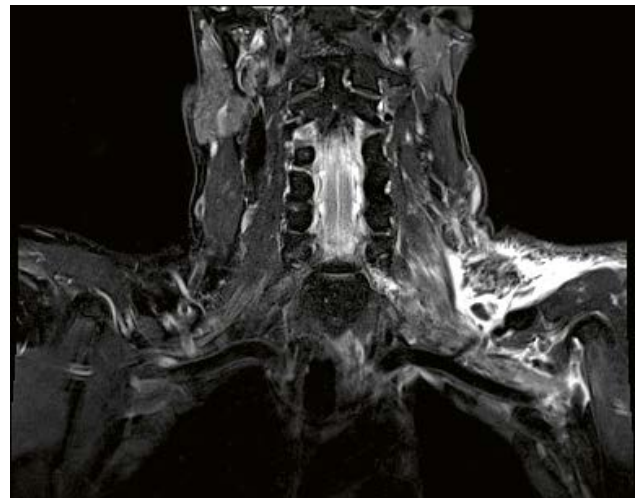
Introduction

Traumatic injury to the brachial plexus is devastating, resulting in significant loss of function and disability. Surgical management is complex, drawing on several surgical techniques ranging from nerve repair to grafting and nerve transfers. Free functioning muscle transfer may also be considered in order to restore stability and function to the upper limb. Surgical reanimation focuses first on restoring elbow flexion and shoulder stabilisation as functional priorities. Grade 3/5 (against gravity) or 4/5 (against resistance) is an expected outcome for these functional groups because intra- and extra-plexus donors are generally available, and the regeneration distances are short. Prior to consideration of any of these procedures, it is important to establish the level of the neurological lesion accurately.

The diagnosis of brachial plexus injuries presents a clinical dilemma due to both complex anatomy and varied symptomology [1]. Imaging with CT myelography and MRI have both been utilised in the evaluation of nerve injuries involving the brachial plexus, with a focus on the identification of preganglionic injuries. In the hyperacute phase post injury, imaging is targeted towards identifying other injuries that may require urgent management such as vascular and orthopaedic injuries. MRI is preferable in many cases thanks to the absence of ionizing radiation, however MR imaging in the hyperacute phase is typically compromised by extensive surrounding oedema and haematoma.

High resolution T2-weighted MR images with fat saturation have been a workhorse in aiding diagnosis and treatment assessment throughout the course of clinical care. Specifically, STIR-prepared 3D SPACE images, and the multiplanar maximum intensity projection (MIP) reconstructions, enable evaluation of the plexus anatomically. Diffusion tensor imaging and tractography have been used

in probing the integrity of nerves which can potentially inform surgical planning. However, imaging the brachial plexus with DTI is technically challenging and presents barriers to implementation [8]. Specific limitations include the small size of the brachial plexus relative to the field-of-view, close proximity to physiological motion, and field inhomogeneities [14].



1 Coronal T2 fat-saturated acquisition on day one post injury (performed at an outside institution). There is significant oedema in the supraclavicular fossa. The extent of this oedema obscures the visualisation of any neural injury making a confident diagnosis extremely difficult. We have found that scanning of the acute post-traumatic plexus is best performed 8–10 weeks post injury to best demonstrate the pathology, following the resolution of the acute post-traumatic oedema. Scanning performed at a later time point also depicts the pathology however many surgical treatments are best instituted early and therefore the 8–10 weeks' time frame is best in our experience.

- The small size of the involved nerves can lead to partial volume and mis-registration artifacts. The plane of acquisition is also important. Sagittal imaging is the ideal plane for visualising the spinal cord. However, given that the brachial plexus runs nearly orthogonal to the plane of the cord, the ideal acquisition for the plexus is axial or axial oblique. Our patient's data was acquired axially.
- Motion can occur as a result of pulsation of the CSF, supra-aortic vessels, and respiratory motion. This leads to misregistration of DTI tractography relative to the anatomical overlay images, resulting in the white matter tracts to project away from their true course [10].
- DTI has historically been based on echo-planar imaging. Although rapid in image acquisition, EPI suffers from image distortions as phase-encoding lines of *k*-space are collected immediately after a single radiofrequency pulse. Geometric distortions occur where there is poor magnetic field homogeneity and susceptibility changes from nearby tissue interfaces [2, 10–12].

The recently developed RESOLVE technique [2] aims to address some of the above-mentioned challenges. RESOLVE is a diffusion-weighted sequence based on multi-shot multi-slice 2D echo-planar imaging. With each excitation the sequence acquires a segment of the data in the readout direction, providing significantly shorter echo spacing compared to the single-shot technique. This in turn reduces susceptibility and blurring effects, as well as making high resolution diffusion imaging possible. However, the multi-shot nature of the sequence exacerbates physiological motion during diffusion preparation. To this end, a navigator echo of the centre *k*-space is acquired at each shot to provide data for phase correction or to trigger a re-acquisition in the case of severe phase errors [3–5].

Segmenting the acquisitions into multiple shots, the RESOLVE technique is significantly slower than the single-shot counterpart, limiting the number of slices and/or diffusion directions that can be acquired in a practical imaging time. To combat this limitation, a blipped-CAIPIRINHA technique is implemented to drastically accelerate RESOLVE technique by simultaneous excitations and acquisitions of multiple slices [6]. These slices are then separated in the reconstruction facilitated by the sensitivity profiles of the multi-channel receive coil [7]. The blipped-CAIPIRINHA technique enhances the separability by introducing an in-plane shift of the simultaneous slices with additional blips in the slice direction applied along with phase-encoding blips. In the following section, we describe the benefit of the addition of such an advanced imaging technique to the anatomic assessment of the traumatic plexus with a pertinent clinical case.

Case Study

Acute care

The patient was a 46-year-old male who sustained a severe upper brachial plexus injury following a downhill mountain bicycle injury. Clinically he presented with left arm pain and clinical signs consistent with an upper plexus injury, including absent sensation in the C5 and 6 dermatomes, 0/5 power in the C5 and 6 myotomes with reduced power in some C7 myotomes and some preservation of C8 and T1 innervation. In particular, he was noted to have weakness of the wrist and fingers. Following initial trauma management according to ATLS principles, his brachial plexus was imaged with anatomical MRI, day one post injury. The initial imaging (Fig. 1) demonstrated a C7 nerve root avulsion and extensive oedema within the supraclavicular fossa which precluded further assessment of the constituent components of the plexus.

His initial surgical management comprised an Oberlin I and II nerve transfer to restore elbow flexion four months after injury. Specifically, redundant fascicles of the ulnar nerve to Flexor Carpi Ulnaris (FCU) were transferred to the biceps branch of the musculocutaneous nerve and redundant fascicles of the median nerve to Flexor Carpi Radialis (FCR) were transferred to the brachialis branch of the musculocutaneous nerve. He subsequently underwent a spinal accessory to suprascapular nerve transfer six months after injury.

Follow-up

The patient did not achieve any recovery of elbow flexion four months after surgery and was referred to the brachial plexus clinic at our institution for an assessment. At that time, the patient's hand function had improved substantially from the initial presentation, but elbow flexion was absent, and the shoulder was unstable. He was referred to the radiology department for imaging of his brachial plexus. He gave informed consent to partake in a research examination of his plexus, which granted access to a prototype sequence SMS-RESOLVE.

The anatomical imaging demonstrated a pseudomeningocele at the C7 level, consistent with the earlier MRI findings of C7 avulsion (Fig. 2A). There was also hyperintensity and a nodular fusiform appearance to the C5 and C6 nerve roots, not shown, consistent with axonotmesis and neuroma in continuity. The C8 and T1 nerve roots appeared normal on anatomic MRI.

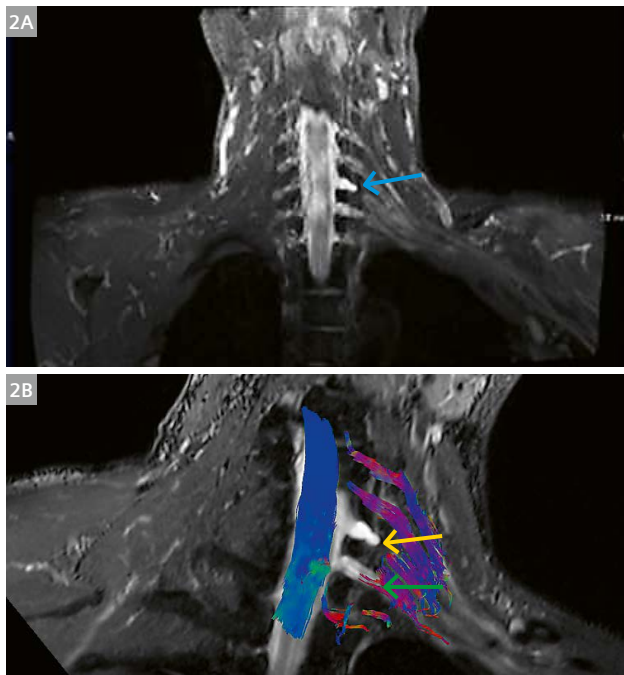
Tractography with 20 directions was also performed using the above-mentioned SMS-RESOLVE DTI technique and overlaid on the anatomical information (Fig. 2B). This demonstrated lack of fiber continuity proximally at the C7 nerve root as expected but also demonstrated a lack of proximal fiber continuity at the C8 level (green arrow

Fig. 2B) – this finding was not expected and served as a potential explanation for the failure of the previous surgical procedure given the nerve fibers transferred to aid elbow flexion (fascicle to FCU) are innervated primarily by C8. Had the proximal injury to C8 been recognised pre-operatively, a different treatment strategy may have been pursued.

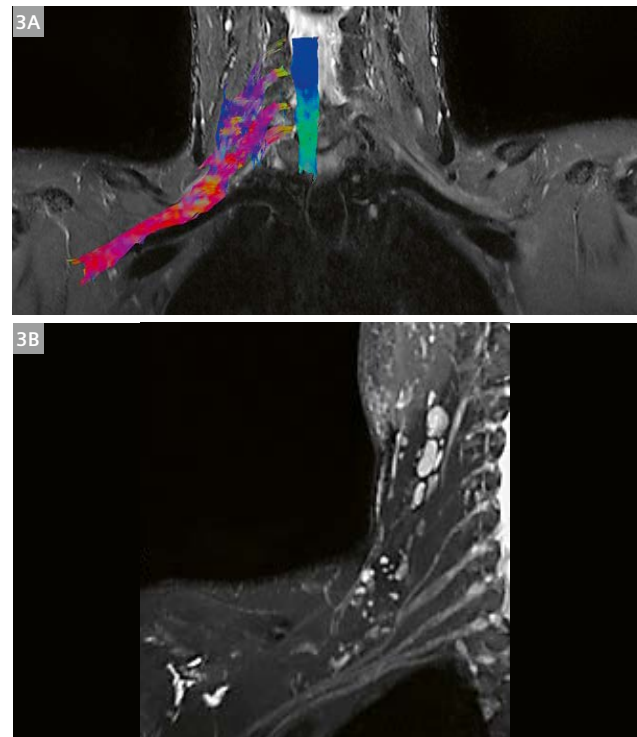
The patient is currently considering the option of free functioning muscle transfer (gracilis) using the phrenic nerve as a donor.

Discussion

MRI DTI tractography is an established neuroimaging technique in determining the location of important fiber tracts and in order to better plan surgical and radiation oncology procedures. It utilises the directional constraints to free water movement (diffusivity) to resolve the directionality of fibers in the CNS [16]. As alluded to in the introduction, the SMS-RESOLVE technique is uniquely suited to tackle the challenges faced with brachial plexus DTI. The read-out segmented EPI aids in providing high resolution scans with reduced susceptibility and blurring effects. Additionally, the shot-by-shot navigators and corresponding phase correction/re-acquisition help reduce the effects of physiological motion including, the small fibres relative to the field-of-view, physiological motions. The SMS technique has also demonstrated the capacity to reduce the imaging time.



2 (2A) Coronal MIP reconstruction of a 3D STIR space MRI demonstrating a pseudomeningocele of the C7 nerve root on the left (blue arrow), consistent with a preganglionic avulsion injury of the C7 nerve root. The remainder of the nerve roots appear intact. (2B) Coronal oblique MIP reconstruction of a 3D STIR space MRI with overlaid DTI tractography, depicting lack of continuity of the proximal fibers of C7 with the source anatomic imaging showing a corresponding pseudomeningocele (yellow arrow). In addition, a feature not seen on the anatomic imaging is an absence of proximal continuity of the C8 nerve root (green arrow).



3 (3A) DTI tractography overlaid on a STIR SPACE anatomic acquisition in a 45-year-old male volunteer. The images depict robust tracks extending from the nerve roots to the proximal aspect of the distal branches. Combined with high resolution anatomic images and clinical correlation regarding neurology, we feel this technique shows significant promise in improving the evaluation of plexus trauma. (3B) Coronal oblique MIP reconstruction from a STIR SPACE acquisition. The proximal components of the Brachial plexus are demonstrated. The upper trunk is formed by the union of the C5 and C6 nerve roots, the lower trunk is similarly formed by the junction of the C8 and T1 nerve roots. The middle trunk represents the continuation of the C7 nerve root.

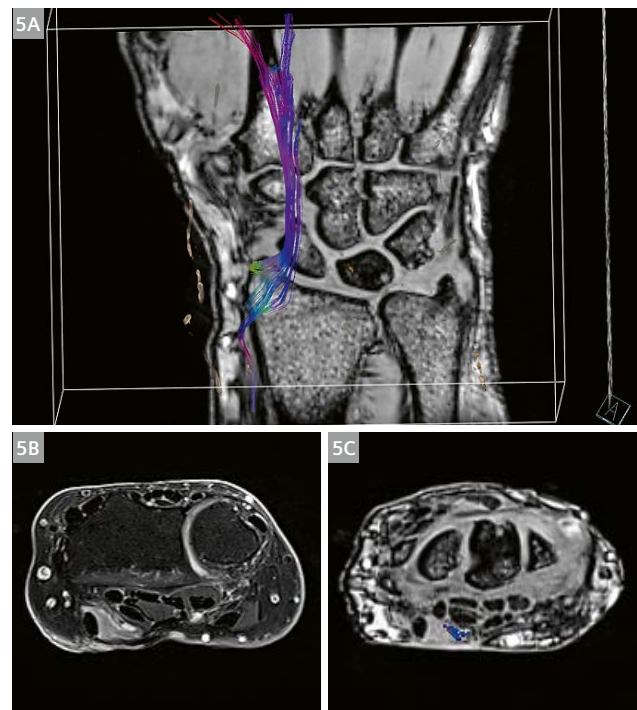
However, brachial plexus DTI using SMS-RESOLVE requires a robust and consistent workflow, including imaging protocols and post-processing techniques. Our imaging department performed numerous scans with volunteers to establish an optimized imaging protocol that balance between, FOV, resolution, SNR, the number of diffusion directions, and overall scan time. Representative volunteer images with DTI tractography and STIR SPACE are shown in Figure 3.

The optimized SMS-RESOLVE based workflow has found wider applications. Figure 4 illustrates a clinical case of a 34-year-old male patient who sustained a stab wound to his buttocks. The anatomic imaging shown on the right demonstrates decreased signal within the sciatic nerve at the site of stabbing injury likely reflecting fibrosis or

hemosiderin. While the extent of injury is inconclusive from the anatomical scan alone, the DTI study demonstrates continuity of the nerve fibers, in this case, combined with the clinical findings of relatively mild weakness in the sciatic nerve distribution, negating the need for surgical exploration. In another case, as shown in Figure 5, SMS-RESOLVE tractography provided evaluation of the relationship of a painful lump in the volar aspect of the wrist to the median nerve for a 74-year-old female patient, with a remote history of glass laceration and surgical repair. This evaluation avoided the need for surgical exploration, by demonstrating that the painful lesion was continuous with the median nerve, consistent with a traumatic neuroma, surgery to this could have resulted in significant loss function of the median nerve which was clinically intact.



4 MRI study of a 34-year-old male patient who sustained a stab wound to his left buttocks. **(4A)** Overlay image of a 20 direction DTI acquisition of the sciatic nerve covering the region of a stab injury. The DTI study demonstrates continuity of the nerve fibers, which in combination with the clinical findings negated the need for surgical exploration. **(4B)** Coronal STIR SPACE acquisition of the left sciatic nerve. There is linear hypointensity within the nerve, which corresponded to the site of knife injury, likely reflecting a combination of hemosiderin and fibrosis.



5 **(5A–5C)** DTI tractography of the median nerve in a 74-year-old female with a remote history of glass laceration and surgical repair as a child in another country – details not available. The patient presented with a palpable and painful lump in the volar aspect of the wrist and imaging was requested to evaluate the relationship to the nerve. Anatomic MRI demonstrating a poorly demarcated mass in the expected location of the median nerve. DTI tractography shows the fibers of the median nerve to pass through the lesion indicating the lesion to be of neural origin – likely a neuroma in continuity given the clinical context. The study prevented a surgical exploration of the lesion which could have resulted in damage to the remaining median nerve.

Conclusion

As demonstrated in the above case, we believe that the addition of DTI tractography to the evaluation of traumatic nerve injuries in general and brachial plexus injuries in particular traumatic can improve the diagnostic accuracy and demonstrate additional pathology that is not evident on the purely anatomical imaging. As clearly shown in this case, the selection of the correct treatment option relies on a correct diagnostic assessment of the level and extent of injury. Advanced imaging can aid in correct patient and procedure selection to allow the best chance of meaningful restoration of function in these patients. The technique is not limited to the brachial plexus and we have had success adding useful information in complex clinical cases elsewhere in the body.

In conclusion, we have presented a case that demonstrates how the addition of DTI tractography, using the SMS-RESOLVE sequence, adds valuable information over and above that of standard MR imaging, assisting in the correct management of the complex injuries sustained in traumatic injury of the brachial plexus.

The ability of SMS-RESOLVE to acquire multiple slices simultaneously results in shorter scan times and less motion artifacts. It is therefore able to generate robust tracking of the complex peripheral nervous system and will likely find more applications in complex surgical planning.

References

- 1 Ho M.J., Ciritsis A, Manoliu A, Stieltjes B, Marcon M, Andreisek G, Kuhn F.P. Diffusion Tensor Imaging of the Brachial Plexus: A Comparison Between Readout-Segmented and Conventional Single-shot Echo-Planar Imaging. *Magn Reson Med Sci*. 2019 Apr 10;18(2):150-157. Doi:10.2463/mrms.mp.2018-0004.
- 2 Porter, D.A., Heidemann, R.M., 2009. High resolution diffusion-weighted imaging using readout-segmented echo-planar imaging, parallel imaging and a two-dimensional navigator-based reacquisition. *Magnetic Resonance in Medicine* 62, 468–475. <https://doi.org/10.1002/mrm.22024>
- 3 Anderson, A.W., Gore, J.C., 1994. Analysis and correction of motion artifacts in diffusion weighted imaging. *Magnetic Resonance in Medicine* 32, 379–387. <https://doi.org/10.1002/mrm.1910320313>
- 4 Ordidge, R.J., Helpert, J.A., Qing, Z.X., Knight, R.A., Nagesh, V., 1994. Correction of motional artifacts in diffusion-weighted MR images using navigator echoes. *Magnetic Resonance Imaging* 12, 455–460. [https://doi.org/10.1016/0730-725X\(94\)92539-9](https://doi.org/10.1016/0730-725X(94)92539-9)
- 5 Nguyen, Q., Clemence, M., Rhornton, J., Ordidge, R.J., 1999. Isotropic Diffusion-Weighted Multishot Imaging using Automatic Reacquisition, in: *Proceedings of the 7th Annual Meeting of ISMRM*. Philadelphia, USA, p. 559.
- 6 Setsompop, K., Gagoski, B.A., Polimeni, J.R., Witzel, T., Wedeen, V.J., Wald, L.L., 2012. Blipped-controlled aliasing in parallel imaging for simultaneous multislice echo planar imaging with reduced g-factor penalty. *Magnetic Resonance in Medicine* 67, 1210–1224. <https://doi.org/10.1002/mrm.23097>
- 7 Cauley, S.F., Polimeni, J.R., Bhat, H., Wald, L.L., Setsompop, K., 2014. Interslice leakage artifact reduction technique for simultaneous multislice acquisitions. *Magnetic Resonance in Medicine* 72, 93–102. <https://doi.org/10.1002/mrm.24898>
- 8 Noguerol T.M., Barousse R, Cabrera, M.G., Socolovsky M, Bencardino J.T., Luna A. Functional MR Neurography in Evaluation of Peripheral Nerve Trauma and Postsurgical Assessment. *RadioGraphics*. 2019 Feb 8;39(2):427-446. <https://doi.org/10.1148/rg.2019180112>
- 9 Rutman A.M., Peterson D.J., Cohen W.A., Moss-Basha M. Diffusion Tensor Imaging of the Spinal Cord: Clinical Value, Investigational Applications, and Technical Limitations. *Curr Probl Diagn Radiol*. 2018 Jul;47(4):257-269. doi: <https://doi.org/10.1067/j.cpradiol.2017.07.005>
- 10 Noguerol T.M., Barousse R, Amrhein T.J., Royuela-del-val J, Montesinos P, Luna A. Optimizing Diffusion-Tensor Imaging Acquisition for Spinal Cord Assessment: Physical Basis and Technical Adjustments. *RadioGraphics*. 2020 Mar 3;40(2):403-427. doi: <https://doi.org/10.1148/rg.2020190058>
- 11 Ho M.J., Manoliu A, Kuhn F.P., Stieltjes B, Klarhöfer, Feiwei T, Marcon M, Andreisek G. Evaluation of Reproducibility of Diffusion Tensor Imaging in the Brachial Plexus at 3.0 T. *Invest Radiol*. 2017 Aug;52(8):482-487. doi:10.1097/RLI.0000000000000363
- 12 Sasiadek M.J., Szewczyk P, Bładowska J. Application of diffusion tensor imaging (DTI) in pathological changes of the spinal cord. *Med Sci Monit*. 2012 Jun;18(6):73–9. doi: 10.12659/msm.882891
- 13 Lerner A, Mogensen M.A., Kim P.E., Shiroishi M.S., Hwang D.H., Law M. Clinical applications of diffusion tensor imaging. *World Neurosurg*. 2014 Jul;82(1-2):96–109. doi: 10.1016/j.wneu.2013.07.083
- 14 Noguerol T.M., Barousse R, Socolovsky M, Luna A. Quantitative Magnetic Resonance (MR) Neurography for Evaluation of Peripheral Nerves and Plexus Injuries. *Quant Imaging Med Surg*. 2017 Aug;7(4):398-421. Doi: 10.21037/qims.2017.08.01
- 15 Kamanth, S. Venkatanarasimha, N. Walsh, M. Hughes, P., 2008. MRI appearance of muscle denervation. *Skeletal Radiol* 37:397-404. <https://doi.org/10.1007/s00256-007-0409-0>
- 16 Mukherjee, P, Berman, J. Chung, S., Hess, C. Henry, R., 2008. Diffusion Tensor MR Imaging and Fiber Tractography: Theoretic Underpinnings. *AJNR*, 29 (4) 632-641. <https://doi.org/10.3174/ajnr.A1051>



Contact

Dr Thomas Lloyd
Department of Radiology
Princess Alexandra Hospital
Ipswich Road
Wooloongabba, Qld 4102
Australia
thomas_lloyd@health.gov.qld.au

Magnetic Resonance Fingerprinting for Precision Imaging in Neuro-Oncology

Domenico Zacà; Guido Buonincontri

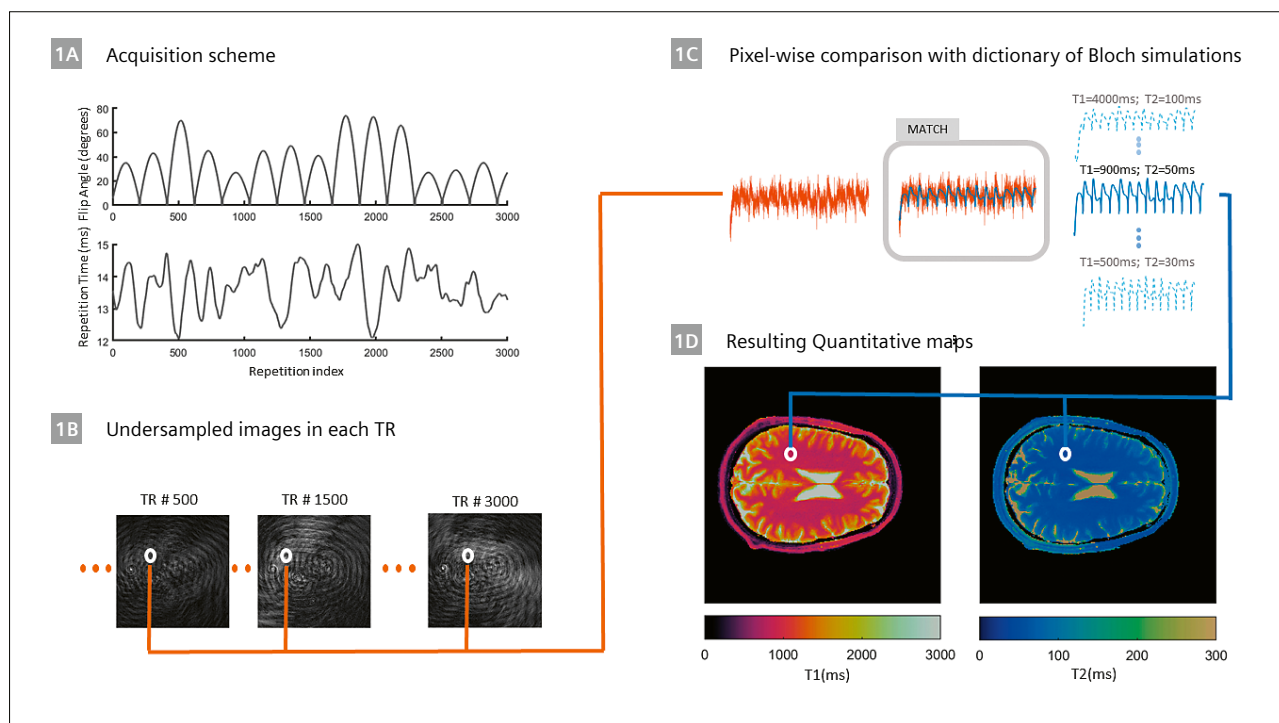
Siemens Healthineers, Italy

Introduction

Brain tumors are one of the greatest health afflictions of our time. Although less prominent than other cancers, affecting around 4 in 100,000 people every year globally, it puts a great burden on patients, carers, and healthcare systems [1]. Recent advances have brought a better understanding of brain-tumor biochemistry, as well as the introduction of new treatments. However, for the most aggressive tumors, many challenges remain – for example, average life expectancy for glioblastoma is still under two years [1]. The standard of care for aggressive tumors includes surgical resection followed by adjuvant treatment and rehabilitation [2]. For effective surgical planning, as well as for treatment evaluation, neuroimaging methods are of primary importance. In this context, precision

imaging requires accurate assessment of the disorder *in situ*, accounting for the often-observed tumor heterogeneity [3], disease progression, presentation after initial treatment, and follow-up during treatment cycles [4]. Due to its superior soft-tissue contrast and the use of non-ionizing radiation, MRI is key to precision imaging. MR exams are repeated often, serving as a major source of information for individualized therapeutic paths, enabling diagnosis, treatment, control, and follow-up tailored to the individual characteristics of each patient [5].

Magnetic resonance imaging is essential in guiding, assisting, and monitoring treatment strategy. Currently, structural MR sequences at fields of 1.5T or above are the standard for brain-tumor imaging. T1-weighted,



1 In Magnetic Resonance Fingerprinting (MRF)¹, acquisition parameters are varied at each TR to keep the magnetization in the transient state (1A). Next, highly undersampled images are acquired in each TR (1B). For each voxel, the acquired data is compared with the clean simulation (1C) to find a match using pattern recognition, then matching results from all voxels are combined to form parameter maps (1D).

¹Work in progress. MR Fingerprinting is not commercially available in some countries. Due to regulatory reasons its future availability cannot be ensured. Please contact your local Siemens Healthineers organization for further details.

T2-weighted, FLAIR, and diffusion-weighted sequences are commonly included in protocols [6]. The images obtained with these sequences provide information about lesion location, brain tissue infiltration, and lesion cellularity. In addition, when contrast media are administered, images become sensitive to processes such as blood-brain barrier infiltration, a phenomenon typical of biologically aggressive neoplasms.

When combined with a patient's clinical history and symptoms, these data are commonly used by the radiologist to perform a differential diagnosis. In addition to a confident diagnosis, accurate delineation of tumor margins has a primary role in therapy planning [7]. Discriminating primary vasogenic edema seen in metastases from the edema with neoplastic cellular infiltration seen in glioblastoma is important to guide surgery and therapy, with a positive impact on patient outcome [8]. To that end, many studies have aimed at probing the underlying tumor microstructure and differentiating the biological characteristics of the tissue. Advanced MR imaging techniques including diffusion tensor imaging, perfusion, and spectroscopy have been used to discriminate glioblastomas from brain metastases and identify areas of peritumoral infiltrations [9]. More specifically, a multiparametric approach combining and comparing the features obtained with basic and advanced techniques could improve both sensitivity and specificity in identifying areas of gliomas that are not contrast enhancing but biologically active [10]. For example, applying machine learning algorithms on hundreds of features extracted from T1, T2, FLAIR, diffusion, and perfusion images has been shown to differentiate between vasogenic edema and tumor infiltration in patients with high grade gliomas with a sensitivity of 86% and a specificity of 89 % [11].

Advanced multiparametric procedures, however, require long scan times since the acquisition of many different basic and advanced sequences is necessary and needs specific postprocessing currently performed offline by dedicated personnel with specific technical expertise. To aid this, many automatic tools for quantitative analysis of neoplastic structures have been developed. Despite many improvements, this remains a challenge [10], owing to the large variability of qualitative MR data commonly used in the clinic. Recent advances have allowed automatic segmentation of brain MR images, achieving robust modelling and segmentation of volumetric data based on Artificial Intelligence (AI). Among these methods, the AI-Rad Companion for brain MR morphometry from Siemens Healthineers recently received 510k and CE labeling [11].

As AI-based medical computer vision enters the field of diagnostic imaging, several tools are needed to achieve automatic classification and interpretation of images, or tumor growth modelling and prediction. Reliable, repro-

ducible, quantitative image data becomes critical – determining the accuracy of decision support and the predictive quality of derived disease models. Consequently, AI-based methods require a rich set of consistent imaging data. Such consistency can be obtained with quantitative MRI methods. In this regard, conventional multiparametric assessments are currently far from entering the clinical arena due to lengthy acquisition and the complexity of processing, as well as questions over their repeatability and reproducibility [12].

MR Fingerprinting in neuro-oncology

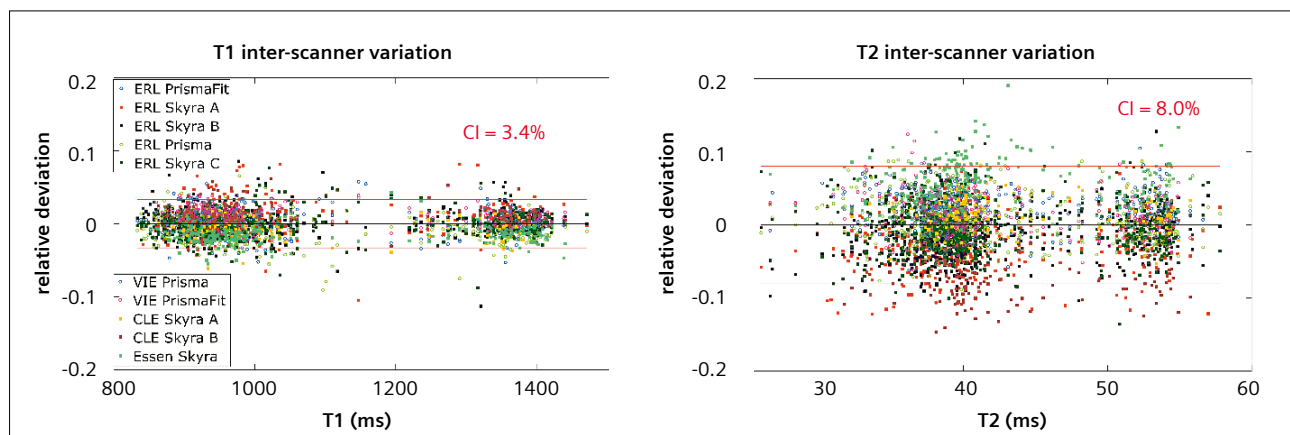
New tools for fast multiparametric estimation have recently been developed, achieving fast multiparametric mapping in a short acquisition time [13]. Among these methods, Magnetic Resonance Fingerprinting (MRF) has now been developed into a Siemens Healthineers product, in partnership with Case Western Reserve University [14]. MRF is a framework for multiparametric mapping relying on transient-state acquisitions [15], achieving multiparametric maps in under 30s. While conventional methods for parameter quantification acquire only one parameter at a time, MRF uses a holistic approach to the signal, including all the relevant information within a single model. This makes it possible to derive many individual parameters at once in an efficient manner.

A scheme of a typical MRF algorithm is shown in Figure 1. Rather than achieving a magnetization steady-state, acquisition parameters are purposely varied in each TR to generate unique tissue responses. For each pulse, an undersampled snapshot is acquired, typically with a non-Cartesian *k*-space acquisition, such as a spiral. In a typical MRF implementation, a dictionary is calculated with the possible physical responses obtained by simulating the transient-state response via the Bloch equations over a range of meaningful tissue parameters (T1, T2, PD, etc.) and system imperfections (e.g., field inhomogeneity). Patterns of acquisition parameters, such as flip angle and TR, are optimized to encode specific magnetization properties at pixel level. After acquisitions, measured signals in individual pixels are compared with calculated dictionary elements. This approach, including multiple parameters within the same model, has the advantage of producing highly accurate maps, with repeatability and reproducibility matching or outperforming other literature methods yet requiring a much shorter scan time [16, 17]. Exemplary 95% confidence intervals for MRF repeatability are reported in Figure 2.

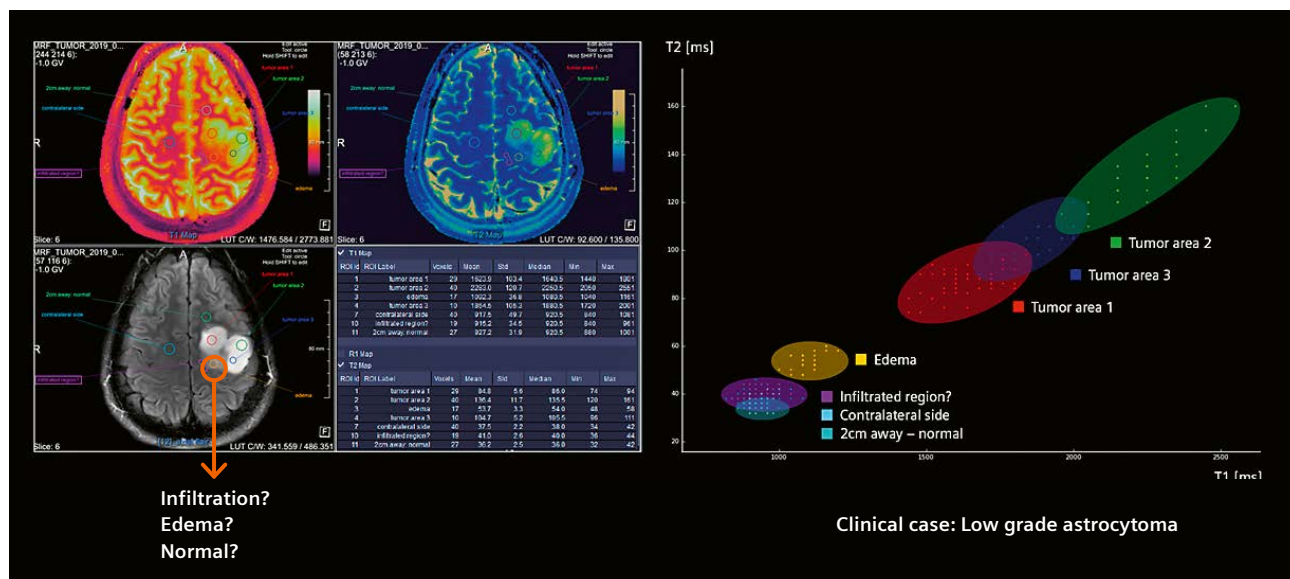
Quantitative relaxometry assessments for neuro-oncology require accurate and reliable tools for confident tissue characterization. Despite initial promise, studies on relaxometry in the early days of MRI found significant overlap between different tumor grades. The results on

tumor tissue characterization were not consistent between studies [18], and more significant diagnosis markers were later found with perfusion and diffusion assessments [19]. However, precise measurements of relaxometry have recently been re-introduced in research studies to complement information from more conventional tumor imaging protocols, as they provide valuable and objective information. For instance, in anti-angiogenic therapy, differentiating response from non-response can be difficult, as enhancement may be faint or subtle due to the decreased vessel wall permeability resulting from therapy. T1 subtraction maps have been used in this setting to improve inter-observer variability and better identify progression [20].

In addition to T1 subtraction maps, native T2 mapping has also provided important findings. In non-enhancing tumors, Response Assessment in Neuro-Oncology (RANO) requires assessment of FLAIR abnormalities, which provide separate information when compared with the enhancement pattern. Here, objective criteria are difficult to establish due to the various sources of pathology, including radiation effects, ischemia, edema, and post-operative gliosis. Recently, studies have found that objective T2 measurements are more specific than T2w images for tumor identification after anti-angiogenic treatments [21], more precisely characterize edema [22], and show a better outcome prediction [23].



2 Graphs show inter-scanner variation of mean T1 and T2 values in all solid matter compartments. Different colors indicate different scanners. Symmetric confidence intervals (CIs) of 1.96 standard deviations are shown. For T1 mean value in solid tissue, CI half-width is 3.4%. For T2 it is 8.0% [data from [16]].



3 Image visualization (left) and scatter plot (right) of the different areas of a low grade astrocytoma, showing a neat discrimination of the various components based on two-dimensional histograms. Courtesy of Professor Siegfried Trattnig, Medical University of Vienna, Austria.

New, more efficient approaches such as MRF, capable of acquiring multiparametric maps in under 30 seconds, are aiding the transition of these findings towards clinical protocols. Initial experiences with MRF in neuro-oncology studies have shown its ability to distinguish different tissue characteristics in both adult and pediatric brain tumors. In a group of 31 adult patients with intra-axial brain tumors, T2 maps were shown to be significantly different between solid tumor regions of lower-grade gliomas and metastases [24]. Likewise, T1 maps of Peritumoral White Matter (PWM) surrounding lower-grade gliomas differed from maps of PWM around glioblastomas [24]. Similar results were obtained in a group of 23 pediatric² and young adult patients [25]. Specifically, the authors reported statistically significant difference in T1 and T2 between low and high grade gliomas as well as between peritumoral and contralateral white matter. These results, although preliminary and yet to be replicated in larger studies, build upon findings showing the value of relaxometry for discriminating different molecular subtypes of tumors and evaluating anti-angiogenic treatment [20]. MRF allows this information to be obtained with a rapid and reproducible acquisition protocol.

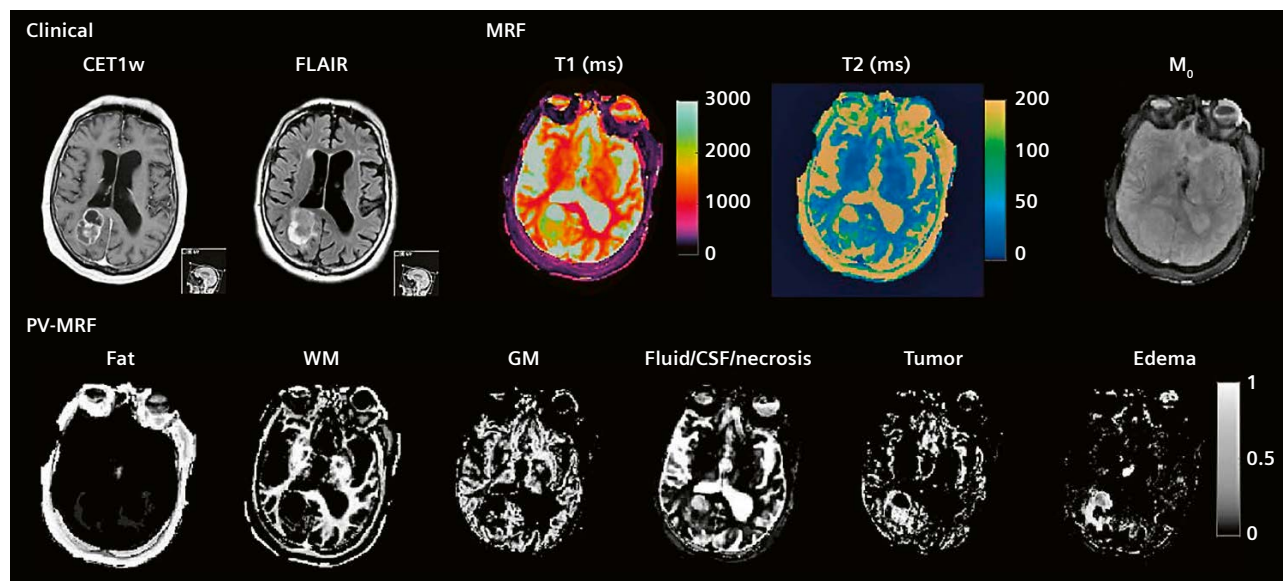
Challenges and opportunities for MRF in neuro-oncology

In addition to analyses based on a single value of T1 and T2 within each voxel, studies are looking into more sophisticated multicomponent analyses to assess tissue microstructure. These include a wealth of information

related to subtle features such as pore size, distribution, and exchange between compartments. While DESPOT modelling and diffusion are established methods to achieve this [26], they often suffer from long acquisition times and complex processing procedures.

With the recent emergence of fast, multiparametric acquisition schemes such as MRF, studying tissue microstructure with more realistic acquisition times has become feasible. In addition to speed, MRF has other inherent advantages for partial-volume modelling. Conventional partial-volume modelling of T1 and T2 mapping involves multi-exponential fits, which are difficult to perform mathematically. In contrast, MRF acquisition generates signals from mixtures which are distinct from pure tissue, allowing for a better discrimination of microstructural components [27]. An example can be seen in Figure 4, showing a segmentation of a small-cell lung cancer metastasis in the brain using dictionary-based partial volume MRF (PV-MRF) and 3D MRF acquisition. Recently, a similar approach has also been used to characterize developmental changes relating to myelination in children from birth² to five years old [28]. This was done by modelling white matter as composed by myelin water, intracellular/extracellular water, and free water, allowing to generate precise myelination trajectories. Similar models could be used to discriminate and follow-up myelin integrity in other disease and treatment cases.

²MR scanning has not been established as safe for imaging fetuses and infants less than two years of age. The responsible physician must evaluate the benefits of the MR examination compared to those of other imaging procedures.



4 Segmentation of a small-cell lung cancer metastasis in the brain using dictionary-based PV-MRF and 3D MRF acquisition. Dictionary matching enables the use of expanded multi-component models and segmentation of more tissue types than conventional partial-volume analysis [from [27]].

Future applications of MRF may include synergistic approaches for treatment planning. In this context, the feasibility of integrating accurate and precise MRF protocols in MR-guided radiation therapy planning has been recently demonstrated [29]. The MRF strategy employed showed increased repeatability and reproducibility for quantification, which is promising for longitudinal quantitative assessment of treatment response for better adaptive therapy, and for large-scale, multi-center clinical trials. There is also promise in including MRF in intra-operative MR solutions such as the Nexaris MR Combi Suite Neurosurgery. Intraoperative MR solutions have recently been shown to significantly improve the management of brain tumor patients by maximizing the extent of resection, and achieving five times more total resection than lightweight surgery [30, 31].

Another advance for treatment planning could be combined PET and multiparametric MRI. The combination of these two modalities for tissue segmentation has recently been shown to provide novel integrated segmentations for effective gamma knife treatment [32]. In this context, optimal combinations of quantitative features from MRF with complementary metabolic information from PET protocols could yield sophisticated tissue characterizations in neuro-oncological applications, with many opportunities for combined MR-PET systems [33], such as the BIOGRAPH mMR. Due to its capability for multi-component estimation in white matter, MRF could also help in the definition of more efficient and less toxic treatment plans. Common findings in patients treated with radiotherapy include vascular damage, hemorrhage, edema, neuroinflammation, astrogliosis, and neuronal cell damage [34,35]. These adverse effects can generate diffuse damage and lead to cognitive decline with a significant impact on the quality of life.

The potential of MRF for oncology is not limited to brain imaging. Research is investigating MRF in other areas of the body, such as chest [36], prostate [37, 38], breast [37], and musculoskeletal system [39–41]. Optimized MRF protocols may aid tumor detection, characterization, and treatment planning in many different applications.

In conclusion, MRF represents a paradigm shift for reliable, repeatable, and consistent signal acquisition and modelling. The recent availability of this technique in the clinical realm may have a significant impact on tumor detection, characterization, and effective treatment planning. Importantly, the clinical MRF sequence uses a standardized implementation, facilitating the pooling of data from different sites and different scanners. This could potentially enable larger scale clinical trials, producing large and consistent datasets. The increased consistency in signal outputs from MRF, compared with more conventional contrast-weighted images, holds great potential for radiomics.

References

- 1 NIH National Cancer Institute. Cancer Facts & Figures 2020.
- 2 Bush NAO, Chang SM, Berger MS. Current and future strategies for treatment of glioma. *Neurosurg. Rev.* 2017;40(1):1-14.
- 3 Turkbey B, Mani H, Shah V, et al. Multiparametric 3T prostate magnetic resonance imaging to detect cancer: Histopathological correlation using prostatectomy specimens processed in customized magnetic resonance imaging based molds. *J. Urol.* 2011;186(5):1818-1824.
- 4 Jacobs AH, Kracht LW, Gossmann A, et al. Imaging in neurooncology. *NeuroRx* 2005;2:333-347.
- 5 European Society of Radiology (ESR). Medical imaging in personalised medicine: a white paper of the research committee of the European Society of Radiology (ESR). *Insights Imaging.* 2015;6:141-155.
- 6 Villanueva-Meyer JE, Mabray MC, Cha S. Current clinical brain tumor imaging. *Clin. Neurosurg.* 2017;81(3): 397-415.
- 7 Njeh CF. Tumor delineation: The weakest link in the search for accuracy in radiotherapy. *J. Med. Phys.* 2008;33(4):136-140.
- 8 Horská A, Barker PB. Imaging of brain tumors: MR spectroscopy and metabolic imaging. *Neuroimaging Clin. N. Am.* 2010;20(3):293-310.
- 9 Kalpathy-Cramer J, Gerstner ER, Emblem KE, Andronesi OC, Rosen B. Advanced magnetic resonance imaging of the physical processes in human Glioblastoma. *Cancer Res.* 2014;74(17):4622-4637.
- 10 Menze BH, Jakab A, Bauer S, et al. The Multimodal Brain Tumor Image Segmentation Benchmark (BRATS). *IEEE Trans. Med. Imaging* 2015;34(10):1993-2024.
- 11 Auntminnie.com. Casey B, Forrest W. Portable head CT, AI for MRI pace Siemens at RSNA; 2019 December 3 [cited 2020 August 10]. Available from: https://www.auntminnie.com/index.aspx?sec=rca&sub=rsna_2019&pag=dis&itemID=127565.
- 12 Deoni S. Quantitative relaxometry of the brain. *Top. Magn. Reson. Imaging.* 2010;21:101-113.
- 13 Buonincontri G. Fast Quantitative Magnetic Resonance Imaging. *Synth. Lect. Biomed. Eng.* 2020; 15(1):i-124.
- 14 Nature research. natureresearch Custom Media, Siemens Healthineers. Diagnostic detectives: Magnetic Resonance Fingerprinting to help radiologists solve disease mysteries; [cited 2020 August 10]. Available from: <https://www.nature.com/articles/d42473-019-00233-1>.
- 15 Ma D, Gulani V, Seiberlich N, et al. Magnetic resonance fingerprinting. *Nature.* 2013;495,187-192.
- 16 Kördörfer G, Kirsch R, Liu K, et al. Reproducibility and repeatability of MR fingerprinting relaxometry in the human brain. *Radiology.* 2019;292(2):429-437.
- 17 Buonincontri G, Biagi L, Retico A, et al. Multi-site repeatability and reproducibility of MR fingerprinting of the healthy brain at 1.5 and 3.0 T. *Neuroimage.* 2019;195:362-372.
- 18 Wagnerova D, Herynek V, Malucelli A, et al. Quantitative MR imaging and spectroscopy of brain tumours: A step forward? *Eur. Radiol.* 2012;22:2307-2318.
- 19 Cha S. Neuroimaging in Neuro-Oncology. *Neurotherapeutics.* 2009;6,465-477.
- 20 Wen PY, Cloughesy TF, Ellingson BM, et al. Report of the Jumpstarting Brain Tumor Drug Development Coalition and FDA clinical trials neuroimaging endpoint workshop (January 30, 2014, Bethesda MD). *Neuro. Oncol.* 2014;16(suppl 7):vii36–vii47.
- 21 Ellingson BM, Lai A, Nguyen HN, Nghiemphu PL, Pope WB, Cloughesy TF. Quantification of Nonenhancing tumor burden in Gliomas using effective T2 maps derived from dual-echo turbo spin-echo MRI. *Clin. Cancer Res.* 2015;21(19):4373-4383.

- 22 Ellingson BM, Cloughesy TF, Lai A, et al. Quantification of edema reduction using differential quantitative T2 (DQ2) relaxometry mapping in recurrent glioblastoma treated with bevacizumab. *J. Neurooncol.* 2012;106(1):111-119.
- 23 Hattingen E, Jurcoane A, Daneshvar K, et al. Quantitative T2 mapping of recurrent glioblastoma under bevacizumab improves monitoring for non-enhancing tumor progression and predicts overall survival. *Neuro. Oncol.* 2013;15(10):1395-1404.
- 24 Badve C, Yu A, Dastmalchian S, et al. Magnetic Resonance Fingerprinting of Adult Brain Tumors: Initial Experience. *Am. J. Neuroradiol.* 2017;38(3):492-499.
- 25 De Blank P, Badve C, Gold DR, et al. Magnetic Resonance Fingerprinting to Characterize Childhood and Young Adult Brain Tumors. *Pediatr. Neurosurg.* 2019;54(5):310-318.
- 26 Does MD. Inferring brain tissue composition and microstructure via MR relaxometry. *Neuroimage* 2018;182:136-148.
- 27 Doshmane A, McGivney DF, Ma D, et al. Partial volume mapping using magnetic resonance fingerprinting. *NMR Biomed.* 2019;32(5):e4082.
- 28 Chen Y, Chen MH, Baluyot KR, Potts TM, Jimenez J, Lin W. MR fingerprinting enables quantitative measures of brain tissue relaxation times and myelin water fraction in the first five years of life. *Neuroimage* 2019; 186:782-793.
- 29 Lu L, Chen Y, Shen C, et al. Initial assessment of 3D magnetic resonance fingerprinting (MRF) towards quantitative brain imaging for radiation therapy. *Med. Phys.* 2020;47(3):1199-1214.
- 30 Kuhnt D, Becker A, Ganslandt O, Bauer M, Buchfelder M, Nimsky C. Correlation of the extent of tumor volume resection and patient survival in surgery of glioblastoma multiforme with high-field intraoperative MRI guidance. *Neuro. Oncol.* 2011;13(12):1339-1348.
- 31 Roder C, Bisdas S, Ebner FH, et al. Maximizing the extent of resection and survival benefit of patients in glioblastoma surgery: High-field iMRI versus conventional and 5-ALA-assisted surgery. *Eur. J. Surg. Oncol.* 2014;40(3):297-304.
- 32 Rundo L, Stefano A, Militello C, et al. A fully automatic approach for multimodal PET and MR image segmentation in gamma knife treatment planning. *Comput. Methods Programs Biomed.* 2017;144:77-96.
- 33 Ropella-Panagis KM, Seiberlich N, Gulani V. Magnetic Resonance Fingerprinting: Implications and Opportunities for PET/MR. *IEEE Trans. Radiat. Plasma Med. Sci.* 2019;3(4):388-399.
- 34 Makola M, Douglas Ris M, Mahone EM, Yeates KO, Cecil KM. Long-term effects of radiation therapy on white matter of the corpus callosum: a diffusion tensor imaging study in children. *Pediatr. Radiol.* 2017;47:1809-1816.
- 35 Panagiotakos G, Alshamy G, Chan B, et al. Long-term impact of radiation on the stem cell and oligodendrocyte precursors in the brain. *PLoS One.* 2007;2(7):e588.
- 36 Hamilton JJ, Jiang Y, Chen Y, et al. MR fingerprinting for rapid quantification of myocardial T1, T2, and proton spin density. *Magn. Reson. Med.* 2017;77(4):1446-1458.
- 37 Chen Y, Panda A, Pahwa S, et al. Three-dimensional MR fingerprinting for quantitative breast imaging. *Radiology.* 2019;290(1):33-40.
- 38 Yu AC, Badve C, Ponsky LE, et al. Development of a combined MR Fingerprinting and Diffusion examination for Prostate cancer. *Radiology.* 2017;283(3):729-738.
- 39 Cencini M, Biagi L, Kaggie JD, Schulte RF, Tosetti M, Buonincontri G. Magnetic resonance fingerprinting with dictionary-based fat and water separation (DBFW MRF): A multi-component approach. *Magn. Reson. Med.* 2019;81(5):3032-3045.
- 40 Lattanzi R, Asslaender J, Cloos M. Rapid proton density, T1 and T2 mapping for comprehensive hip cartilage evaluation with magnetic resonance fingerprinting. *Skeletal Radiol.* 2017;46:1313.
- 41 Cloos MA, Assländer J, Abbas B, et al. Rapid Radial T1 and T2 Mapping of the Hip Articular Cartilage With Magnetic Resonance Fingerprinting. *J. Magn. Reson. Imaging.* 2019;50(3):810-815.

Contact

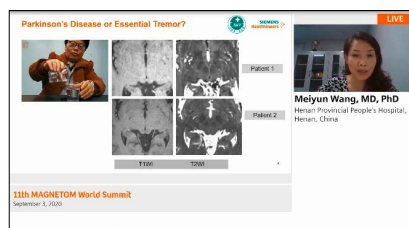


Domenico Zaccà
Siemens Healthineers
SHS EMEA SEU ITA S&PSM-DI&AT&US DI-MR
Via Vipiteno 4
20128 Milano
Italy
domenico.zacca@siemens-healthineers.com

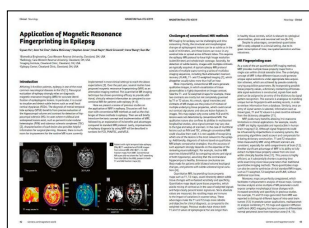


Guido Buonincontri
Siemens Healthineers
SHS EMEA SEU ITA S&PSM-DI&AT&US DI-MR
Via Laurentina 455
00142 Roma
Italy
guido.buonincontri@siemens-healthineers.com

Learn more about MR Fingerprinting



Clinical Benefits of MR Fingerprinting
Meiyun Wang
Henan Provincial People's Hospital, China



Application of MRF in Epilepsy
Dan Ma, et al.
Case Western Reserve University, Cleveland, OH, USA

For imaging examples, articles, talks, motivation and technique, please visit
[siemens.com/magnetom-world](https://www.siemens.com/magnetom-world)
> Hot Topics > MR Fingerprinting

Breast MRI on 1.5T MAGNETOM Sola

Sindre Øverstad

Department of Radiology, Radiumhospitalet, Oslo University Hospital, Oslo, Norway

The .exar1 protocol is available for download at:

www.siemens.com/magnetom-world

> Clinical Corner > Protocols > Breast MRI

Introduction

Creating an MRI-protocol always involves a compromise between image resolution, image contrast, signal-to-noise ratio (SNR), and scan time. MRI of the breasts can be a somewhat uncomfortable procedure. Proper use of support cushions and head rest is helpful, but it still needs to be done in prone position. This gives limitations to the total examination time to prevent motion artifacts due to patient discomfort. MAGNETOM Sola unleashes advanced acceleration- and imaging techniques at 1.5T that can be combined to shorten scan time and improve the image quality. Using the combination of the 18-channel Breast coil and the 18-channel Body coil, we have developed a multiparametric breast MRI protocol requiring approximately 15 minutes scan time (Table 1). The protocol is in accordance with current state-of-the art technical requirements for the three main indications: screening, staging, and treatment evaluation of breast cancer [1, 2].

Patient setup and preparation

The patient is positioned on the Breast 18 coil in prone position. We also use the Body 18 coil on the back of the patient in order to increase the signal received from the axilla and sternum. The light weight of the Body 18 coil (1.6 kg / 3.5 lbs. including cable) provides insignificant added discomfort to the patient, and the straps used to fixate the coil are used to give support to the arms.

We aim to position the breasts as close to the center of the coil as possible. To fixate the breasts we use the adjustment lever on both sides of the Body 18 coil. This is done with caution, as we are very aware not to cause discomfort to the patient or alter the anatomy of the breasts.

	# slices	Slice Thickness (mm)/gap	TR	TE	TA (min:sec)	Voxel size (mm)	FOV (mm)	Matrix	Avg.	Coil(s)	iPAT
Tra T2w Dixon	84	2.0/0%	3080	81	5:03	0.75 × 0.83 × 2.00* 0.38 × 0.38 × 2.00**	390 x 240	468 x 320	1	Breast 18 + Body 18	GRAPPA: 2 SMS: 3
Tra DWI b0/b800 ZOOMit ^{PRO}	34	4.0/25%	6200	63	4:39	1.83 × 1.83 × 4.00* 0.92 × 0.92 × 4.00**	330 x 161.3	180 x 88	b0: 8 b800: 8	Breast 18	GRAPPA: 2
Tra TWIST-VIBE Dixon	80	2.0/20%	6.8	TE 1: 2.39 TE 2: 4.77	5:39	0.78 × 0.78 × 2.00	337.5 x 200	432 x 256	1	Breast 18 + Body 18	CAIPI: 4

Table 1: Sequence parameters for breast MRI at 1.5T MAGNETOM Sola.

*Acquired resolution

**Interpolated resolution

Protocol

Morphology

2D or 3D

To choose between 2D- and 3D-techniques means a choice between in-plane resolution and multiplanar reconstruction (MPR). Whereas a 3D TSE sequence (SPACE) provides superior MPR using isotropic 1 mm³ voxels, thin 2D TSE sequences provides superior submillimeter in-plane details. MAGNETOM Sola allows for 2 mm 2D TSE slices without slice spacing (with the use of two concatenations). This enables high image details with surprisingly acceptable MPR. Our radiologists use MRP mostly for comparison with ultrasound and mammography, and prefer the better in-plane details that the 2D images provides. The new simultaneous multislice (SMS) technique enables us to cover 16.8 cm (84 slices) within comparable scan time to 3D SPACE. When SMS is applied to TSE-sequences, it yields an increase in specific absorption rate (SAR). However, we rarely exceed the limiting values operating in Normal Mode. This may be of bigger concern when scanning at 3T.

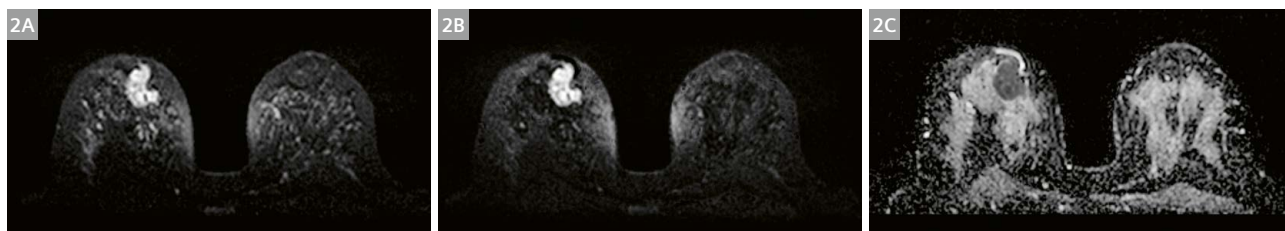
A trade-off with 2D is slightly inferior morphology of small lymph nodes when oblique oriented to the image plane.

Dixon or not Dixon

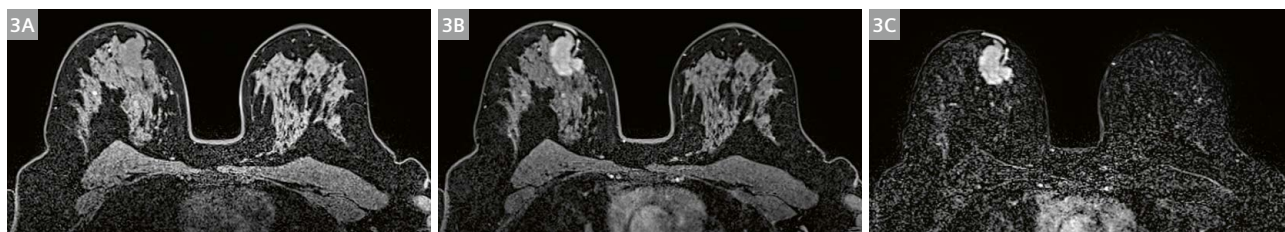
The Dixon fat-water separation technique has the advantages of specific fat images (fat-only) and robust and homogenous fat free imaging of water (water-only) in the same sequences. Thus, using Dixon enables not only superior image quality, but also reduced scan time. The fat-only images are superior to T1W for depiction of fat. The T2W water-only images are superior to frequency-selective fat sat for homogeneity and superior to STIR regarding scan time and SNR, and can be performed after the injection of Gadolinium if necessary. Because Dixon unfortunately is unavailable for 3D SPACE, we have chosen the thin interleaved 2D images (Fig. 1). For depicting blood and proteinous liquid at T1W we use the pre-contrast phase from the dynamic sequence (VIBE-Dixon) (Fig. 3A).



1 Transversal T2W Dixon in-phase (1A), fat-only (1B), and water-only (1C) showing a tumor in the upper medial quadrant of the right breast.



2 Transversal DWI using b800 (2A), calculated b-value 1400 (2B), and ADC map (2C) showing restricted diffusion in a tumor in the upper medial quadrant of the right breast.



3 Transversal T1W TWIST-VIBE Dixon pre-contrast (3A) and first contrast phase (52 sec) (3B) of the breasts. Our radiologists also use the subtraction images (3C) routinely.

Diffusion-weighted images (DWI)

What kind of EPI?

MAGNETOM Sola offers three kinds of diffusion-weighted imaging: standard, segmented (RESOLVE), and zoomed 2D RF excitation (ZOOMit^{PRO}). We have found the ZOOMit^{PRO} sequence to be superior. This technique includes both breasts in one FOV with good fat saturation. Given equal resolution, ZOOMit^{PRO} also appears sharper. The fat saturation is not better with any of the other DWI techniques, except STIR-EPI. However, STIR is too time- and SNR-consuming for regular use. The fat suppression sometimes fails at the transition between the breast and the thoracic wall, but this area rarely contains glandular tissue. We have found that scanning each breast individually with a reduced FOV only result in an increase of scan time with no added benefit of artifact reduction. If necessary, changing to sagittal image plane and careful placing of the B₀ shim box may improve the fat saturation in a particular area.

According to a new consensus on DWI of the breasts from EUSOBI we acquire the DWI with a resolution $\leq 2 \times 2 \text{ mm}^2$ in-plane and a slice thickness of 4 mm [3]. In addition, we interpolate the in-plane resolution to $0.92 \times 0.92 \text{ mm}^2$. The recommended b-values are b0 and b800, and in addition we calculate a heavily DW image set of b1400. ZOOMit^{PRO} provides a nice contrast between tumor, glandular tissue, and fatty background. There is usually some remaining signal from glandular tissue at b800, but the calculated b1400 images produce a homogeneous low signal background, increasing the conspicuity of tumor.

The ZOOMit^{PRO} also manages 3 mm slice thickness, but then the SNR is starting to be critical. In our experience, the quality of the ADC map is heavily dependent on the SNR. Thus, we prefer 4 mm slice thickness. We also equal the signal averaging at b0 and b800 to further improve the SNR of the ADC-map (Fig. 2).

Dynamic Contrast Enhanced (DCE) imaging

State-of-the-art DCE imaging in the breast emphasizes morphology over kinetics and typically uses a temporal resolution of 60–90 seconds in order to provide very high spatial resolution [2]. We have chosen the time resolved TWIST-VIBE Dixon sequence that enables very high spatial resolution producing detailed morphology even on MPR, reasonable time resolution, and high contrast to background. The use of the Dixon technique offers superior fat removal. Subtraction images are calculated in-line. In this way the radiologists have the advantage of both interpreting the contrast enhancing abnormalities surrounded by the non-enhancing tissue (native water-only Dixon images) and differentiate enhancing structures from proteinous liquid and blood (subtraction images). Our images are done with a temporal resolution of just over 52 seconds, and the voxel size acquired is $0.78 \times 0.78 \times 2.00 \text{ mm}^3$ (Fig. 3).

Ultrafast breast imaging is arising. Malign lesions enhance earlier and faster than benign lesions [2]. MAGNETOM Sola offers another acceleration technique, GRASP-VIBE, which enables ultrafast time resolution of ≤ 10 seconds and good spatial resolution. GRASP-VIBE utilizes motion insensitive radial k-space sampling and compressed sensing. However, even at comparable spatial resolution, the GRASP-VIBE is more blurred than the TWIST VIBE-Dixon and the image contrast is lower, possibly do to inferior fat suppression. Our breast imaging specialized radiologists prefer to use the TWIST-VIBE Dixon in clinical routine.

Acknowledgments

Thanks to radiographers Evy Storengen Nøstvold and Edmund Reitan and radiologist Knut Håkon Hole for invaluable help with developing the protocol and preparing the manuscript. Thanks to the breast imaging specialized radiologists Marit Muri Holmen and Siri Helene Bertelsen Brandal for clinical on-site considerations through the process of developing and testing of our breast imaging protocol.

Contact

Sindre Øverstad, BSc, RT(R) (MR) (CT)
Radiographer
Oslo universitetssykehus HF
Radiumhospitalet
Ullernchausseen 70
0379 Oslo
Norway
Tel. +47 93659267
sindre.overstad@gmail.com



References

- 1 Mann, R. M. et al. Breast MRI: EUSOBI recommendations for woman's information. *European Radiology* 25, 3669-3678 (2015).
- 2 Mann, R. M., Cho, N. & May, L. Breast MRI: State of the Art. *Radiology* 2019, 292;520-536 (2019).
- 3 Baltzer, P. et al. Diffusion-weighted imaging of the breast – a consensus and mission statement from EUSOBI International Breast Diffusion-Weighted Imaging working group. *European Radiology* 30, 1436-1450 (2019).

Personalized Treatment for Patients with Prostate Cancer Using MRI-guided Transurethral Ultrasound Ablation (TULSA)

Joyce Bomers, Ph.D.¹; Cameron Wright, M.Sc.²; Jurgen Fütterer, M.D., Ph.D.¹

¹Department of Imaging, Radboud University Nijmegen Medical Centre, Nijmegen, The Netherlands

²Profound Medical Inc., Mississauga, Canada

Background

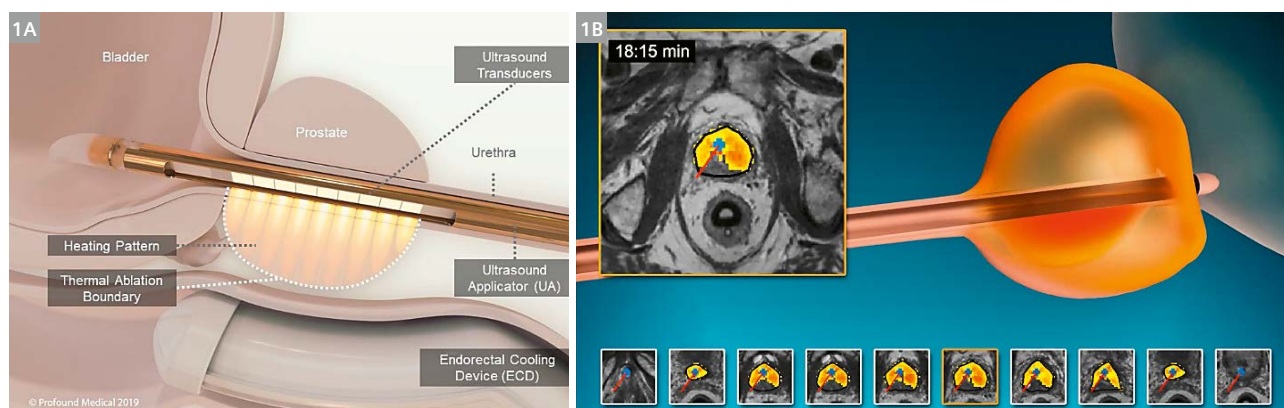
The lifetime risk of being diagnosed with prostate cancer (PCa) is one in six [1]. Although PCa can be lethal, most men who are diagnosed with PCa will not suffer clinically significant consequences from the disease during their lifetime. According to (inter)national guidelines, when a patient has localized PCa treatment the conventional treatment options include radical prostatectomy (RP) and radiation therapy (RT), which treat the whole prostate regardless where the underlying pathology is located. The comorbidity associated with this type of treatment in combination with a relatively high cancer specific survival (92%) has a tremendous impact on quality of life and cost. Approximately 15–20% of the patients who undergo prostatectomy will suffer from treatment-induced urinary dysfunction and 8–36% will have to live with erectile dysfunction [2, 3].

Several new interventions have been developed hoping to offer non-inferior oncological control with an improved safety profile, including minimally invasive

modalities such as high-intensity focused ultrasound, cryoablation, and laser ablation [4]. At their inception these technologies performed whole-gland ablation, but as PCa screening and disease localization have improved primarily due to the advent of mpMRI [5], there has been a shift to targeted treatment. Targeted therapy treats the dominant lesion plus an additional thermal safety margin, with the rationale this should offer the best compromise between oncological control and morbidity.

The concept of targeted therapy is still relatively new and therefore controversial, and has stricter inclusion requirements, meaning patients with multi-focal and/or diffuse disease are likely not ideal candidates. This underscores the need for a modality that can deliver safely and effectively both whole-gland and targeted treatment.

MRI-guided transurethral ultrasound ablation (TULSA) has been used as a primary treatment for whole-gland treatment [6, 7] as well as targeted treatment [8, 9] and will be explored in more detail.



1 MRI-guided transurethral ultrasound (TULSA) procedure. **(1A)** Rendering of ultrasound applicator and endorectal cooling device. **(1B)** Ablation zone is prescribed on intraoperative transverse T2-weighted images from prostate apex to base, and the ablation is observed in real-time with thermometry.

TULSA overview

TULSA is a newer technology which uses high-intensity thermal ultrasound to destroy prostate tissue by treating the prescribed boundary to an ablative temperature of 55 °C. The procedure takes place entirely in the MRI suite with the patient under general anesthesia or regional block. A rigid transurethral ultrasound catheter is guided into the prostate and then secured with an MRI-compatible robot that provides linear and rotational motion of the device within the prostatic urethra during treatment planning and the ablation. The ultrasound catheter has ten separate elements, each which are independently controlled for acoustic power and frequency. A rectal device is inserted which cools the rectum with cold water (Fig. 1A).

Device localization is performed with a high-resolution sagittal 3D T2-weighted SPACE sequence (TR 1700 ms; TE 97 ms; Slice thickness 1 mm; FOV 256 mm; Resolution 1 x 1 x 1 mm). Treatment planning is performed with transverse T2-weighted images (qtse: TR 7500 ms; TE 101 ms; Slice thickness 3 mm; FOV 260 mm; Resolution 1 x 1 x 3 mm) and monitored in real-time with a segmented EPI MRI thermometry sequence (TR 45 ms; TE 8 ms; Slice thickness 4 mm; FOV 256 mm; Resolution 2 x 2 x 4 mm) (Fig. 1B).

One of TULSA's distinguishing features that allows it to ablate large volumes of tissue yet still offer conformal ablation is the automated controller. During the ablation real-time thermometry images acquired by the MRI are sent to the TULSA software every ~6 s. These images are processed immediately upon arrival, and the controller in turn calculates the optimal device rotation rate, acoustic power and acoustic frequency for all active ultrasound elements. This process repeats itself indefinitely until the ablation is completed. The control parameters are adjusted to achieve the fine balance of reaching the 55 °C temperature at the prescribed boundary in the shortest possible treatment time, but not overshooting into surrounding structures. Over time (~50 minutes for a whole-gland ablation) the ultrasound catheter is rotated through the prostate via the robotic arm, delivering a consistent thermal dose to the targeted volume.

Whole-gland TACT trial

The most extensive and up-to-date clinical data regarding TULSA comes from the TACT trial (NCT02766543). This was a multi-center, prospective, single-arm clinical trial where patients with low- to intermediate-risk, biopsy-proven, localized PCa (Table 1) were treated with TULSA as a first-line therapy. From September 2016 until February 2018 115 men were enrolled across 13 different institutions in 5 different countries. The main objectives of the study were safety and early oncological control at one year

as determined by PSA, biopsy, and mpMRI. Every patient regardless of their specific disease characteristic received whole-gland ablation but with sparing to the urethra and apical sphincter. Repeat TULSA was not allowed. At the time of writing 2-year follow-up is available for 48/115 patients (42%).

Procedural outcomes

The median (IQR) ablation time was 51 minutes (39–66), achieving 98% thermal coverage. The spatial precision of the TULSA ablation was 1.4 mm. Patients were discharged the same day (55%) or admitted overnight (45%), mostly depending on the local hospital protocol.

Safety outcomes

No ≥ Grade 4 adverse events, no intraoperative complications, no rectal injury, and no rectal fistula were observed. A total of 12 Grade 3 (severe) adverse events occurred in 9 (8%) men, including genitourinary infection (4%), urethral stricture (2%), urinary retention (2%), urethral calculus and pain (1%), and urinoma (1%), all resolved by the 12-month visit.

No patient had severe erectile dysfunction. Of the 92 patients at baseline who had erections sufficient for penetration, 75% maintained this at one year, and this increased to 83% in those patients with two-year follow-up, indicating a continued recovery. Moderate urinary incontinence (Grade 2, pads) was reported by 3 patients (2.6%), with no new incontinence at 2 years. The patient-reported IPSS (International Prostate Symptom Score) questionnaire was used to quantify urinary symptoms after the intervention, where a score 1–7 represents mild, 8–19 moderate and 20–35 severe symptoms. The median IPSS was unchanged from 7 at baseline to 6 at one year and 5 at two years after TULSA.

Oncological outcomes

Median (IQR) PSA reduction at one year was 95% (91–98%) with a median nadir of 0.3 ng/ml and was stable at two years. Median decrease in perfused prostate volume changed by 91% at 12 months, decreasing from a median of 37 cc at baseline to 3 cc.

Median age, age	65 (59–69)
PSA, ng/ml	6.3 (4.6–7.9)
Grade Group Distribution, n (%)	72 with GG2 (63%) 43 with GG1 (37%)
Targeted prostate volume, cc	40 (32–50)

Table 1: Patient characteristics at baseline for whole-gland TACT trial.

From biopsy results there was no evidence of cancer in 72 (65%) men and 16 (14%) had low-volume GG1. Among the 68 men with GG ≥ 2 at baseline, 54 (79%) were free of GG ≥ 2 at 12 months. Similarly, 20 of 26 (77%) men with high-volume GG1 at baseline had either no cancer or low-volume GG1 (< 3 cores and < 50% per core) at 12 months. Overall, histological improvement (eradication of GG2, shift from high to low-volume GG1, or eradication of GG1 disease) occurred in 75–80% of men across all risk subgroups.

12-month MRI showed a 96% negative predictive value for absence of GG2 disease on 1-year biopsy.

TULSA case example: whole-gland ablation

A 68-year-old male arrived in our clinic in 2017 with suspicion of localized PCa in the left midgland peripheral zone based on elevated PSA and mpMRI findings (PSA 6.9 ng/ml, PI-RADS 5, prostate volume 52 cc). Baseline mpMRI findings were concordant with the MRI-targeted biopsy, revealing 2 positive cores with a total cancer core length of 12 mm (Grade Group 2).

The patient underwent whole-gland TULSA with urethra and apical sphincter sparing, with the treatment plan shown in Figure 2A. The total ablation time lasted 42 minutes, with the patient discharged the following day. The maximum heat deposition at the end of treatment (Fig. 2B) and the corresponding immediate post-ablation

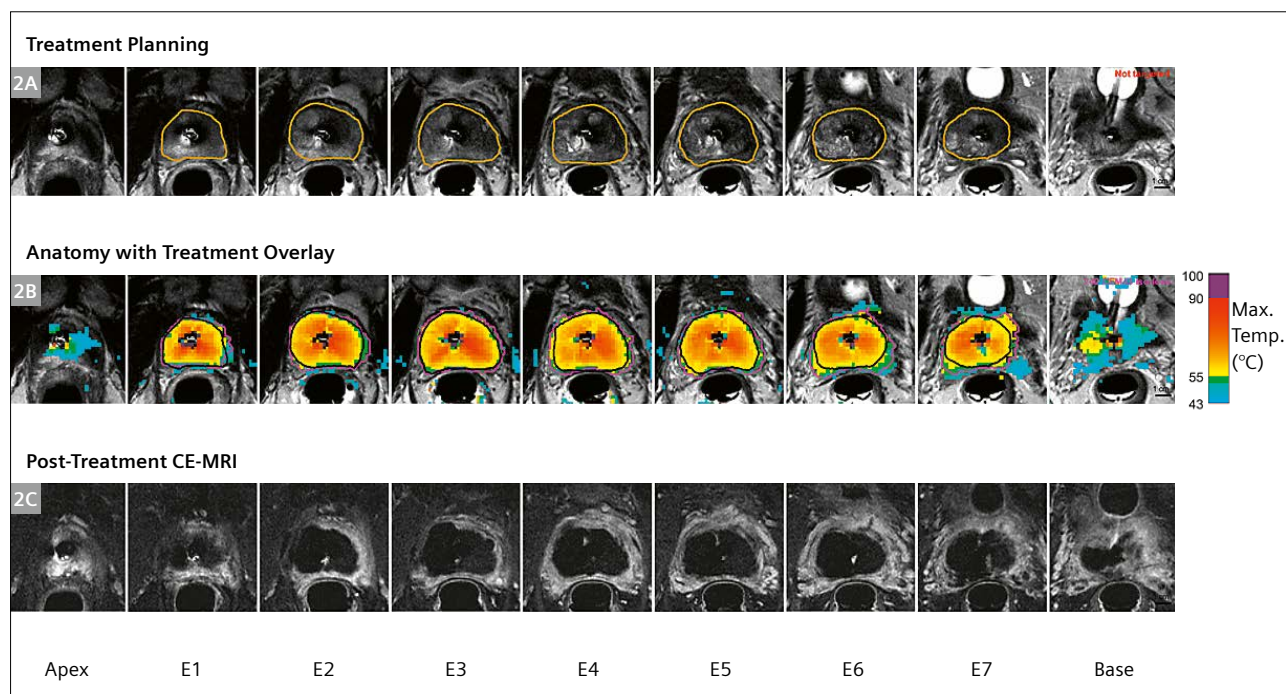
contrast scan revealing immediate cell kill can be seen in Figure 2C.

One-year follow-up visit was promising, with the patient experiencing no urinary incontinence, no rectal injuries, and an IPSS improvement from 14 to 8. Oncological control at 12 months was demonstrated by a low and stable PSA of 0.41 ng/ml, negative mpMRI and a negative 12-core biopsy.

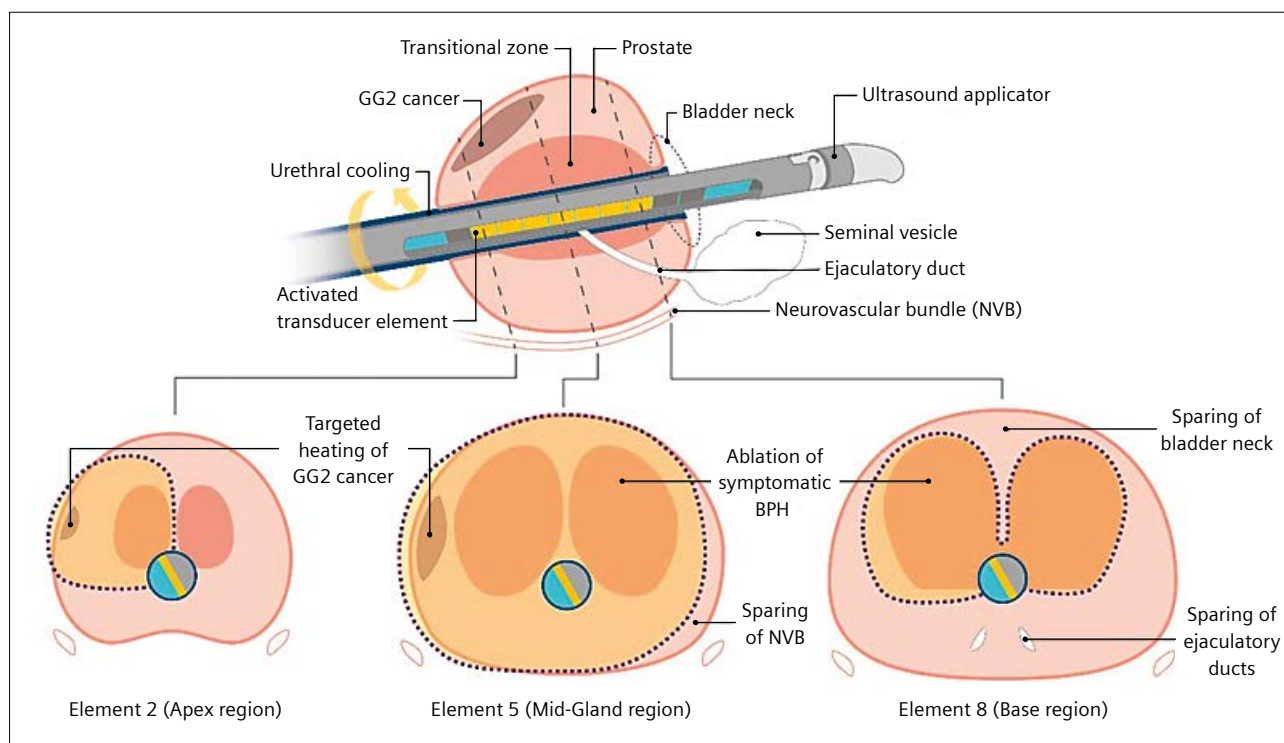
TULSA personalized care

As discussed earlier, in the last decade PCa disease localization has greatly improved. This has given treating physicians the option to spare viable prostate tissue and treat only the source of tumor. Opting for targeted therapy is not solely a clinical decision however, as the patient's wishes and underlying health conditions must also be considered, providing a better platform for the patient to control their own care. Possible treatment options with TULSA include whole-gland, whole-gland with nerve sparing, hemi-ablation, or quadrant ablation. Figure 3 illustrates a hypothetical custom treatment plan with TULSA.

If one considers the TACT trial as 'worst-case' for safety and morbidity as the ablation was performed on the whole gland without nerve sparing, it is reasonable to expect a safety improvement moving to partial ablation, although this must still be confirmed through more extensive clinical trials.



2 (2A) Treatment plan outlined on transverse T2w planning sequence. (2B) Maximum heat deposition in temperature at the end of treatment. (2C) Post-ablation contrast scan showing immediate cell kill based on non-perfused volume.



- 3** Personalized TULSA treatment. A patient presents with both localized intermediate-risk prostate cancer and urinary symptoms prior to treatment. A treatment plan is devised to target only the dominant lesion with a thermal safety margin, as well as the source of adenoma causing urinary obstruction. The apical sphincter, the left side of the neurovascular bundle, the ejaculatory ducts, and the bladder neck are spared from the ablation volume, in order to offer the best compromise between oncological control and function.

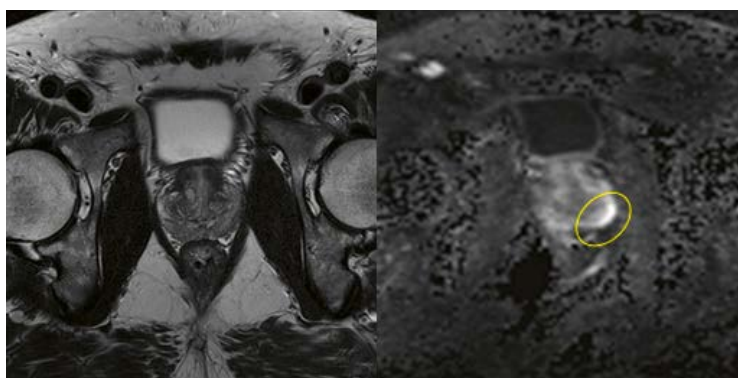
TULSA case example: hemi-ablation

A 60-year-old male with intermediate-risk, unilateral, localized PCa (PSA 15 ng/ml, Grade Group 2, PI-RADS 4) arrived at our clinic in 2018. mpMRI findings were concordant with positive biopsy location with the lesion apparent on DWI, outlined in yellow (Fig. 4).

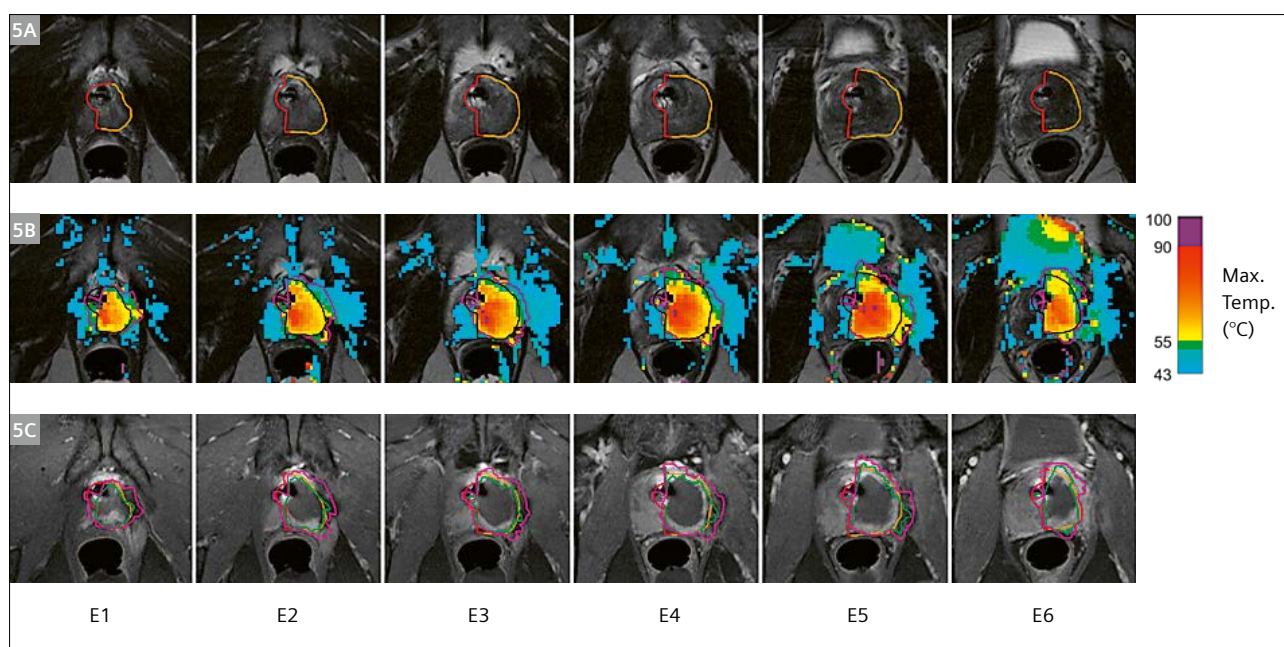
The individualized treatment plan was developed by a multi-disciplinary team including urologists and radiologists, and presented to the patient before the treatment. It was determined the patient would undergo hemi-gland

ablation, which would spare one side of the neurovascular bundle, while still targeting the dominant lesion (Fig. 5). The ablation time lasted 35 minutes, with the patient discharged the following day.

At 2 years post-TULSA the patient underwent mpMRI which revealed no suspicions and the PSA was stable at 3.9 ng/ml, a decrease of 74% from baseline which is expected for a focal treatment. No changes to urinary, bowel, or sexual function were noted.



- 4** Screening image for patient who underwent targeted TULSA treatment. Biopsy showed single lesion Grade Group 2 which was concordant on mpMRI (PI-RADS 4). The lesion is outlined in yellow. Based on the tumor characteristics it was decided the patient would undergo a hemi-ablation on the left side.



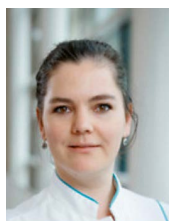
5 Hemi-ablation treatment with TULSA. Elements E1–E6 were enabled on the left lobe to deliver spatially precise ablation in order to reduce toxicity. The treatment plan (**5A**) was determined in advance of the therapy. The ablation lasted only 35 minutes (**5B**) and the immediate treatment effects can be visualized on contrast MRI with the non-perfused volume.

Conclusion

TULSA is a new technology which has demonstrated promising early oncological results with a well-tolerated safety profile. As PCa disease localization continues to improve, it is expected that targeted treatment will become increasingly part of localized PCa management. As MRI is already embedded within TULSA, used both to guide, plan, and monitor treatment, TULSA is well-positioned to address the changing landscape of PCa disease management.

References

- 1 Siegel RL, et al. Cancer statistics, 2020. *A Cancer Journal for Clinicians*. 2020;70(1):7-30.
- 2 Sanda MG, et al. Quality of life and satisfaction with outcome among prostate-cancer survivors. *The New England journal of medicine*. 2008;358(12):1250-1261.
- 3 Resnick MJ, et al. Long-term functional outcomes after treatment for localized prostate cancer. *The New England journal of medicine*. 2013;368(5):436-445.
- 4 McClure TD, et al. Partial gland ablation in the management of prostate cancer: a review. *Current Opinion Urology*. 2017;27(2):156-160.
- 5 Padhani AR, et al. Prostate imaging-reporting and data system steering committee: PI-RADS v2 status update and future directions. *European Urology*. 2019;75(3):385-396.
- 6 Chin JL, et al. Magnetic resonance imaging-guided transurethral ultrasound ablation of prostate tissue in patients with localized prostate cancer: a prospective phase 1 clinical trial. *European Urology*. 2016;70(3):477-455.
- 7 Eggener S, et al. Pivotal trial of MRI-guided transurethral ultrasound ablation in men with localized prostate cancer: two-year follow-up. *The Journal of Urology*. 2020;203(4):e369-e369.
- 8 Ramsay E, et al. Evaluation of focal ablation of magnetic resonance imaging defined prostate cancer using magnetic resonance imaging controlled transurethral ultrasound therapy with prostatectomy as the reference standard. *Journal of Urology*. 2013;197(1):255-261.
- 9 Anttinen J, et al. Feasibility of MRI-guided transurethral ultrasound for lesion-targeted ablation of prostate cancer. *Scandinavian Journal of Urology*. 2019;53(5):295-302.



Joyce Bomers



Jurgen Fütterer

Contact

Professor Jurgen Fütterer, M.D., Ph.D.
Department of Imaging
Radboud University Nijmegen Medical Centre
Geert Grooteplein Zuid 10
6525 GA Nijmegen
The Netherlands
Tel. +31 (0)24 361 40 11
jurgen.futterer@radboudumc.nl

New Advances in Radiomics of Liver Imaging

Roberto Cannella¹, Tommaso Vincenzo Bartolotta^{1,2}

¹Section of Radiology – BiND, University Hospital “Paolo Giaccone”, Palermo, Italy

²Department of Radiology, Fondazione Istituto Giuseppe Giglio, Ct.da Pietrapollastra, Cefalù (Palermo), Italy

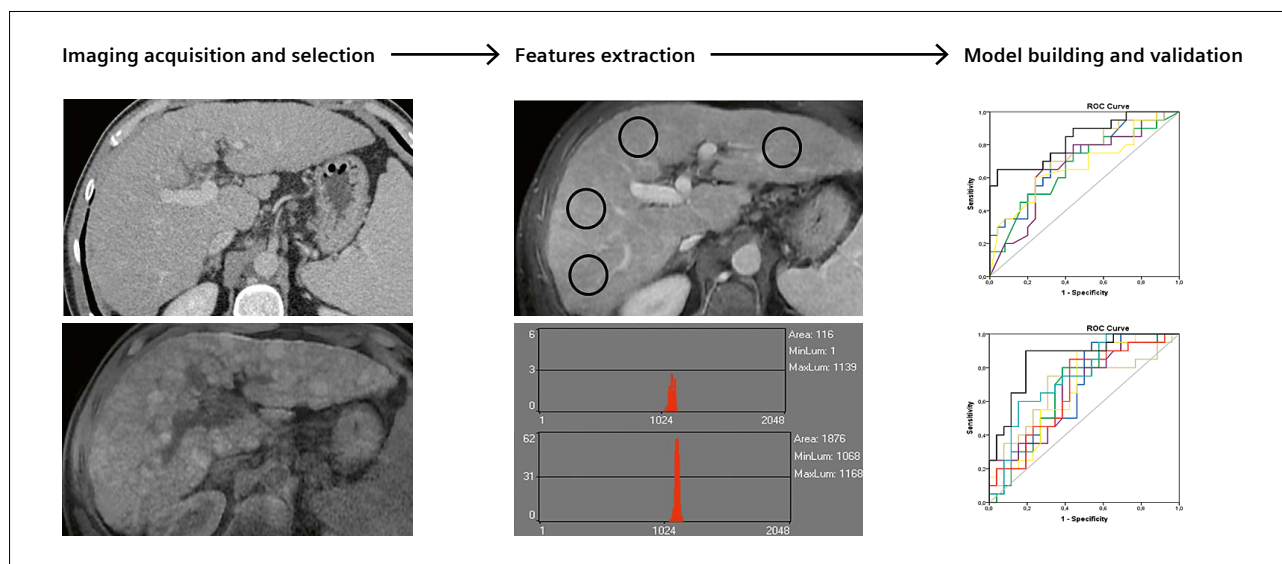
Introduction

Interpretation of liver imaging studies remains challenging in clinical practice due to the complex presentation of chronic liver disease and the presence of multiple focal liver lesions arising in normal and cirrhotic liver with overlap in imaging appearance. Radiomics is currently emerging as a new promising tool for quantitative analysis of liver imaging studies that could potentially increase diagnostic accuracy in the assessment of focal liver lesions, predict treatment response and prognosis after loco-regional or systemic therapies, and stratify the risk of advanced fibrosis and cirrhosis in patients with chronic liver disease [1].

Radiomics allows to extract a large amount of mathematical data through the analysis of the distribution and relationships of pixel densities/intensities within a defined region of interest, providing additional quantitative information from medical images that cannot be evaluated by human eyes [2]. These large amounts of quantitative data can be combined with patients' clinical characteristics, laboratory markers, histopathological parameters, or

genetic data in order to provide predictive models that will help guide physicians to the most appropriate form of management [3]. Radiomics can be applied to any type of imaging study, including ultrasound, CT, MRI, and PET/CT, but most liver studies are currently based on CT or MRI examinations [4]. Although multiple experimental studies have shown promising results from radiomics, with excellent performance for diagnostic, prognostic, and predictive applications in liver imaging, there are several challenges for the adoption of radiomics in clinical practice. Differences in image acquisition, features extraction, and radiomics software pose challenges for the repeatability or application of radiomics models in large populations [3].

In this paper, we aim to discuss the basis of the radiomics workflow and review the new advances and current applications of radiomics in liver imaging, with an emphasis on the current knowledge about radiomics applications in the field of chronic liver disease and focal liver lesions.



1 Schematic of radiomics workflow.

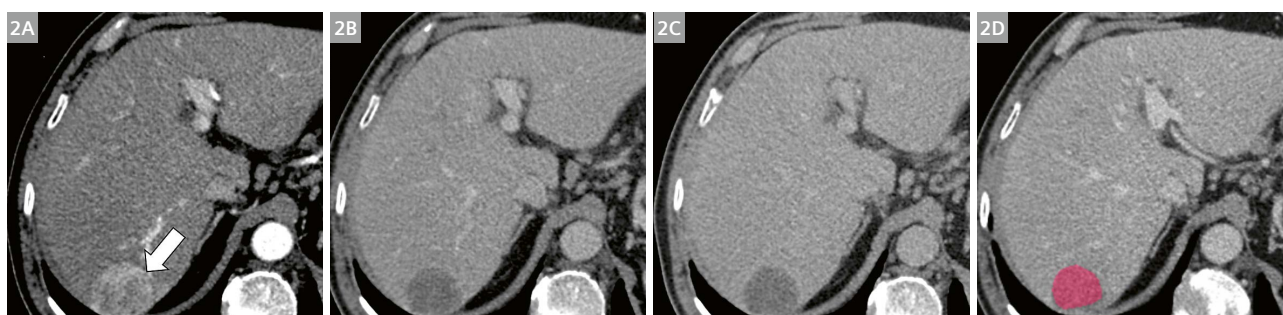
The radiomics workflow

Radiomics analysis is based on a multistep process that includes image acquisition, lesion segmentation, features extraction, features selection and reduction, predictive model building, final validation, and clinical interpretation of the results (Fig. 1) [4–7]. Acquisition of radiological imaging studies is one of the most important steps for radiomics, since scanning and technical parameters are known to influence the reproducibility of radiomics features. In particular, the reconstruction algorithm and slice thickness have an impact on the reproducibility of radiomics features on contrast-enhanced CT images [8–10]. Differences in acquisition protocols complicate the retrospective evaluation of CT or MRI studies acquired with different scanners [11]. It is also important to select the optimal phase/sequence for image analysis. Pre-contrast images are not affected by the contrast administration, but the segmentation may be not feasible if the lesion cannot be distinguished from the background hepatic parenchyma. However, pre-contrast images may provide more reliable assessment of the liver parenchyma in patients with chronic liver disease. Contrast-enhanced images may provide better lesion visualization, but the type, timing, and amount of contrast agent can be additional confounding factors, especially for images acquired in the arterial phase.

Segmentation can be performed manually by experienced radiologists using semi-automatic, or automatic software [11]. Manual segmentation is currently the gold standard in most radiomics studies, but it is often time consuming and is prone to intra- and inter-reader variability [4, 6, 12]. Semi-automatic or automatic software can provide more rapid and reproducible results, but they are prone to errors in cases of imaging artifacts, or unexpected liver anatomy or lesions. When analyzing focal liver lesions, the segmentation is usually performed by drawing an ROI within the tumor margins (Fig. 2). The ROI can be positioned on a single slice (2D ROI) on the largest tumor cross section, or it can include the whole lesion (3D ROI) [7]. When assessing diffuse liver disease, the

segmentation can be performed using a single ROI with fixed diameters positioned on a specific hepatic segment (usually in the right lobe) in a single slice and not including large hepatic vessels or focal live lesions; using multiple ROIs with fixed diameters on different hepatic segments or different levels; or using ROIs that include the whole liver parenchyma or specific segments, usually at the level of the porta hepatis. Although 3D and whole-liver segmentations can capture more tissue heterogeneity, the clinical advantage remains debatable, since studies have demonstrated that single-slice analysis is often sufficient for the evaluation of chronic liver disease and focal lesions, and more practical for the radiological workflow.

Several in-house or commercially available radiomics research software programs allow users to extract a large number of radiomics features. Radiomics features are usually classified as first-, second-, or third-order features [4]. First-order features are obtained from the analysis of the gray-level histogram within a defined ROI, without considering spatial relationships between pixels. The most common histogram-based features include mean (average of the pixels within the ROI), standard deviation (dispersion from the mean), skewness (asymmetry of the histogram), kurtosis (peakedness/flatness of the histogram), and entropy (image irregularity or complexity) [5]. Second-order texture features consider the spatial relationship between pixels and most commonly include the gray-level co-occurrence matrix (GLCM), which quantifies the arrangements of pairs of pixels with the same values in a specific direction, and the gray-level run length matrix (GLRLM), which quantifies consecutive pixels with the same intensity in a specific direction. Third-order or higher order features evaluate spatial relationships between three or more pixels using statistical methods after applying filters or mathematical transforms. These features include fractal analysis, wavelet transforms, and Laplacian transforms of Gaussian-filtered images. Due to the large number of extracted parameters, a features reduction should be performed in order to exclude features that are not reproducible or redundant, and to avoid overfitting problems [8].



2 A 76-year-old man with hepatitis C-related cirrhosis and hepatocellular carcinoma: Contrast-enhanced CT imaging shows a 4 cm liver lesion with arterial phase hyperenhancement (2A, arrow), and washout in portal venous (2B) and delayed (2C) phases. Example of lesion segmentation was performed on portal venous phase (2D).

Final radiomics models should be tailored to validate the accuracy of uncorrelated features according to the specific outcome. The choice of statistical methods depends on multiple factors, such as evaluation of primary outcome, number of features, and number of analyzed lesions. Validation in an independent or external patient cohort is necessary in order to test the real performance of radiomics [12].

Radiomics in chronic liver disease

Chronic liver disease covers a wide spectrum of liver pathologies, the incidence of which has been increasing in recent years. The most common etiologies of chronic liver disease include chronic viral hepatitis (primarily hepatitis B and C), alcoholic hepatitis, and nonalcoholic fatty liver disease (NAFLD). These may evolve into advanced fibrosis and cirrhosis, with possible complications such as portal hypertension, decompensated hepatic failure, and development of hepatocellular carcinoma. In particular, the presence of significant and advanced fibrosis has been reported as an independent predictor of mortality caused by chronic liver disease [13].

Although liver biopsy is considered the reference standard for the diagnosis and staging of fibrosis in patients with chronic liver disease, it has known complications such as pain, hemorrhage, and infections. It is also prone to sampling errors due to the heterogeneous distribution of fibrosis in the hepatic parenchyma, and to inter- and intra-reader variability. Several imaging-based noninvasive methods have been developed for assessing hepatic fibrosis in patients with chronic liver disease. They include shear wave elastography, MR elastography, diffusion-weighted imaging, and liver surface nodularity [14]. Recently, radiomics has been applied to liver imaging for the noninvasive assessment of hepatic fibrosis, with several studies reporting a fair-to-good diagnostic performance for the detection of advanced fibrosis or cirrhosis [15–23]. Most of these studies applied radiomics on CT or MR imaging, using pre-contrast or portal venous phase images. Overall, similar diagnostic performance was observed regardless of the etiology of the chronic liver disease. However, it should be noted that most current radiomics studies have evaluated patients with chronic viral hepatitis B or C. Nonalcoholic fatty liver disease, which is becoming the major cause of chronic liver disease and cirrhosis in Western countries, was investigated by only a minority of studies [15, 16, 18].

In the initial experience of Lubner et al. [18] quantitative texture analysis was performed on contrast-enhanced CT images from 289 patients with different etiologies of chronic liver disease, with a fair-to-good performance in discriminating between different stages of fibrosis. In a subsequent study, Lubner et al. [19] enrolled a cohort of

556 patients that included both healthy subjects and patients with hepatitis C and various degrees of hepatic fibrosis. Texture features were extracted by drawing an ROI that covered the entire liver. A good diagnostic performance was achieved for detecting significant and advanced fibrosis of models incorporating multiple features. A multiparametric approach that combines radiomics features and other CT-based methods for staging hepatic fibrosis has demonstrated excellent results in the stratification of fibrosis degree, improving the performance of individual parameters [21]. A recent study of MRI [15] investigated the performance of texture analysis in NAFLD patients, reporting a fair accuracy of entropy and standard deviation for the diagnosis of significant and advanced fibrosis, based on pre-contrast sequences.

Compared to other noninvasive imaging-based methods for assessment of hepatic fibrosis, the major advantage of radiomics and texture analysis is that they can also be applied retrospectively to extract additional data from images that have already been acquired, and can potentially be performed with any type of imaging study. However, a lack of standardization, variability in radiomics features and available software, and vulnerability to image acquisition parameters still pose significant challenges for applying radiomics in routine clinical practice. Further studies should focus on validation in multicenter cohorts, and on comparison with other non-invasive techniques for fibrosis evaluation.

Radiomics in focal liver lesions

Focal liver lesions include a wide spectrum of benign and malignant lesions that can occur in both normal liver and in cirrhosis. The differential diagnosis of focal liver lesions should consider the background liver parenchyma, presence of risk factors, clinical parameters, and imaging appearance on multiphasic contrast-enhanced studies. Although some lesions may demonstrate typical enhancement patterns on CT or MR images, the differential diagnosis in clinical practice remains challenging, and a histopathological confirmation is often required to reach the final diagnosis.

In patients without history of chronic liver disease or extrahepatic malignancies, focal liver lesions are most commonly benign, and the differential diagnosis includes hemangioma, focal nodular hyperplasia (FNH), and hepatocellular adenoma (HCA). Differentiating between FNH and HCA is challenging due to the overlap in the imaging appearance and the presence of multiple subtypes of HCA [24]. While FNHs are indolent lesions, HCAs carry a risk of complications such as hemorrhage and malignant transformation. Lesion biopsy is therefore often required to reach the definitive diagnosis [24]. Recent studies have demonstrated that the application of radiomics could help

increase the diagnostic performance for the differential diagnosis between FNH and HCA, with significant improvements compared to conventional qualitative evaluations [25, 26]. In particular, a retrospective study [26] reported that texture-based parameters obtained from gadoxetate disodium-enhanced MRI on T2-weighted and hepatobiliary phase imaging can distinguish FNH from HCA in up to 96% of cases.

In patients with underlying cirrhosis or chronic liver disease, hepatocellular carcinoma (HCC) represents the most common primary malignancy, accounting for up to 90% of all liver cancers [27, 28]. Several studies have adopted a radiomics approach to quantify lesion heterogeneity in HCC. In particular, recent studies have explored the potential of radiomics for preoperative assessments of HCC with prediction of recurrence-free survival and overall survival after curative resection, recurrence following liver transplantation, correlation with histopathological markers of HCC aggressiveness (i.e., microvascular invasion), and evaluation of treatment response in patients undergoing locoregional therapies or systemic therapies in cases with advanced tumors [29–40]. Anh et al. [31] found that imaging findings and texture-based features on preoperative gadoxetate disodium-enhanced MRI were helpful for predicting early recurrence after curative resections in patients with single HCC. Feng et al. [35] developed a preoperative radiomics model for prediction of microvascular invasion based on gadoxetate disodium-enhanced MRI. Park et al. [38] investigated the role of CT-based texture analysis in the prediction of therapeutic response in HCC after transcatheter arterial chemoembolization.

Conclusions

Radiomics is emerging as a promising tool with large potential for the assessment of chronic liver disease and focal liver lesions, providing excellent diagnostic performance for multiple applications in research studies. Future implementation of radiomics models should focus on addressing current limitations that pose challenges for its application in everyday clinical practice.

References

- Lubner MG, Smith AD, Sandrasegaran K, Sahani DV, Pickhardt PJ. CT Texture Analysis: Definitions, Applications, Biologic Correlates, and Challenges. *Radiographics*. 2017;37(5):1483-1503.
- Vernuccio F, Cannella R, Comelli A, Salvaggio G, Lagalla R, Midiri M. [Radiomics and artificial intelligence: new frontiers in medicine.]. *Recenti Prog Med*. 2020;111(3):130-135.
- Gillies RJ, Kinahan PE, Hricak H. Radiomics: Images Are More than Pictures, They Are Data. *Radiology*. 2016;278(2):563-577.
- Lewis S, Hectors S, Taouli B. Radiomics of hepatocellular carcinoma. *Abdom Radiol (NY)*. 2020;doi:10.1007/s00261-019-02378-5.
- Miranda Magalhaes Santos JM, Clemente Oliveira B, Araujo-Filho JAB, Assuncao-Jr AN, de M Machado FA, Carlos Tavares Rocha C, et al. State-of-the-art in radiomics of hepatocellular carcinoma: a review of basic principles, applications, and limitations. *Abdom Radiol (NY)*. 2020;45(2):342-353.
- Varghese BA, Cen SY, Hwang DH, Duddalwar VA. Texture Analysis of Imaging: What Radiologists Need to Know. *AJR Am J Roentgenol*. 2019;212(3):520-528.
- Cannella R, La Grutta L, Midiri M, Bartolotta TV. New advances in radiomics of gastrointestinal stromal tumors. *World J Gastroenterol* 2020;26(32):4729-4738
- Berenguer R, Pastor-Juan MDR, Canales-Vázquez J, Castro-García M, Villas MV, Mansilla Legorburo F, et al. Radiomics of CT Features May Be Nonreproducible and Redundant: Influence of CT Acquisition Parameters. *Radiology*. 2018;288(2):407-415.
- Ahn SJ, Kim JH, Lee SM, Park SJ, Han JK. CT reconstruction algorithms affect histogram and texture analysis: evidence for liver parenchyma, focal solid liver lesions, and renal cysts. *Eur Radiol*. 2019;29(8):4008-4015.
- Meyer M, Ronald J, Vernuccio F, Nelson RC, Ramirez-Giraldo JC, Solomon J, et al. Reproducibility of CT Radiomic Features within the Same Patient: Influence of Radiation Dose and CT Reconstruction Settings. *Radiology*. 2019;293(3):583-591.
- Koçak B, Durmaz EŞ, Ateş E, Kılıçkesmez Ö. Radiomics with artificial intelligence: a practical guide for beginners. *Diagn Interv Radiol*. 2019;25(6):485-495.
- Wakabayashi T, Ouhmich F, Gonzalez-Cabrera C, Felli E, Saviano A, Agnus V, et al. Radiomics in hepatocellular carcinoma: a quantitative review. *Hepatol Int*. 2019;13(5):546-559.
- Chalasani N, Younossi Z, Lavine JE, Charlton M, Cusi K, Rinella M, et al. The diagnosis and management of nonalcoholic fatty liver disease: Practice guidance from the American Association for the Study of Liver Diseases. *Hepatology*. 2018;67(1):328-357.
- Petitclerc L, Gilbert G, Nguyen BN, Tang A. Liver Fibrosis Quantification by Magnetic Resonance Imaging. *Top Magn Reson Imaging*. 2017;26(6):229-241.
- Cannella R, Borhani AA, Tublin M, Behari J, Furlan A. Diagnostic value of MR-based texture analysis for the assessment of hepatic fibrosis in patients with nonalcoholic fatty liver disease (NAFLD). *Abdom Radiol (NY)*. 2019;44(5):1816-1824.
- Daginawala N, Li B, Buch K, Yu H, Tischler B, Qureshi MM, et al. Using texture analyses of contrast enhanced CT to assess hepatic fibrosis. *Eur J Radiol*. 2016;85(3):511-517.
- House MJ, Bangma SJ, Thomas M, Gan EK, Ayonrinde OT, Adams LA, et al. Texture-based classification of liver fibrosis using MRI. *J Magn Reson Imaging*. 2015;41(2):322-328.
- Lubner MG, Malecki K, Kloke J, Ganeshan B, Pickhardt PJ. Texture analysis of the liver at MDCT for assessing hepatic fibrosis. *Abdom Radiol (NY)*. 2017;42(8):2069-2078.
- Lubner MG, Jones D, Kloke J, Said A, Pickhardt PJ. CT texture analysis of the liver for assessing hepatic fibrosis in patients with hepatitis C virus. *Br J Radiol*. 2019;92(1093):20180153. Epub 2018 Oct 11.
- Park HJ, Lee SS, Park B, Yun J, Sung YS, Shim WH, et al. Radiomics Analysis of Gadoxetic Acid-enhanced MRI for Staging Liver Fibrosis. *Radiology*. 2019;290(2):380-387.
- Pickhardt PJ, Graffy PM, Said A, Jones D, Welsh B, Zea R, et al. Multiparametric CT for Noninvasive Staging of Hepatitis C Virus-Related Liver Fibrosis: Correlation With the Histopathologic Fibrosis Score. *AJR Am J Roentgenol*. 2019;212(3):547-553.

- 22 Wu Z, Matsui O, Kitao A, Kozaka K, Koda W, Kobayashi S, et al. Hepatitis C related chronic liver cirrhosis: feasibility of texture analysis of MR images for classification of fibrosis stage and necroinflammatory activity grade. *PLoS One*. 2015;10(3):e0118297.
- 23 Zhang X, Gao X, Liu BJ, Ma K, Yan W, Liling L, et al. Effective staging of fibrosis by the selected texture features of liver: Which one is better, CT or MR imaging? *Comput Med Imaging Graph*. 2015;2:227-236.
- 24 Nault JC, Couchy G, Balabaud C, Morcrette G, Caruso S, Blanc JF, et al. Molecular Classification of Hepatocellular Adenoma Associates With Risk Factors, Bleeding, and Malignant Transformation. *Gastroenterology*. 2017;152(4):880-894.e6.
- 25 Cannella R, Borhani AA, Minervini MI, Tsung A, Furlan A. Evaluation of texture analysis for the differential diagnosis of focal nodular hyperplasia from hepatocellular adenoma on contrast-enhanced CT images. *Abdom Radiol (NY)*. 2019;44(4):1323-1330.
- 26 Cannella R, Rangaswamy B, Minervini MI, Borhani AA, Tsung A, Furlan A. Value of Texture Analysis on Gadoteric Acid-enhanced MRI for Differentiating Hepatocellular Adenoma from Focal Nodular Hyperplasia. *AJR Am J Roentgenol*. 2019;212(3):538-546.
- 27 European Association for the Study of the Liver. EASL Clinical Practice Guidelines: Management of hepatocellular carcinoma. *J Hepatol*. 2018;69(1):182-236.
- 28 Marrero JA, Kulik LM, Sirlin CB, Zhu AX, Finn RS, Abecassis MM, et al. Diagnosis, Staging, and Management of Hepatocellular Carcinoma: 2018 Practice Guidance by the American Association for the Study of Liver Diseases. *Hepatology*. 2018;68(2):723-750.
- 29 Chen S, Zhu Y, Liu Z, Liang C. Texture analysis of baseline multiphasic hepatic computed tomography images for the prognosis of single hepatocellular carcinoma after hepatectomy: A retrospective pilot study. *Eur J Radiol*. 2017;90:198-204.
- 30 Zhou Y, He L, Huang Y, Chen S, Wu P, Ye W, et al. CT-based radiomics signature: a potential biomarker for preoperative prediction of early recurrence in hepatocellular carcinoma. *Abdom Radiol (NY)*. 2017;42(6):1695-1704.
- 31 Ahn SJ, Kim JH, Park SJ, Kim ST, Han JK. Hepatocellular carcinoma: preoperative gadoxetic acid-enhanced MR imaging can predict early recurrence after curative resection using image features and texture analysis. *Abdom Radiol (NY)*. 2019;44(2):539-548.
- 32 Brenet Defour L, Mulé S, Tenenhaus A, Piardi T, Sommacale D, Hoeffel C, et al. Hepatocellular carcinoma: CT texture analysis as a predictor of survival after surgical resection. *Eur Radiol*. 2019;29(3):1231-1239.
- 33 Oh J, Lee JM, Park J, Joo I, Yoon JH, Lee DH, et al. Hepatocellular Carcinoma: Texture Analysis of Preoperative Computed Tomography Images Can Provide Markers of Tumor Grade and Disease-Free Survival. *Korean J Radiol*. 2019;20(4):569-579.
- 34 Ning P, Gao F, Hai J, Wu M, Chen J, Zhu S, et al. Application of CT radiomics in prediction of early recurrence in hepatocellular carcinoma. *Abdom Radiol (NY)*. 2020;45(1):64-72.
- 35 Feng ST, Jia Y, Liao B, Huang B, Zhou Q, Li X, et al. Preoperative prediction of microvascular invasion in hepatocellular cancer: a radiomics model using Gd-EOB-DTPA-enhanced MRI. *Eur Radiol*. 2019;29(9):4648-4659.
- 36 Xu X, Zhang HL, Liu QP, Sun SW, Zhang J, Zhu FP, et al. Radiomic analysis of contrast-enhanced CT predicts microvascular invasion and outcome in hepatocellular carcinoma. *J Hepatol*. 2019;70(6):1133-1144.
- 37 Wilson GC, Cannella R, Fiorentini G, Shen C, Borhani A, Furlan A, et al. Texture analysis on preoperative contrast-enhanced magnetic resonance imaging identifies microvascular invasion in hepatocellular carcinoma. *HPB (Oxford)*. 2020;S1365-182X(20)30079-4.
- 38 Park HJ, Kim JH, Choi SY, Lee ES, Park SJ, Byun JY, et al. Prediction of Therapeutic Response of Hepatocellular Carcinoma to Transcatheter Arterial Chemoembolization Based on Pretherapeutic Dynamic CT and Textural Findings. *AJR Am J Roentgenol*. 2017;209(4):W211-W220.
- 39 Yu JY, Zhang HP, Tang ZY, Zhou J, He XJ, Liu YY, et al. Value of texture analysis based on enhanced MRI for predicting an early therapeutic response to transcatheter arterial chemoembolisation combined with high-intensity focused ultrasound treatment in hepatocellular carcinoma. *Clin Radiol*. 2018;73(8):758.e9-758.e18.
- 40 Mulé S, Thieffin G, Costentin C, Durot C, Rahmouni A, Luciani A, et al. Advanced Hepatocellular Carcinoma: Pretreatment Contrast-enhanced CT Texture Parameters as Predictive Biomarkers of Survival in Patients Treated with Sorafenib. *Radiology*. 2018;288(2):445-455.

Contact

Professor Tommaso Vincenzo Bartolotta, M.D., Ph.D.
 Department of Radiology
 Fondazione Istituto Giuseppe Giglio
 Ct.da Pietrapollastra
 Via Pisciotto,
 90015 Cefalù (Palermo)
 Italy
tommasovincenzo.bartolotta@unipa.it



Roberto Cannella, M.D.
 Section of Radiology – BiND
 University Hospital “Paolo Giaccone”
 Via del Vespro 129
 90127 Palermo
 Italy
rob.cannella89@gmail.com



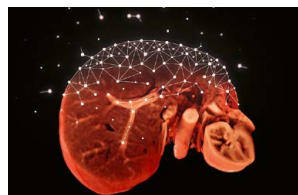
Try them on your system

Trial licenses for many of the applications featured in this issue of MAGNETOM Flash are available as a trial license free of charge for a period of 90 days.



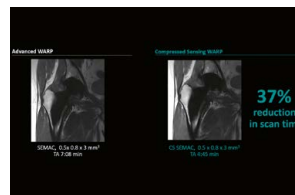
Whole-Body Dot Engine

Reliably perform whole-body MRI in 25 minutes.



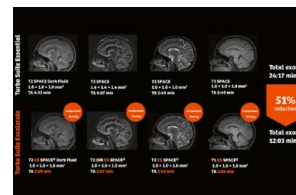
Compressed Sensing GRASP-VIBE

Beyond speed. Beyond motion.



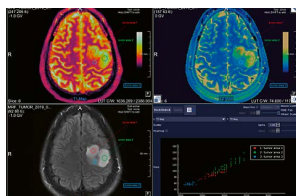
Compressed Sensing SEMAC

Highly accelerated musculo-skeletal imaging in patients with whole joint replacements based on SEMAC with Compressed Sensing.



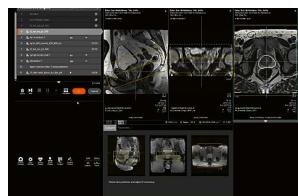
Compressed Sensing SPACE

Compressed Sensing (CS) speeds up data acquisition with sparse data subsampling.



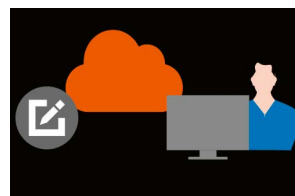
MR Fingerprinting

Quantitative tissue maps enabling improved tissue characterization.



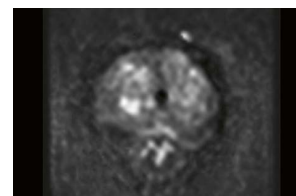
Prostate Dot Engine

Improved image quality and consistency of prostate MRI exams.



MR Protocols Module

Centrally manage & distribute your standardized protocols.



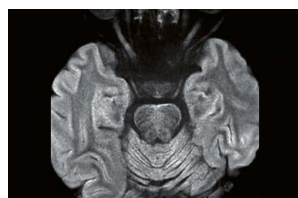
ZOOMit^{PRO}

Zoomed diffusion-weighted imaging for increased lesion conspicuity.



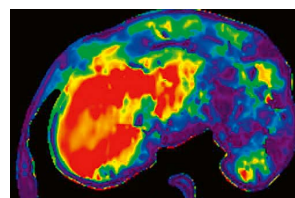
Simultaneous Multi-Slice

Setting the pace in MRI acceleration for TSE and DWI.



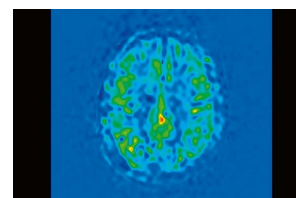
RESOLVE

Experience a higher level of diagnostic confidence with sharp, high-resolution diffusion-weighted images largely free of geometric distortions.



MR Elastography

MR Elastography is a non-invasive method to detect and follow chronic liver disease.



PCASL

Improved 2D or 3D brain perfusion imaging.

For further details, product overviews, image galleries and general requirements visit us at:

www.siemens-healthineers.com/magnetic-resonance-imaging/options-and-upgrades

Reduced Stress and Consistent Contrast-enhanced MRI Scans with Precisely Timed, Automated Injection Enabled by MR-Injector Coupling

A Joint Development by Bayer and Siemens Healthineers

Gregor Thoenner¹; Manuela Rick¹; Petra Bildhauer¹; Jens Gühring¹; Dieter Faust¹; Barbara De Napoli²; Ron Barbat³; Sri Shriram³

¹Siemens Healthineers, Magnetic Resonance Imaging, Erlangen, Germany

²Bayer Medical Care B.V., Pharmaceuticals, Maastricht, The Netherlands

³Bayer Healthcare, Pharmaceuticals, Indianola, USA

Introduction

Contrast-enhanced MR imaging procedures, such as MR angiography (MRA) or dynamic contrast-enhanced (DCE) imaging in oncology, require precise timing of contrast injection and MR data acquisition to hit the first pass of contrast agent in the body region or tissue of interest.

If all the required steps are performed carefully and in the right order, MRA and DCE can be performed with high

consistency and reproducibility. However, conducting a test bolus scan alone typically involves user interactions with three different monitors and devices (see Table 1). In daily clinical practice, typically, MRA is a one-per-day examination and consequently many technologists do not routinely perform such exams. Also, calculating the delay time between injection and scanning, considering

	Conventional workflow	Enhanced ISI workflow
Preparation	1. Localizer imaging to gain anatomical overview 2. Vessel scout to gain overview where big vessels are located	
Test Bolus	3. Plan and prepare test bolus examination 4. Set-up test bolus protocol & Arm the injector 5. Prepare patient for the injection 6. Arm the scan on the MR console (prescans are performed)	
	7. Start contrast agent injection on the injector console 8. Start MR acquisition at the same time with second hand	7. precisely synchronized start of injection and scan with one click
Time Delay (TD) Calculation	9. Open mean-curve application and load test bolus data 10. Derive time-to-arrival 11. calculate TD based on time-to-center and formula	8. Select supplying vessel in pre-loaded test bolus images with one click for automated calculation of TD
MRA	12. (9.) Plan and scan pre-contrast T1w 3D protocol 13. (10.) Set up injection protocol & arm injector 14. (11.) Wait-for-user-to-start dialogue (@scanner) to enter contrast agent and volume applied 15. (12.) Arm the post-contrast scan (prescans are performed) 16. (13.) Prepare patient for second injection and breath-hold exam	
	17. Start contrast agent injection on the injector console 18. Monitor time elapsed 19. Apply breath-hold command 3–4 seconds before intended start of scanning (TD) 20. Start the scan at TD 21. "Continue breathing"	14. One click to: – Inject contrast – Apply timed Auto-voice command before TD – Auto-start scan at TD – "Continue breathing" command

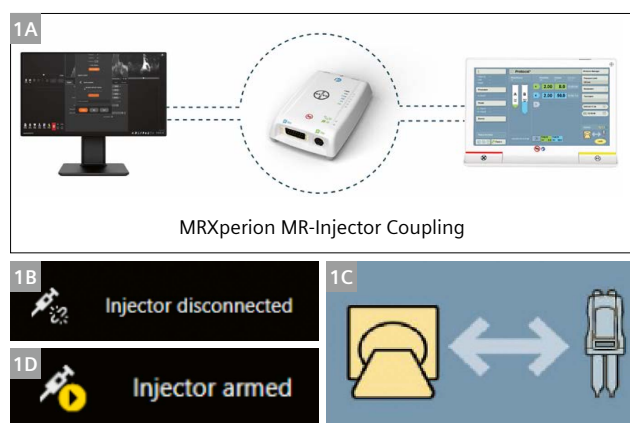
Table 1: Comparison between conventional workflow and enhanced ISI workflow.

when the center of k -space is acquired, is often regarded as a challenge. Along with the lack of routine practice, this can cause uncertainty and errors in the workflow that may result in imperfect timing. If the bolus is missed, the MRA may show venous enhancement or improper arterial filling, and in DCE the lesion-to-background contrast will not be optimal. If an examination is of reduced quality or non-diagnostic, this may lead to repeated administration of contrast, delayed diagnosis, additional costs, and tensions between radiologist and technologist.

Imaging System Interface (ISI) for MR-Injector Coupling

Bayer Healthcare and Siemens Healthineers have jointly developed a hardware and software interface (ISI – Imaging System Interface) enabling active coupling between the Medrad® MRXperion MR Injection System (in short, “injector”) and the MR scanner (Fig. 1)¹. It establishes a direct reliable connection between the MR scanner and the injector control system, allowing a technologist at the MR operator console to release injections remotely, which helps to overcome the aforementioned challenges. Combined with intuitive guidance provided by the Angio Dot Engine or the Abdomen Dot Engine, this provides a self-contained, intuitive workflow for high-quality and consistent contrast-enhanced procedures.

¹Work in progress: the application is currently under development and is not for sale in the U.S. and in other countries. Its future availability cannot be ensured. Note: This feature may not be available in all regions/countries at the time of publication.

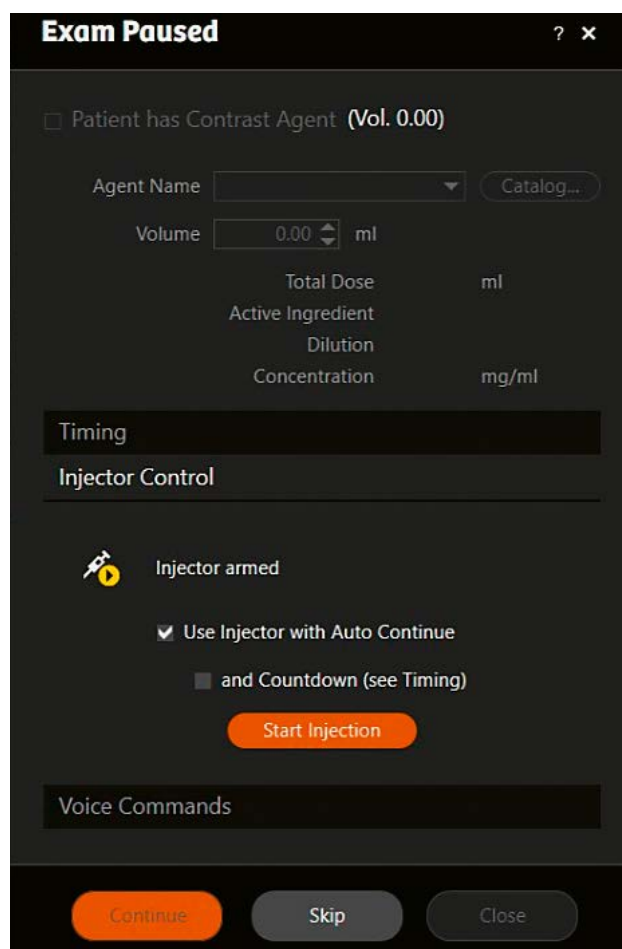


1 (1A) Schematic view of scanner-injector coupling via the ISI box. On the MR console, the status of the scanner-injector coupling is displayed as: not connected (1B), connected or armed. After confirming the injection protocol (“Lock”) and ensuring that tubes and syringes are cleared of air (“Arm”) on the injector console (1C) the status on the MR console changes to “Injector armed” (1D). From this point on, it is possible to initiate the contrast application directly from the MR console, seamlessly embedded in different workflows.

Conventional versus enhanced ISI Workflow

An MRA of the carotids is used in Table 1 to illustrate the enhanced ISI workflow in comparison with a conventional examination. The related advantages can be generalized to various other CE examinations.

As shown in Table 1, the ISI workflow is predominantly similar to the conventional workflow, but decisive and critical steps are assisted and the user interaction is reduced to the essentials. If the coupling between the injector and the MR scanner is established as described in Figure 1, both the scan and the injection can be initiated with one single mouse click in the MR scanner user interface (Fig. 2). Among other things, this enables precise synchronization between contrast injection and start of the test bolus MR sequence for the accurate calculation of contrast arrival in the target region.



2 Pause dialogue before first contrast injection. Injector and MR are coupled via ISI, the injector is armed. Selecting the tick box “Use Injector with Auto Continue” will facilitate a synchronized release of contrast injection and scan whenever the user presses “Start Injection”.



- 3** Interaction dialogue of the Angio Dot Engine after the test bolus measurement. After selecting a feeding artery in test bolus images, the contrast enhancement curve in the respective ROI is displayed as a red curve. Optionally it is also possible to display the contrast dynamics in a vein to make sure that the k -space center is acquired before the venous enhancement is pronounced. The dialogue box intuitively visualizes when and how the post-contrast scan will be performed, when the breath-hold commands will be applied and when the center of k -space will be acquired. The experienced user may always change the settings.

Within the Angio Dot Engine workflow (Fig. 3), the user is also guided and assisted in deriving the patient-specific delay time for MRA. The acquired test bolus datasets are automatically pre-loaded and the user is only required to select a feeding artery in the images. The software will then automatically derive when the peak of enhancement is reached, and by accounting for specific parameters, such as time-to-center of k -space, the optimal delay time between injection and start of the post-contrast scan will be calculated.

With the ISI workflow application of contrast and start of measurement are synchronized, so the user has to press just one button, "Start Injection", instead of manually

injecting contrast on the injector console while giving breath-hold commands to the patient in a timely fashion via the Patient Intercom, and finally starting the actual MR data acquisition manually after the derived delay time on a third device – the MR scanner console. As shown in Figure 4, the automatically derived delay time is prepopulated. By choosing "Use Injector with Auto Continue" and "Countdown" in the acquisition step of the post-contrast images, the scanner software will not only automatically initiate the contrast but start image acquisition at the right time. The required breath-hold commands will also be played exactly when needed.

Summary

In a conventional setting, the technologist is required to constantly plan, monitor, and time the various steps on the injector and scanner workstations for contrast-enhanced procedures – resulting in reduced efficiency, high stress, and potentially suboptimal image quality.

The MR-Injector coupling via ISI is a software and hardware solution that simplifies synchronized contrast injection and scanning by guiding the user through an intuitive workflow, with clicks and interactions reduced to the essentials. With consistent and reproducible studies, this helps to save time, improve operational efficiency, and reduce stress.

Furthermore, the solution is designed to support scenarios such as remotely assisted scans with the *syngo* Virtual Cockpit, where an expert controls the scanner virtually from a remote location. This can help to transform care delivery by providing advanced contrast-enhanced imaging services in remote areas, instead of requiring patients to travel to distant, centralized expert medical centers.

Acknowledgments

The authors would like to thank Sharon Standish, Sean Berecek and William Hohn, and the extended Bayer team (Bayer U.S. LLC, Pharmaceuticals, Indianola, PA, USA) for their valuable support.

- 4 Wait-for-user-to-start dialogue before main contrast injection. Volume and type of contrast agent can be specified. In the "Timing" section, the delay time between injection and start of image acquisition (see Figure 3) is already pre-populated. The section "Injector Control" shows that the injector is armed and that the protocol will be performed with automated countdown and automated start. As soon as "Start injection" is pressed, the contrast injection is initiated, the countdown starts, and 8.9 seconds before "zero" (= start of the imaging sequence) the voice command is played.

Contact

Gregor Thörmer, Ph.D.
Global Segment Manager
MRI in Oncology
Siemens Healthineers
Tel.: +49 (0)9131 84-7726
gregor.thoermer@siemens-healthineers.com



Exam Paused

☒ Patient has Contrast Agent (Vol. 0.00)

Agent Name

Volume

0.00 ml

Total Dose

Active Ingredient

Dilution

Concentration

ml

mg/ml

Catalog...

Timing

Break time

Total Time

Countdown

0 s

0 s

27 s

☒ Auto Continue

Start Countdown

Injector Control

Injector armed

☒ Use Injector with Auto Continue

☒ and Countdown (see Timing)

Start Injection

Voice Commands

Before Scan

Hold breath (inhaled).

8.9 s

After Scan

Continue breathing.

2.7 s

Continue

Skip

Close

Revisiting 3T: Pearls and Pitfalls Compared with 1.5T

Cédric Buttin¹; Nicolas Dechâtre²; Corentin Mauris³; Allan Thuret¹

¹MR Technologist, IRM74 Economic Interest Group, Annecy, France

²Specialist Application MR, Medical Professionals, Annecy, France

³MR Technologist, Medical-Technical Advisor, IRM74 Economic Interest Group, Annecy, France

Introduction

Today, 3-tesla MRI plays an increasingly significant role in the world of medical imaging. Approximately 1,250 to 1,300 MRI scanners are operated in France, 85% of which are 1.5-tesla systems, and 15% of which are 3-tesla systems.

In France, up to now, 3T MRI scanners have mainly been used in university hospitals or for research purposes. However, private entities are now increasingly tending to opt for the high-field MRI systems.

The Economic Interest Group IRM74 is also affected by this change of direction in the choice of field strength. In 2019 and 2020, for instance, our fleet of MRI scanners was enhanced by two new MAGNETOM Lumina with BioMatrix systems, one at the Annecy-Genevois Hospital site (Metz-Tessy, 2019¹) and the other at our Annecy site, where it replaced a MAGNETOM Aera system (Fig. 1A–D).

A total of seven MAGNETOM MRI systems from Siemens Healthineers are currently used by our facility:

- 1.5T: MAGNETOM Avanto Fit (x1),
MAGNETOM Aera (x1),
MAGNETOM Amira with BioMatrix (x1),
MAGNETOM Altea with BioMatrix (x2)
- 3T: MAGNETOM Lumina with BioMatrix (x2)

The aim of this article is to share our experience of this new innovation and to give our radiology colleagues (technologists) a better understanding of 3-tesla MRI.

The advantages, explained by physics

Improved signal-to-noise ratio

Increasing the magnetic field strength increases the proton mass (E) aligned in parallel with B_0 , which is responsible, in particular, for producing more signal.

Equation 1

$$\Delta E = \gamma \cdot \hbar \cdot B_0$$

where γ is the gyromagnetic ratio, and \hbar is Planck's constant.

The signal-to-noise ratio formula is

Equation 2

$$\frac{S}{N} \sim \omega_0 \cdot f(T_1, T_2)$$

where ω_0 is the Larmor frequency (which depends on B_0), $f(T_1, T_2)$ is the relaxation factor, and $\Delta\omega$ is bandwidth detection.

With a static magnetic field strength (B_0) (changing from 1.5 to 3-tesla), the signal-to-noise ratio obtained at 3T is twice that obtained at 1.5T².

Equation 3

$$SNR(3T) = 2 \cdot SNR(1.5T)$$

This increase in the signal-to-noise ratio principally has two benefits:

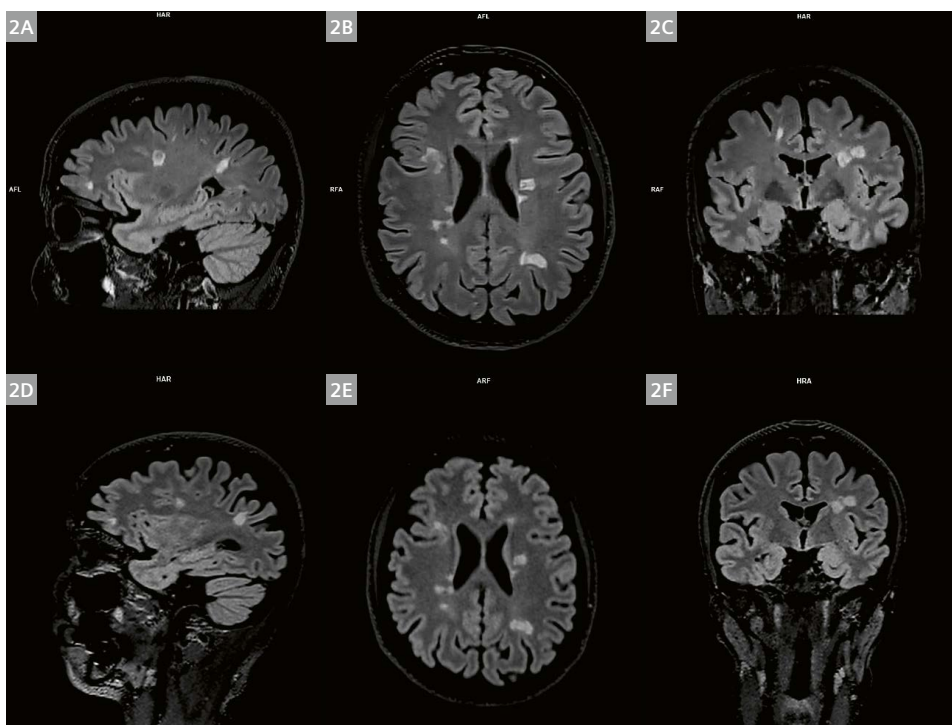
- Increased spatial resolution (Figs. 2, 3, and 4)
- Reduced acquisition time

¹Mauris C., Fernandes G., Dechâtre N. and Jaccoud A., *Introducing 3T MR Imaging with the New MAGNETOM Lumina*, MAGNETOM Flash (75) 4/2019, RSNA Edition 2019, 16-23.

²This 2-fold increase is a theoretical increase. In practice, depending on the examined body region the effective gain in SNR is lower (or higher) also depending on T1/T2 times, effect of gadolinium, etc. Semelka et al. show that the statistically significant increase in SNRs in various abdominal tissues ranged from 1.3- to 3.5-fold at 3T compared to 1.5T. (See also Ramalho M, Vasco H, Semelka RC, et al. Quantitative and Qualitative Comparison of 1.5 and 3.0 Tesla MRI in Patients With Chronic Liver Diseases. JMRI 29:869–879 (2009) <https://onlinelibrary.wiley.com/doi/pdf/10.1002/jmri.21719>)



1 MAGNETOM Lumina with BioMatrix XK 36/200 MRI system (1A–1C) equipped with an Interflex pneumatic door (1D).



2 Examination to monitor multiple sclerosis on a MAGNETOM Lumina 3T (tra_cs_space_dark_fluid_3D_iso (2B) with sagittal (2A) and coronal (2C) reconstructions) compared with the previous examination performed on a MAGNETOM Aera 1.5T (sag_caipirinha_space_dark_fluid_3D_iso (2D) with transversal (2E) and coronal reconstructions (2F)).

In theory, the difference in contrast between the tissues and the gadolinium is greater.

Despite the lower relaxivity of contrast agents (CA) at 3T in relation to 1.5T, the shortening effect on T1 remains greater at 3T (Fig. 5) in their presence.

In addition, thanks to the lengthening of T1 (Table 1), 3T enables T1 to be enhanced by the contrast agents (Fig. 6) which suggests that smaller doses of contrast agent can be injected.

As previously mentioned when discussing the issue of injected volumes in pediatrics³, our future work will focus on decreasing the dose of gadolinium contrast agent injected into the patient on the MAGNETOM Lumina system in prostate, abdominal, and MRA imaging.

In spectroscopy, there are various advantages of higher field

Firstly, the much larger chemical shift improves spectral resolution. The signal contribution improves differentiation of low concentrations of metabolites. Combined together,

these two aspects will also enable us to achieve a reduced acquisition time.

However, increasing the magnetic field also has a disadvantage as it is also responsible for a greater susceptibility effect (distortion, signal loss at air/tissue interfaces) which makes shimming optimization even more important.

The chemical shift artifact is also increased which is a challenge particularly when using CSI.

An increase in magnetic susceptibility artifacts.

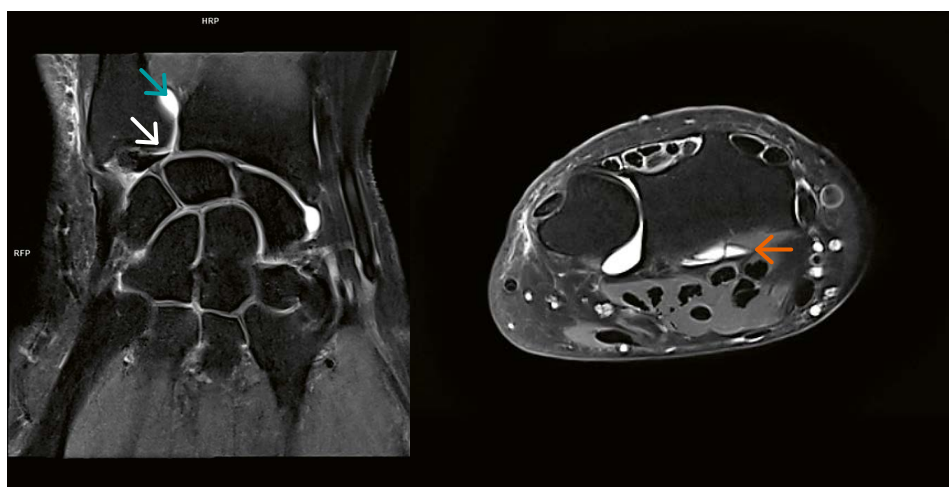
Due to the increased magnetic field, spin dephasing plays a more significant role as the T2* effect does which produces a greater susceptibility effect, and the size of the artifact is also more important as it improves detection of microbleeding.

Equation 4

$$\text{Size of Susceptibility artifact} \sim \frac{(\Delta \text{Susceptibility}) \cdot B_0 \cdot TE}{\text{Bandwidth}}$$



3 Peritendinous flexor tendon sheath effusion from the carpal tunnel to the long fingers with the sequence PD FS TSE COR sms – 2.5 mm, 400 x 640, FOV 138 x 220 (3A) and PD FS TSE SAG – 2.5 mm, 384 x 384, FOV 120 (3B). Synovial effusion with the sequence PD FS TSE TRA sms, 2 mm, 266 x 448, FOV 71 x 120 (3C).



4 Disinsertion of the radial enthesis of the TFCC joint disk (white arrow) associated with a distal radioulnar joint effusion (petrol arrow) with the sequence PD FS TSE COR sms – 2.5 mm, 352 x 352, FOV 80 x 80. Cyst on the palmar side of the wrist joint (orange arrow) with the sequence PD FS TSE TRA sms – 2.5 mm, 280 x 560, FOV 70 x 140.

³Colafati, G.S., Rossi, E., Carducci, C. et al. Half-dose versus full-dose macrocyclic gadolinium at 3-T magnetic resonance imaging in pediatric bone and soft-tissue disease. *Pediatr Radiol* 48, 1724–1735 (2018). <https://doi.org/10.1007/s00247-018-4204-y>

Therefore, in the absence of a 180° RF pulse, as for spin echo sequences, GRE-type sequences are more sensitive to magnetic susceptibility. The use of conventional GRE or SWI sequences (Fig. 7) for the detection of bleeding, brain perfusion in stroke or tumor studies, and BOLD-type functional MRI sequences will therefore be improved at 3T.

Shortening effect on T1 for the liver: 1.5T vs. 3T

$$T1 \text{ observed} = 1 / (1/T1 + [CA] * r1)$$

T1 liver with 1.5T \approx 600 ms

T1 liver with 3T \approx 800 ms

CA is concentrated by 0.1 mmol/l

$r1 \text{ 1.5T} = 5 \text{ l/(mmol*s)}$

$r1 \text{ 3T} = 4,8 \text{ l/(mmol*s)}$

With 1.5T

$$T1 \text{ observed} = 1 / (1/0.6 + 0.1 * 5) = 461 \text{ ms (23\% reduction)}$$

With 3T

$$T1 \text{ observed} = 1 / (1/0.8 + 0.1 * 4,8) = 578 \text{ ms (28\% reduction)}$$

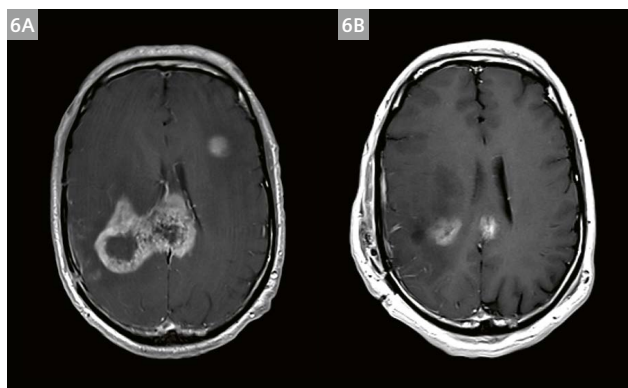
- 5** Greater shortening effect of T1 with 3T versus 1.5T with contrast agents.

Time-of-flight imaging with better contrast (Fig. 8)

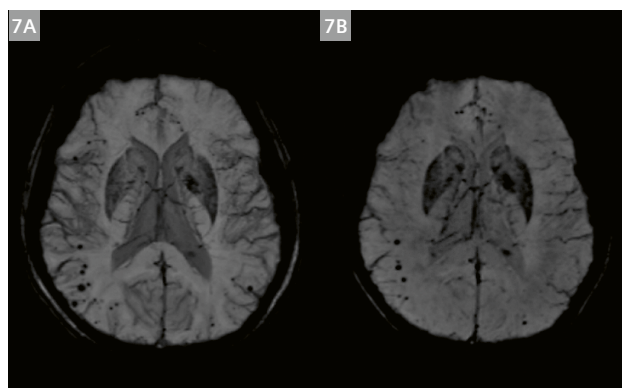
The increase in the static magnetic field B_0 enables lengthening of T1 and results in improved saturation of the spins in stationary tissue and therefore improves contrast. At 3T, the SNR makes it possible to optimize spatial resolution and therefore to improve the detection of small blood vessels (better inflow effect). The distal vessel view is therefore a real improvement.

Tissue	T1 [ms]			
	0.35T	1.0T	1.5T	3.0T
Fat	201	241	259	292
Liver	284	423	493	641
White Matter	474	683	787	832
Gray Matter	588	813	921	1331
Skeletal muscle	471	732	868	1162
Blood			1200	1500
CSF			4430	4500

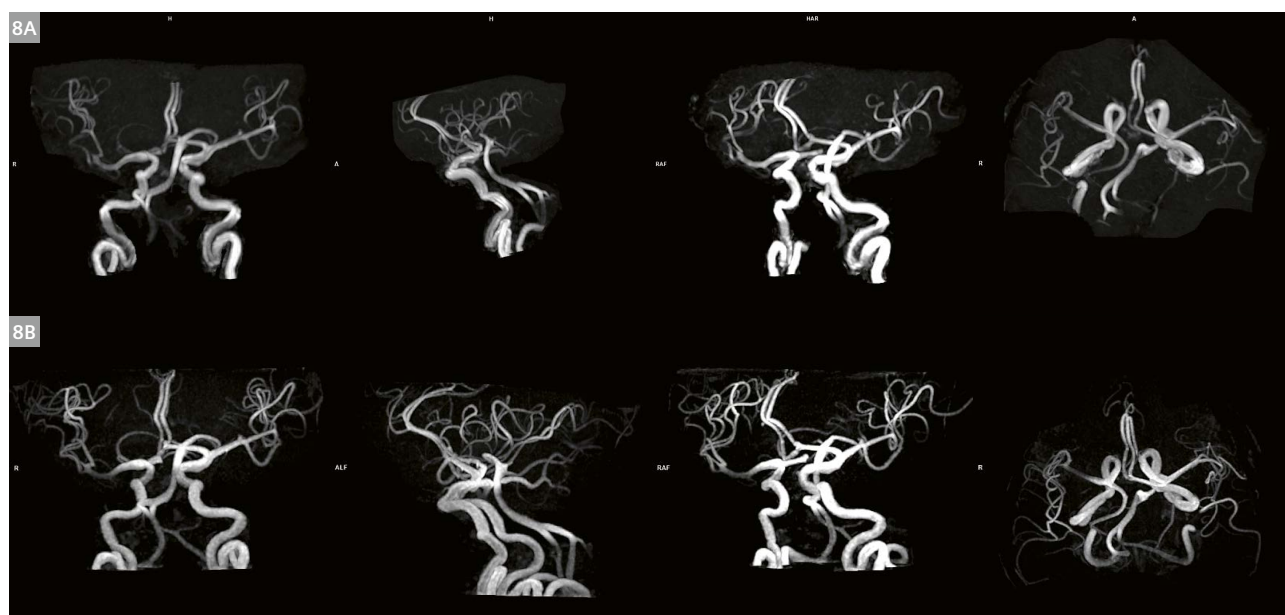
Table 1: T1 value depending on magnetic field strength.



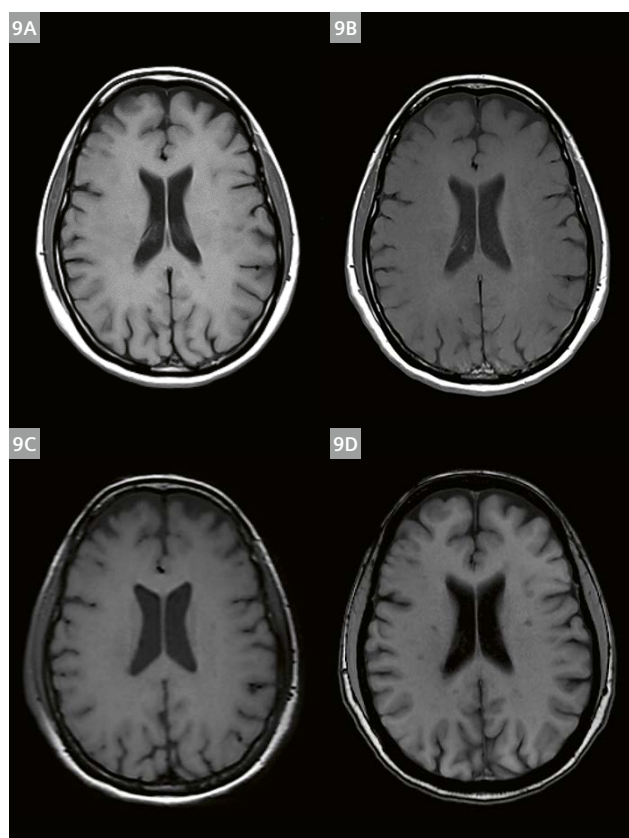
- 6** Monitoring a right temporal-insular glioblastoma with a left frontal metastasis, a few millimeters in size. Operated right temporal and insular lesions. Review following chemoradiotherapy. Regarding the right temporal insular region, this contrast uptake progresses towards the insular region, the splenium of the corpus callosum, and the internal capsule on the T1 TSE TRA sequence (**6A**) performed on a MAGNETOM Lumina 3T compared with the previous MRI performed on a MAGNETOM Aera 1.5T (**6B**). Appearance of new contrast uptakes of the left cingular gyrus. A very good contrast is confirmed after injection of the contrast agent.



- 7** Examination to monitor microbleeding, indicating a cerebral amyloid angiopathy (CAA) on a MAGNETOM Lumina 3T (SWI TRA MIP (**7A**)) compared with its previous examination acquired on a MAGNETOM Altea 1.5T (SWI TRA MIP (**7B**)).



8 TOF TRA sequences performed on the same patient, reconstructed in MIP in different planes, obtained on a MAGNETOM Altea 1.5T (**8A**) and then on a MAGNETOM Lumina 3T (**8B**). Notable improvement in the view of the circle of Willis and the distal arteries at 3T.



9 T1 TRA obtained on a MAGNETOM Aera 1.5T in TSE (**9A**) and on a MAGNETOM Lumina 3T with the sequences TSE (**9B**), SPACE MPR (**9C**), and GRE (**9D**).

Disadvantages and solutions to resolve them

Acoustic noise increase

At 3T, acoustic noise increases, in theory, in relation to the 1.5T system as the magnetic field is stronger and therefore the vibrations produced by the strong currents passing through the copper (gradient) coils should be multiplied in proportion to the field. In practice, however, this is not the case, as the 3T gradient amplifiers and shock absorbers (filter behind the amplifiers) compensate for this noise so that, ultimately, a 3T system only produces slightly more noise than a 1.5T system.

It is important to provide the patient with all the necessary hearing protectors such as ear plugs and head phones.

Less T1 contrast between tissues

Mainly observable in neurological and spinal imaging, this issue can present a real challenge especially for radiologists who have to become familiar with this particular differentiation between tissues with a “flattened contrast” effect, especially in TSE (Fig. 9), and who have to accept that they must adapt their clinical routine to accommodate this constraint.

This loss of T1 contrast for tissues at 3T in relation to 1.5T is related to the increase in T1 which leads to a convergence of the relaxation times of white and gray matter (Fig. 10). This reduction in contrast can also be observed when comparing healthy tissue and pathological tissue.

So the result is poorer differentiation between gray matter (GM) and white matter (WM), especially with spin echo (SE) or turbo spin echo (TSE) sequences.

In addition to this natural “loss” in contrast, a cross-talk phenomenon also exists whereby each slice saturates the signal of its adjacent slice (Fig. 11). This phenomenon is particularly related to

- the gap between slices (the larger the gap, the less cross talk there is);
- the slice excitation profile (“No SAR” – “normal” – “rapid” RF pulse mode);
- the flip angle (with greater sensitivity with SE than in GRE).

With SE, the RF pulses act like magnetization transfer pulses which therefore “flatten” the contrast in neuro imaging.

The only neuro indications that benefit from lengthening of T1 are TOF (no more slice entry phenomenon and improved suppression of stationary tissue), ASL, and perfusion.

Solution: Use gradient echo-type sequences which are less sensitive to this phenomenon than spin echo sequences, such as a FLASH sequence (rapid, low SAR, less magnetization transfer effect, and good WM-GM contrast) but also less sensitive on small lesions, entry slice phenomenon, so vessels appear spontaneously as a hypersignal without the use of any contrast agents.

It is also possible to work with TSE-type sequences using inversion recovery pulse sequences in order to improve contrast, but care should be taken when using contrast agents with this type of sequence.

The magnetic susceptibility artifacts are increased

As mentioned above, this can be an advantage of the T2 gradient echo sequences. It can, however, also be a

disadvantage, particularly if there are any metal objects in the patient. Field distortion and loss of signal, already observed with 1.5T systems, will be even greater.

Solution: Spin echo sequences can be prioritized as they present less heterogeneity of the field due to their 180° rephasing pulse. The TE can also be reduced to minimize dephasing. To do so, it can be useful to increase the bandwidth, taking account of the resulting drop in signal-to-noise ratio. As far as possible, increasing the matrix to decrease the voxel size can also reduce this artifact. Prioritize saturation with IR (STIR) or using WARP-type options with VAT or even SEMAC for which it is necessary to optimize SAR management.

The B_1 artifact

There is one artifact – the B_1 artifact – that can be observed at 3T but not at 1.5T. This is characterized by a non-homogeneous signal or even a loss of signal (Fig. 12).

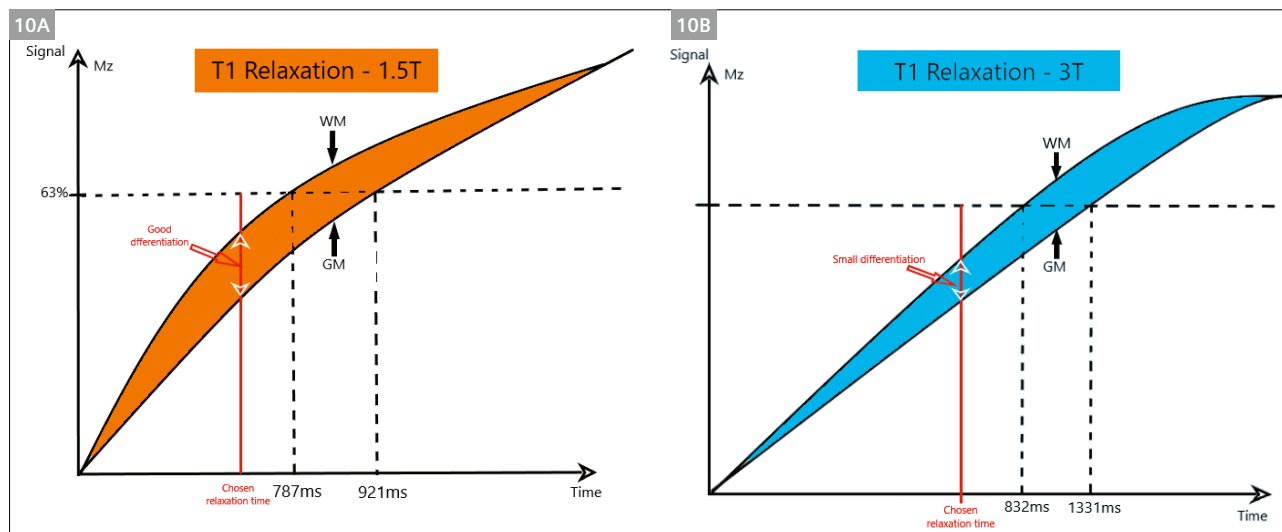
B_0 corresponds to the main magnetic field, whereas B_1 corresponds to the radio frequency field. Therefore, the B_1 artifact is related to a problem involving the use of radio frequency waves.

This problem results from a far greater and more intense variation of the flip angles at 3T which result in a lack of contrast uniformity and a possible loss of signal.

The variations in the B_1 (RF) field do not depend on the manufacturer but are related to patients themselves, and to the body region being investigated.

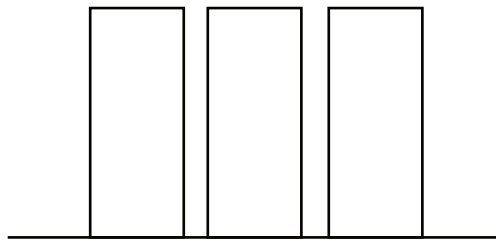
Therefore, significant variations in flip angles lead to a variability in the excitation of spins which respond differently in terms of contrast and signal.

This phenomenon is often reduced to the dielectric effect by considering the wavelengths in the tissues as a function of the strength of the magnetic field:



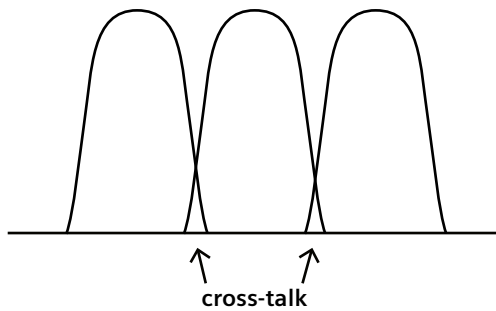
10 T1 1.5T (**10A**) longitudinal relaxation curves versus 3T (**10B**) for white matter (WM) and gray matter (GM) showing that their differentiation decreases at 3T, and therefore the contrast is weaker.

11A



Ideal slice profiles

11B



Actual slice profiles

- 11** Each slice affects the signal of adjacent slices through cross-talk.
 With permission from www.mriquestions.com, ©2020 AD Elster, ELSTER LLC

12A



12B



- 12** B₁ artifact characterized by a signal void (orange arrow) on TSE SAG T1 (12A) and T2 (12B) sequences.

At 3T, the wavelengths become the same size as, or even smaller than, the regions being investigated (Fig. 13). The phenomenon is mainly observed in thicker body regions such as the abdomen and pelvis, and also in skull investigations.

Solution: The issue has been addressed with the introduction of TrueForm technology, where the phase of the excitation is modulated in a way that more homogeneous excitations are achieved in large exam volumes. In addition, and in case of still pronounced artifacts, it is possible to select a B_1 image filter instead of “pre-scan normalize” or “normalize” filters.

The SAR is much higher than at 1.5T

The SAR is defined as the RF power absorbed per unit of mass of a patient, and is measured in Watts per kilogram (W/kg). We can also say that it is the amount of energy per unit of time and dissipated in the body.

It is proportional to B_0^2 and therefore:

Equation 5

$$SAR \text{ with } 3T = 4 \cdot SAR \text{ at } 1.5T$$

with the same flip angle and the same RF pulse (same shape and length).

Equation 6

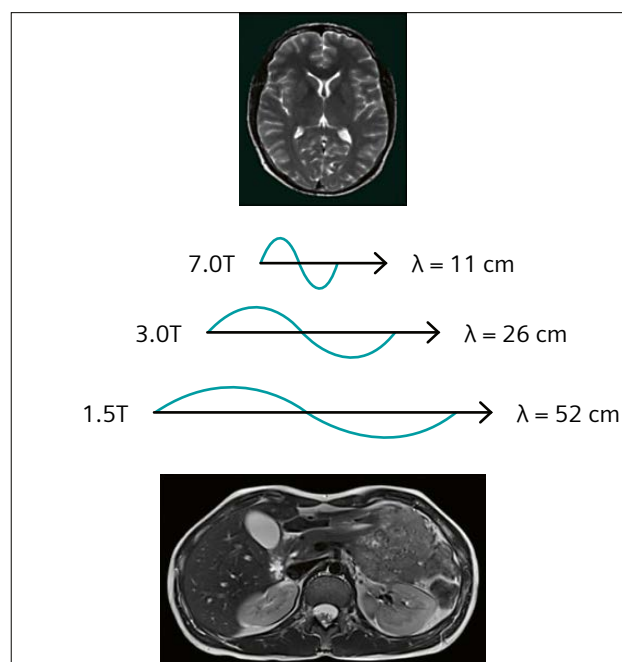
$$SAR \sim \frac{\sigma \omega_0^2 |B_1|^2}{m}$$

σ is the tissue conductivity, ω_0 is the Larmor precessional frequency – (reminder $\omega = \gamma \cdot B_0$), and m is the body mass.

This can lead to an increase in the patient's body temperature.

In order to mitigate any risk to the patient, RF exposure levels are set by the IEC (International Electrotechnical Commission) with, in particular, IEC 60601-2-33 (3rd Edition) (Table 2).

Solution: For the patient's safety and to optimize the duration of the examination, the sequence order should be anticipated when designing the acquisition protocol. For example, after an SAR intensive sequence such as a TSE sequence with a high echo train length or an STIR sequence with an inversion recovery pulse, it is advisable to continue with a sequence that has less energy, such



13 RF wavelengths in tissue as a function of field strength.
With permission from www.mriquestions.com, ©2020 AD Elster, ELSTER LLC

	Whole-Body SAR	Partial Body SAR	Head SAR
Body Region	Whole-Body	Partial Body	Head
Normal (W/kg)	2	2–10 α	3.2
First Level (W/kg)	4	4–10 α	3.2
Second Level (W/kg)	> 4	> (4–10) α	> 3.2
Short duration SAR	The SAR limit over any 10 s period shall not exceed two times the stated values		

Table 2: SAR limits for volume transmit coils (averaging time of 6 min)

α : The limit scales dynamically with the ratio “exposed patient mass / patient mass”

Normal operating mode: Partial body SAR = 10 W/kg – (8 W/kg * exposed patient mass / patient mass)

First level controlled operating mode: Partial body SAR = 10 W/kg – (6 W/kg * exposed patient mass / patient mass)

Averaging time of 6 minutes.

as a gradient echo sequence. This means that the patient will not be exposed to a high energy deposition for an overly long period of time and also makes it possible to avoid lengthy acquisition pauses between each sequence. To reduce the SAR:

- increase the TR, which will allow more time between each RF wave, reducing the frequency of energy deposition in the patient. However, the acquisition time is longer.
- reduce the number of slices therefore less RF pulses are necessary.
- reduce the flip angle to reduce the energy transmitted to the patient.
- reduce the echo train length making it possible to reduce the number of successive RF pulses over time.
- remain in Normal mode (do not go to First Level).
Note that you should not go to First Level for pregnant women, pediatric patients, people approaching death, sedated patients, or patients with fever. The patient must be monitored carefully and the room temperature must fulfill the recommended requirements.

At 3T, other solutions are possible to reduce the SAR. There is a higher signal-to-noise ratio and therefore more room for maneuver in terms of image optimization. This makes it possible to use acceleration factors such as parallel imaging, thereby limiting the number of RF waves.

Conclusion

While 3T MRI offers undreamt of possibilities, it can also be a source of concern compared to managing conventional 1.5T systems.

A static magnetic field (B_0) that is twice as powerful generates more signal, enables acquisition times to be reduced, and leads to more resolved imaging. In practice, however, this increase in the static field also can generate undesirable physical phenomena – although these can be easily overcome.

As is often the case with MRI, it's all about compromise!

- 14** Pop-up window indicating that the SAR limits have been exceeded and prompting the user to change their settings in order to remain in Normal SAR mode. Suggestions for changing the number of slices, the TR and the flip angle are directly accessible. It is also possible to go to First Level.



Cédric Buttin



Allan Thuret



Corentin Mauris

Contact

Corentin Mauris
Medical Electroradiology Technician
Medical-technical advisor
GIE IRM74
18, Rue de la Césièrre
74000 Annecy
France
Tel.: +33 4 50 51 81 75
c.mauris@irm74.org

Upgrading *syngo.via* VB30 to VB40 – What's New in MRI?

Corentin Mauris¹; Marc Férat²

¹GIE IRM74, Groupement d'Intérêt Economique Imagerie par Résonance Magnétique, Annecy, France

²Siemens Healthineers, Customer Services, Remote Services Center, Erlangen, Germany

In May 2020, the Economic Interest Group IRM74, upgraded its two *syngo.via* servers from software version VB30 to VB40.

Below, you can find details about the new features added to enhance daily use for radiographers and radiologists, together with a description of the advanced software.

General MR

Sorting has been redesigned in the **Series Navigator**, in particular by adding a number in front of each series for easier identification. The diffusion b-value is displayed between brackets (Fig. 1A), in a similar manner to the TE value for multiple scan series or when the series are sorted in Dixon, which makes viewing much clearer for the user.

Note also that the presence of an icon makes it easier to identify a series generated by the user in the list of series (Fig. 1B).

New **display types**, such as Cinematic VRT (Fig. 2A) and MIP/MinIP fusion (Fig. 2B), are available in the bottom left corner menu of the screen.

The display mode and slice thickness can now be changed more quickly with the aid of the blue shortcuts at the side (Fig. 3).

This tool can be used on new layouts created from a private account and when using them to improve memorization of the required series (**Smart Layout** tool: Segment learning button – Fig. 4).

The system then takes into account approximately 30 DICOM attributes from the dragged sequence in order to search for the series that best matches the required series.

If you wish to display several well-defined series, it is possible to zoom-in on specific segments. This is done by selecting the segments by holding down the Ctrl key and right-clicking on **Enlarge segments** (Fig. 5). Simply double-click to return to the original display.

Easy Reading layout now displays series with the same orientation in segments of the same size.

When studying dynamic series (particularly if there are multiple phases as is the case with TWIST and GRASP-VIBE), the **4D cinematic imaging** tool facilitates the temporal location of the displayed phase (Fig. 6). This is now available in all MR workflows.

When **studying 3D volumes**, the reference line is now hidden automatically when scrolling through the series so that it does not interfere with viewing.

An **export in non-DICOM image format** (practical for saving images to an external storage device for presentation purposes, for example) is now available from any

To read the full article, please visit

 www.siemens.com/MAGNETOM-World

> **Clinical Corner** > **Application Tips**

Upgrading syngo.via VB30 to VB40 – What's New in MRI?

Cordelia Maier¹, Marc Fiebert²

¹GEA, Groupe d'Études Économiques par Médecine Magnétique, Annecy, France
²Siemens Healthineers, Customer Services, Remote Services Center, Erlangen, Germany

In May 2020, the Economic Interest Group RM74, updated to two syngo.via servers from software version VB30 to VB40.

Below, you can find details about the new features added to enhance daily use for radiologists and radiologists, together with a description of the advanced software.

General MR

Spring has been redesigned in the **Series Navigator**, in particular by adding a number in front of each series for easier identification. The diffusion b-value is displayed between brackets (Fig. 1A), in a similar manner to the TE value for multiple scan series when the series are sorted in **DSort**, which makes viewing much clearer for the user.

Note also the presence of an icon makes it easier to identify a series generated by the user in the list of series (Fig. 1B).

New **display types**, such as **Cinematic VFI** (Fig. 2A) and **MRBrainShift** (Fig. 2B), are available in the bottom left corner menu of the screen.

The display mode and slice thickness can now be changed more quickly with the aid of the blue shortcut at the side (Fig. 3).

The system can now also memorize radiologists' habits when dragging and dropping their series so that they are displayed according to their preferences the next time.

This tool can be used on new layouts created from a private account and when using them to improve memorization of the required series (**Smart Layout** tool: Segment learning button – Fig. 4).

The system then takes into account approximately 30 DICOM attributes from the dragged sequence in order to search for the series that best matches the required series.

If you wish to display several well-defined series, it is possible to zoom in on specific segments. This is done by selecting the segments by holding down the Ctrl key and right-clicking on **Enlarge segments** (Fig. 5). Simply double-click to return to the original display.

Easy Reading layout now displays series with the same orientation in segments of the same size.

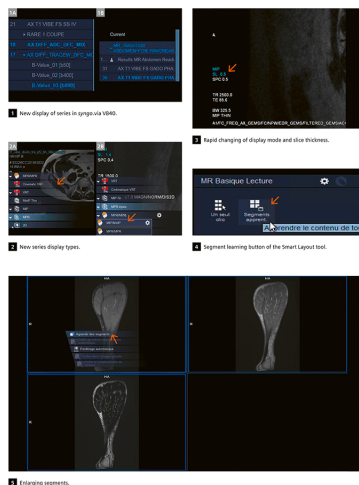
When studying dynamic series (particularly if there are multiple phases as in the case with **TWIST** and **GRASP-VIBE**), the **4D Cinematic** imaging tool facilitates the temporal location of the displayed phase (Fig. 6). This is now available in all MR workflows.

When studying 3D volumes, the reference line is now hidden automatically when scrolling through the series so that it does not interfere with viewing.

An **expert in non-DICOM image format** (practical for saving images to an external storage device for presentation purposes, for example) is now available from any workflow (previously only available in MR head) (Fig. 7).

When the user closes an examination by 'ignoring the findings', the dialog box that asked for confirmation in the previous version has now disappeared.

MAGNETOM Flash (77) 2020



1 New display of series in syngo.via VB40.



2 New series display types.



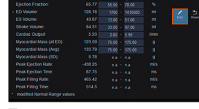
3 Segment learning button of the Smart Layout tool.



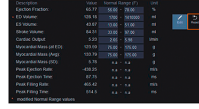
4 Easy Reading layout now displays series with the same orientation in segments of the same size.



5 When studying dynamic series, the 4D Cinematic tool facilitates the temporal location of the displayed phase.



6 When studying 3D volumes, the reference line is now hidden automatically when scrolling through the series.



7 An expert in non-DICOM image format is now available from any workflow.



8 When the user closes an examination by 'ignoring the findings', the dialog box that asked for confirmation in the previous version has now disappeared.

MAGNETOM Flash (77) 2020

MR Prostate

A new feature for automatic segmentation of the prostate gland is now available from the **Biopsy Support** (Fig. 8A). An automatic prostate volume calculation is carried out if the system has been configured to do so (Fig. 8B). It can also be generated again afterwards at any time. Radiologists can then modify the contours according to their expectations, by using the manual correction tools (Fig. 8C).

A quick and easy configuration needs to be carried out once by clicking on the settings icon and indicating which series to use (depending on the sequence names used on the user's shift). Prostate segmentation works for T2-weighted TSE or SPICE cross-sectional series (Fig. 9 orange arrows).

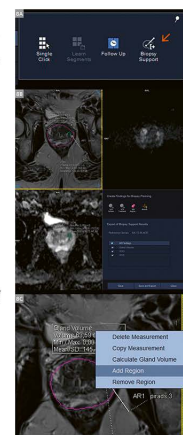
Note that it is still possible to analyse the gland volume using the three measurements technique. For that, you need to hold down the **SHIFT** button while drawing the three measures (one in each standard anatomic plane) and right-clicking on **Calculate Gland Volume**.

The user can also create VOIs to define a target for US-guided biopsy (Fig. 8D). The data can be exported to the PACS or to any fusion biopsy support system with the **RTS (Radiotherapy Structure Set)** standard format. The fusion can then be used as a reference during the biopsy.

Displaying the MR Spectroscopy Analysis step can also be disabled in the configuration settings to avoid overloading the list of viewing stages (Fig. 9).

The report has been completely revised. The display is now clear and much more complete, including the color scheme and **PI-RADS 2.1** report (see the **Findings Wizard** section for the other workflows).

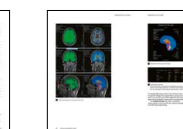
The report can be exported in various formats: CSV or standard PDF format (Fig. 12).



8 MR Prostate automatic segmentation.

siemens.com/magnetom-world

5



MR Cardiac Analysis

For multi-phase cases, a user-defined layout can be created (Fig. 39A).

It is now possible to create private layouts with spatial and/or temporal synchronization. It is now also possible to set series in the most relevant segment position by dragging and dropping series (for example, SA and LA) and different time points (for example, sorted into columns) in the layout (Fig. 39B).

The synchronization tool can also be used to set up a movie synchronization group (Fig. 39C).

It is now possible to adjust the EndoVFI contour more easily by moving the visible control points with the aid of the **Control Point Edit** tool (Fig. 40).

• Switch between EndoVFI with the respective buttons (on the left A shortcut).

• Add more control points simply by clicking on the contour or delete existing control points by right-clicking on them.

• The changes are propagated in the same way as with the **Slider** tool.

Furthermore, all the relevant values (SV, EF, TDDTS volume, Mass) are now always visible for both ventricles in the **VAG** segment (Fig. 41). This facilitates comparison of the left and right ventricles.

It is now also possible to **modify the preferred normal range** according to other criteria, for example, on different publications or for pediatric patients (Fig. 42). You can view these normal ranges according to criteria in the **Findings Details** of the **Findings Navigator**, and edit the normal values if needed.

Don't forget to select the **SDS** button again to save the changes.

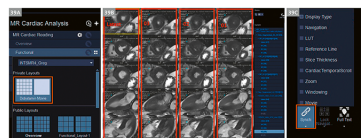
You can always 'reset' the normal ranges to the factory settings after confirming the safety pop-up window (Fig. 43).

The normal values can be modified for all the available options (VAG, VAG NORM, VO, VO NORM).

The modified normal values are saved by the user; consequently, a pediatric radiologist can use different values.

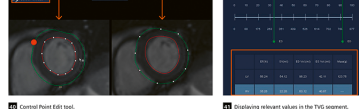
TDDTS mode can now be enabled by default when opening the MR Cardiac Analysis application. Open 'MR Cardiac Function Properties' and enable the contour drawing 'only within EDE's in your chosen mode (Fig. 44).

Wall thickness is automatically included in the findings. It is also possible to create a **VGVVD** finding directly from the **Findings Details** dialog box (Fig. 45).

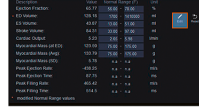


39 New configuration functionalities in MR Cardiac Analysis with the creation of a private layout (39A) and the possibility of spatial and/or temporal synchronization (39B) and (39C).

MAGNETOM Flash (77) 2020



40 Control Point Edit tool.



41 Displaying relevant values in the VAG segment.



42 Modifying the normal value ranges according to criteria.



43 Resetting the normal values.

siemens.com/magnetom-world

19

MAGNETOM Flash (77) 2020

MR Spectroscopy

Several improvements have been made to the MR Spectroscopy workflow.

It is now possible to view the selection of multiple voxels in all orientations (Fig. 46). This makes it possible to adjust the voxels selected in high-quality at the same time.

To do so, all the selected voxels must be of the same category (high quality or low quality). Voxels are selected simply by holding down the **CTRL** key and left-clicking with the mouse.

In addition, the **display's performance in manual phasing** has been improved (Fig. 47).

Manual phasing is a tool from the **Corner menu** which is available for advanced users (requires the **spectroscopy** license).



46 Selecting multiple voxels in the different planes.

47 Manual phasing of the spectrum.



Contact
Cordelia Maier
Medical Electronics Technology Technician
MR/CT Technical Advisor
GE, MR/CT
10, Rue de la Croix
24000 Angoulême
France
E-mail: c.maier@siemens-healthineers.com



Contact
Marc Fiebert
Siemens Healthineers
Customer Services
Remote Services Center
Siemens Healthineers AG
Siemensstr. 10
91052 Erlangen
Germany
E-mail: m.fiebert@siemens-healthineers.com

Case Report: CMR of Myocardial Inflammation Regression in Convalescence of Acute Myocarditis Caused by SARS-CoV-2

Felipe Toth Renda Dias; Fernanda Albano; Lara Leite; Camila Silveira; Bruno A. de Azevedo; Manuel Nicolas Cano; Silvia Judith Fortunato de Cano; Carlos E. Prazeres¹; Juliana M. Bello; Adriano Carneiro; Valeria M. Moreira; Tiago A. Magalhães; Carlos Eduardo Rochitte

¹Hospital do Coração de São Paulo, HCOR, Cardiovascular CMR and CCT sector, São Paulo, Brazil

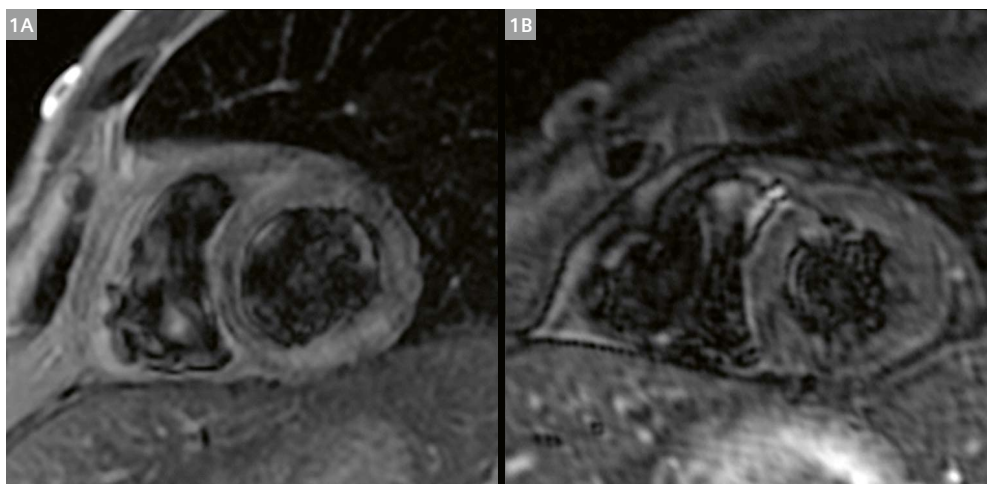
Abstract

A patient with recent COVID-19 infection and chest pain was diagnosed with acute myocarditis caused by SARS-CoV-2. Cardiovascular magnetic resonance (CMR) imaging performed on presentation and two months later demonstrated myocardial inflammation regression, defined by disappearance of myocardial edema on T2-weighted images, and significant decline in the extent of late gadolinium enhancement (LGE) between CMR exams. Despite the favorable imaging and clinical evolution of the acute myocarditis, T1 and T2 myocardial values and extracellular volume measurements remained slightly elevated in segments previously affected by edema and LGE compared to unaffected segments.

Case report

A 58-year-old male patient with dyslipidemia receiving rosuvastatin and with a positive RT-PCR for COVID-19 from April 28, 2020, arrived at the emergency department of a tertiary hospital in São Paulo, Brazil, on May 12, 2020. He presented with intermittent chest pain radiating out to the left arm and lasting four hours with progressive worsening. On admission, a hypothesis of acute coronary syndrome

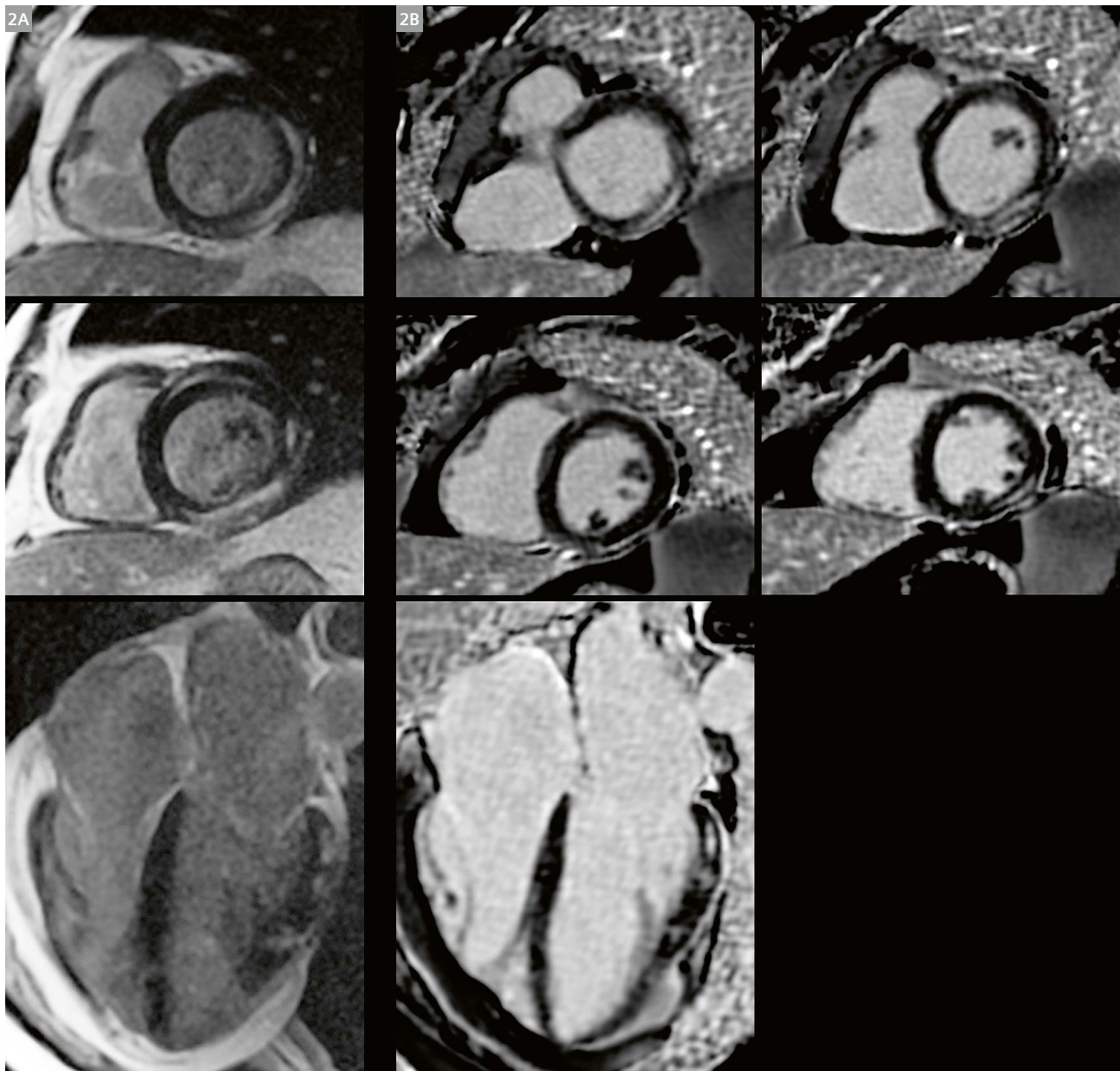
was made. ECG showed sinus rhythm without ST segment elevation, and troponin I was elevated with 8.3 ng/mL (reference value: below 0.034 ng/dL). He was medicated with 200 mg aspirin and 600 mg clopidogrel, and referred for invasive coronary cardiac catheterization. An uneventful procedure was performed showing a 40% stenotic ostial lesion in the first diagonal branch, without signs of unstable coronary plaque. Acute coronary syndrome was therefore ruled out. Due to the patient's previous COVID-19 infection, a new RT-PCR was performed on the day he was admitted, and returned a positive result. He was placed on the intensive care unit, and a progressive increase in troponin (up to 12.5 ng/mL) was observed. This led to a new working diagnostic hypothesis of acute myocarditis secondary to COVID-19. COVID-19 serological tests showed elevated IgG and IgM levels (41.86 AU/ml and 1.81 AU/ml, respectively), confirming a current infection by SARS-CoV-2. Other acute viral infections were ruled out by specific serological tests: negative tests for Coxsackie B antibodies, adenovirus, HIV, toxoplasmosis, cytomegalovirus, Epstein-Barr virus (last three tests: IgM negative and IgG positive, indicating previous infection). He was then referred for a cardiovascular magnetic resonance (CMR)



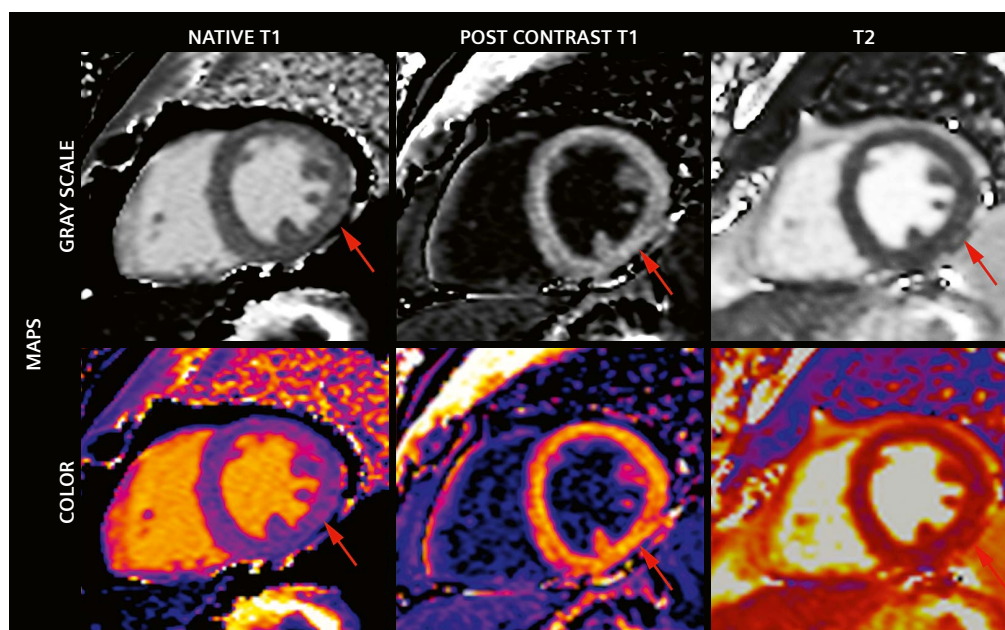
1 Myocardial Edema Regression: left ventricle short-axis T2-weighted images during acute phase of myocarditis (**1A**) with evident increase in signal intensity in inferior and inferolateral segments; resolution of the increased myocardial signal intensity in the same segments on images from a CMR exam two months later (**1B**).

exam. The left ventricle showed preserved dimensions and ejection fraction (LVEF of 64%). Myocardial edema in the basal and middle anteroseptal and inferolateral segments were noted (Fig. 1A). Late gadolinium enhancement at mid-wall and subepicardial layers in basal and middle anteroseptal and inferolateral segments was also observed, compatible with non-ischemic myocardial injury (Fig. 2A) and confirming the acute myocarditis diagnosis. Losartan was then introduced to the therapeutic regimen. The patient showed a decline in troponin levels (2.94 and 0.7 ng/mL) and clinical improvement, and was discharged

on May 19, 2020, for outpatient follow-up. On July 13, 2020, nine weeks after his hospitalization, the patient returned, asymptomatic, to undergo a follow-up CMR. Preserved cardiac chamber dimensions and LVEF, and resolution of myocardial edema were seen (Fig. 1B). Myocardial LGE was still present (Fig. 2B), though its extent was significantly decreased compared to baseline CMR (9 vs. 4 LV segments with LGE, and 15.4 g or 11.1% of LV mass vs. 5.3 g or 3.7% of LV mass, Fig. 2B). In the follow-up CMR, myocardial maps were also acquired, and native T1 and T2 values and extracellular volume (ECV)



2 Myocardial Late Gadolinium Enhancement (LGE) Regression: long-axis (bottom row) and short-axis LGE images during acute phase of myocarditis (2A) and at two-month follow-up CMR exam (2B); significant reduction of the extent of LGE seen in the short-axis and long-axis views.



3 Myocardial Maps: native T1, post-contrast T1 and T2; grayscale (top row) and color (bottom row) maps; red arrows indicate inferolateral segments with mildly elevated myocardial T1 and T2 values compared to inferoseptal values (see text).

were still elevated in the lateral wall compared to segments without LGE (native T1 myocardial values: 1014 ms vs. 982 ms; T2 values: 50 ms vs. 42 ms; and ECV 27% vs. 23%, respectively, Fig. 3). Despite the lack of myocardial T1 and T2 values on the baseline CMR, resolution of myocardial edema in T2w images and the reduction of LGE extent over the two-month period between the two CMR exams, along with the clinical improvement, indicate in this case a favorable evolution of myocardial inflammation after COVID-19 myocarditis. Nonetheless, elevated T1, T2, and ECV myocardial values in segments previously affected by LGE and edema compared to unaffected segments suggest that myocardial abnormalities may persist for a longer period with still-unknown clinical relevance in the specific context of COVID-19.

Conclusion

To our knowledge, this is the first case of convalescent COVID-19 with demonstration of myocardial inflammation regression in a short-term CMR follow-up for acute myocarditis caused by COVID-19. The case report also shows how Compressed Sensing CINE and free-breathing myocardial delayed enhancement (MDE) allowed good diagnostic imaging even in a patient who was severely short of breath. However, despite the favorable evolution of the myocardial inflammation, the follow-up CMR also indicated that myocardial abnormalities may continue beyond two months. Further research on the clinical relevance of this in a COVID-19 setting is needed.

References

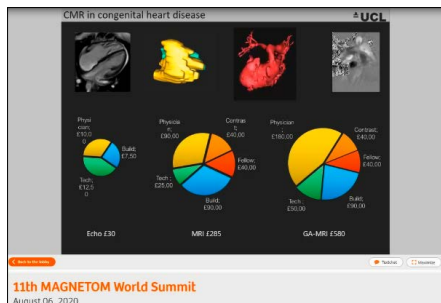
- 1 Huang L, Zhao P, Tang D, Zhu T, Han R, Zhan C, et al. Cardiac Involvement in Patients Recovered from COVID-19 Identified Using Magnetic Resonance Imaging. *JACC Cardiovasc Imaging*. 2020;S1936-878X(20)30403-4. doi: 10.1016/j.jcmg.2020.05.004. Epub ahead of print.
- 2 Puntmann VO, Carerj ML, Wieters I, Fahim M, Arendt C, Hoffmann J, et al. Outcomes of Cardiovascular Magnetic Resonance Imaging in Patients Recently Recovered from Coronavirus Disease 2019 (COVID-19). *JAMA Cardiol*. 2020:e203557. doi: 10.1001/jamacardio.2020.3557. Epub ahead of print.
- 3 Rudski L, Januzzi JL, Rigolin VH, Bohula EA, Blankstein R, Patel AR, et al. Multimodality Imaging in Evaluation of Cardiovascular Complications in Patients with COVID-19: JACC Scientific Expert Panel. *J Am Coll Cardiol*. 2020;76(11):1345-1357. doi: 10.1016/j.jacc.2020.06.080. Epub 2020 Jul 22.

Contact

Carlos Eduardo Rochitte
Cardiovascular CMR and CCT Coordinator
Hospital do Coração, HCOR,
Cardiovascular CMR and CCT sector
Rua Desembargador Eliseu Guilherme, 147
Paraíso – São Paulo – SP – Brazil
Zip – 04004-030
rochitte@gmail.com



Learn more!

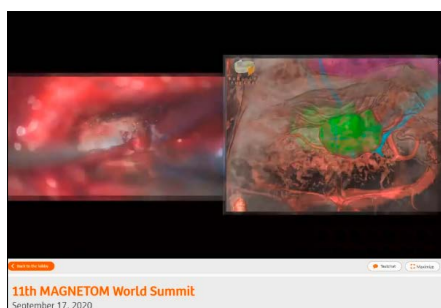


CMR in congenital heart disease

11th MAGNETOM World Summit
August 06, 2020

AI and Deep Learning. Where is CMRI heading to?

Vivek Muthurangu
University College London, UK



Towards Precision Surgery in Neurosurgery

11th MAGNETOM World Summit
September 17, 2020

Towards Precision Surgery in Neurosurgery

Bernard Bendok
Mayo Clinic, Phoenix, AZ, USA

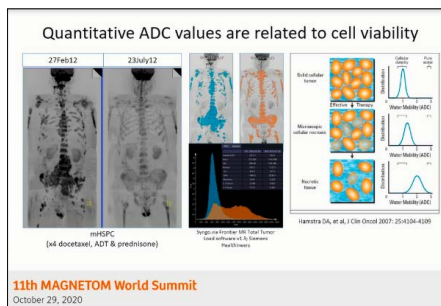


Rapid 3D multi-contrast evaluation of the brain

11th MAGNETOM World Summit
September 3, 2020

Wave CAIPI for Routine Clinical Brain MRI

Susie Huang
Harvard Medical School, MGH, Charlestown, USA



Quantitative ADC values are related to cell viability

11th MAGNETOM World Summit
October 29, 2020

Malignant Bone Disease Imaging in the Era of Precision Medicine

Anwar Padhani
Mount Vernon Cancer Centre, London, UK

Don't miss the talks delivered by experienced and renowned experts at the MAGNETOM World Summit

www.siemens-healthineers.com/MWS2020-recordings

New Clinical Possibilities and Increased Productivity after Upgrading from MAGNETOM Aera to MAGNETOM Sola Fit

Philip Chappel, MD

ZNA Jan Palfijn Hospital, Merksem, Belgium

Introduction

ZNA Jan Palfijn is an important general hospital in the north of the city of Antwerp in Belgium, covering almost all medical fields. The hospital serves outpatients in an outpatient clinic, as well as patients admitted to the hospital or receiving treatment in the day hospital. ZNA Jan Palfijn has a large, recently renovated emergency department and an important intensive care unit.

The hospital also includes an orthogeriatric department where orthopedists and geriatrists work together to provide optimal orthopedic treatment for vulnerable elderly patients. In 2016, the institute became part of the Iridium Cancer Network, a network of multidisciplinary doctors, nurses, and an extensive counselling team who strive for the optimal diagnosis, treatment, and aftercare of each individual cancer patient in the Greater Antwerp and Waasland region. The network has the specific technology and knowledge needed to offer intraoperative radiotherapy, radiosurgery, prostate brachytherapy, and innovative radiotherapy in clinical trials if necessary. In this context, we acquired a new PET-CT scanner in June 2018.

The medical imaging department at ZNA Jan Palfijn offers all imaging techniques: conventional radiography, mammography (the services are recognized as mammographic screening centers), computer tomography (CT), magnetic resonance imaging (MRI), and ultrasound examinations. Medical imaging is also used for infiltration of joints (under ultrasound or fluoroscopic guidance), fine needle aspiration cytology or FNAC (e.g., for thyroid gland nodules), and core biopsy (e.g., for breast lesions) whenever accurate visualization is important and a minimally invasive, non-operative technique is preferable.

We have one 1.5T MRI scanner in our facility, on which we perform a full range of MRI examinations – from neurological to musculoskeletal, abdominal, and breast. Cardiac MRI is the only examination we do not perform. When Siemens Healthineers offered us the possibility to upgrade our existing MAGNETOM Aera 1.5T system to a MAGNETOM Sola Fit with BioMatrix technology (Fig. 1), we considered this a good opportunity to expand our

clinical capabilities, reduce our acquisitions times, and increase our patient throughput at a very attractive cost-benefit ratio compared to installing an entirely new system.

We decided to purchase the world's first MAGNETOM Sola Fit upgrade and take part in the customer use test from Siemens Healthineers. In order to really compare and demonstrate the changes in MR scanning achieved with the upgrade, we installed a teamplay receiver on our MAGNETOM Aera system shortly before the upgrade. Additionally, we granted Siemens Healthineers the rights to analyze our system service data so that we could look into more detailed scan parameters. In order to make datasets comparable, we chose time periods with a comparable number of working days, avoiding times with a high number of holidays or vacations. The MAGNETOM Aera data presented here covers the period from June 19 to July 28, 2019, and the MAGNETOM Sola Fit data covers October 2 to November 10, 2019. In this article, we share our results after having operated the upgraded system for almost a year.



1 MAGNETOM Sola Fit at our institute.

Installation

The installation of the upgrade had to be really fast as we didn't have a back-up MRI system and couldn't scan any patients at all during the installation process. We received the MAGNETOM Sola Fit upgrade kit in the first week of August 2019. Even though this was the first installation of its kind globally, the upgrade went very smoothly and fast, taking a total of 13 working days for de-installation of old components, installation of the Sola Fit components as well as tuning and ramp-up. Due to a missing CE label, the go-live of the system was unfortunately delayed for another two days. The upgrade itself included new RF components, new electrical cabinets, new covers with BioMatrix touch panels, a new patient table, a new 32-channel spine coil with respiratory sensors, a new tiltable 20-channel head/neck coil with CoilShim technology, and a new MRI workplace with a large-screen monitor. All our existing licenses were transferred, and existing coils could be used after the upgrade. The upgrade also came with a new 18-channel transmit/receive knee coil, a 16-channel flexible shoulder coil, and new Turbo Suite licenses containing the latest acceleration techniques from Siemens Healthineers.

On the very first day of going live, the scanner already produced high-quality images. In the first week, we scanned volunteers and patients in the time slots we usually worked with in the past (to allow the technicians to get used to the new protocols and work environment). During the second week, we were able to scan patients within a shortened schedule and without significant delays at the end of the day.

New work environment

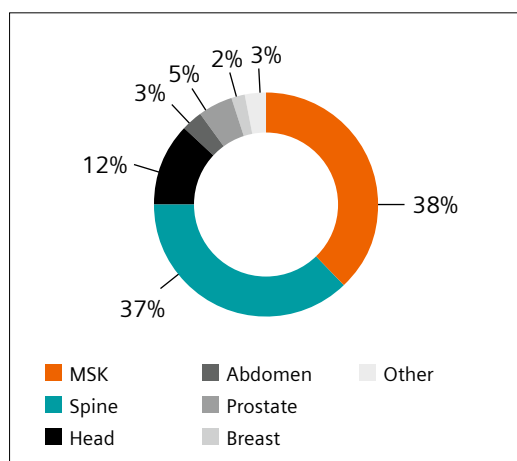
The upgrade not only brought many hardware changes, but also a completely new work environment and changes

to our workflows. In our medical imaging department, we have six technologists working with the MRI system. To help them become comfortable in working with the new equipment, we ordered online pretraining via the PEPconnect training platform from Siemens Healthineers, and two weeks of onsite training. After this training period, our technicians felt quite comfortable scanning in the new environment.

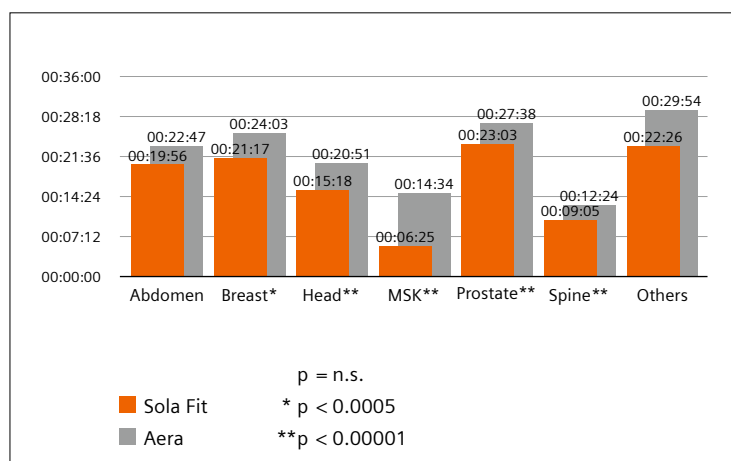
We gave ourselves really challenging goals for the time slots of our different examinations. In an intensive iterative approach between myself, head of the MRI unit, and the local Siemens Healthineers application specialist, each of our protocols were adapted to make use of the new sequences and acceleration techniques. In the end, we succeeded in performing all examinations in the given time slots while maintaining our high image-quality requirements.

Before-and-after comparisons

Our case mix before and after upgrading to the MAGNETOM Sola Fit system stayed more or less the same, though the period we chose for our productivity comparison showed a small shift from spine examinations to musculoskeletal (MSK) examinations. Generally, our case mix mainly consists of MSK (~40%), spine (~35%), and brain examinations (~15%) (Fig. 2). We also perform prostate, pelvis, breast, and abdominal scans. After the upgrade, we achieved significant improvements in all these clinical areas. As shown in Figure 3, the median examination times per body area were reduced across the board. The reductions are statistically relevant. In the following sections, we will show selected results as examples for the different regions.



2 Example case mix for MAGNETOM Sola Fit (Oct – Nov 2019).

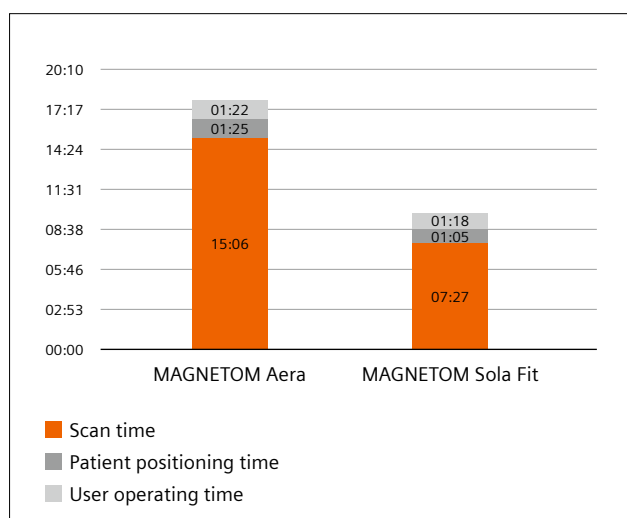


3 Mean exam duration for MAGNETOM Aera vs. Sola Fit per body region; statistical significance tested with Wilcoxon rank sum test for equal medians.

1. Musculoskeletal examinations

For standard MSK examinations, we mostly used 2D proton density (PD) sequences and fat-saturated T2 sequences in the different planes. After the upgrade, we adjusted, for instance, our knee protocols to one 2D PD sequence using Simultaneous Multi-Slice and one 3D SPACE sequence using Compressed Sensing acceleration and reconstruction of the different planes. Depending on the indication, we also follow this strategy for ankle examinations.

For routine knee examinations, this strategy allowed us to reduce the median examination time from 18 minutes to 10 minutes (Fig. 4).



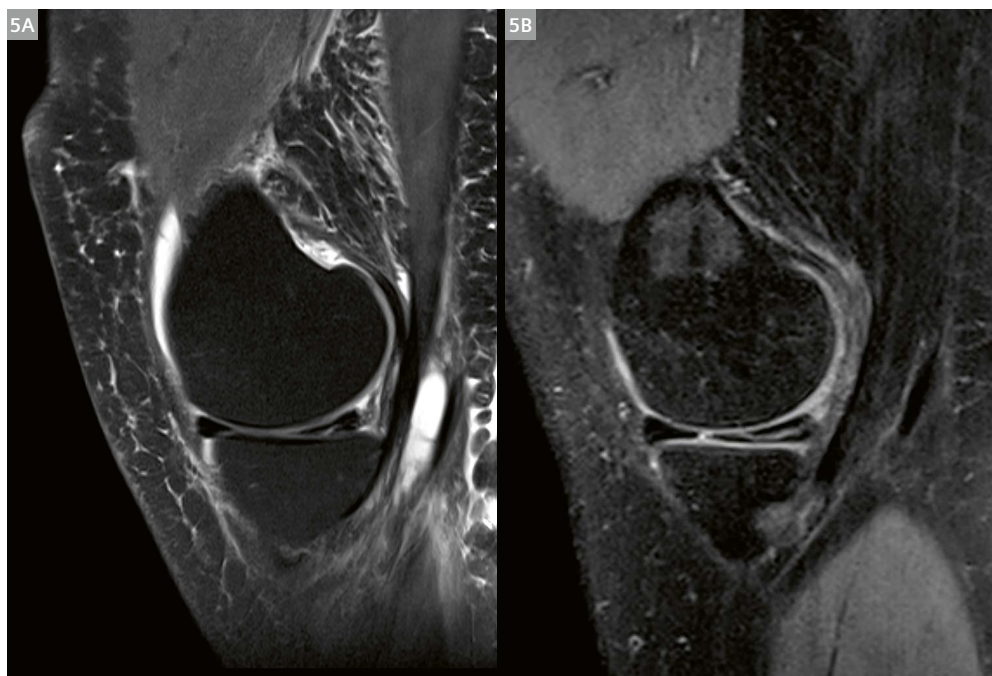
4 Median examination times for routine knee examinations before and after the upgrade.

The following knee examinations (Fig. 5) of horizontal tears of the posterior horn of the medial meniscus performed before and after the upgrade demonstrate how we reduced the overall acquisition time by 50% while maintaining diagnostic quality and information in our clinical images. Instead of running three T2 TSE FS sequences for all orientations, we now acquire only one 3D SPACE sequence. This allows us to reconstruct all planes and dramatically reduces the scan time.

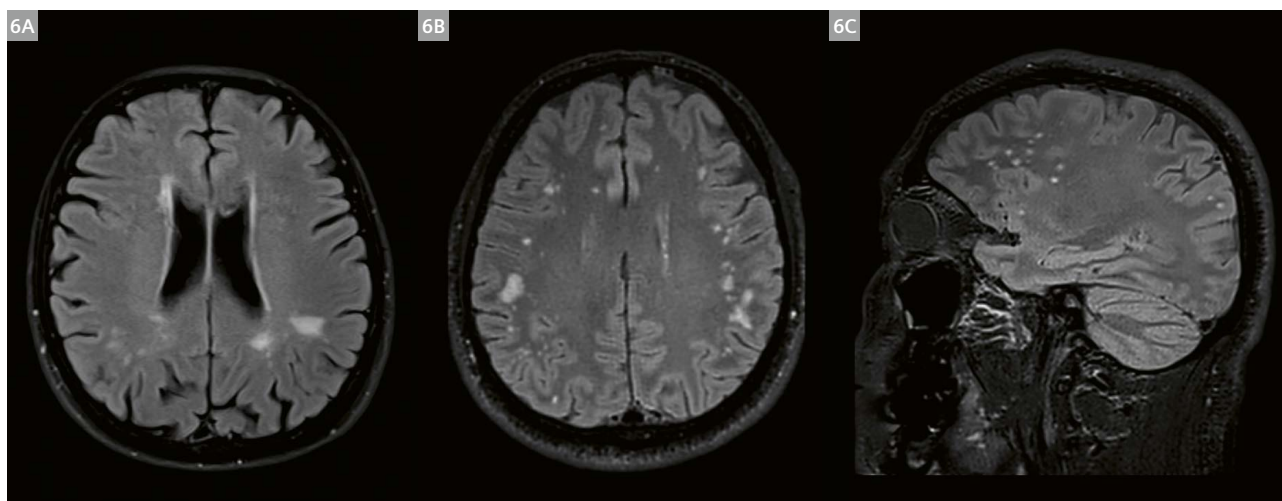
With the upgrade, we also acquired a new transmit/receive knee coil with 18 channels. This coil has a wider opening, which now allows us to scan nearly all obese patients, or knees with large swellings, where before we had to use the body coil. For shoulder imaging, we have the new flexible Shoulder Shape coil which achieves a better fit with the patient's anatomy and leads to a higher signal-to-noise ratio in general.

2. Neurological examinations

Our standard brain protocol consists of sagittal T1, transversal diffusion, T2 TSE, T2 FLAIR, and Time-of-Flight sequences where needed. After the upgrade, we now use Compressed Sensing acceleration for the FLAIR as well as the Time-of-Flight sequences. The following example (Fig. 6) shows two comparable cases acquired before the upgrade using a 2D FLAIR, and after the upgrade using 3D SPACE FLAIR with Compressed Sensing. As well as providing additional information through the different planes, the 3D SPACE FLAIR also has a higher and isotropic resolution of 0.6 mm and shows better white matter delineation.



5 Image (5A) is a T2 TSE FS acquisition before the upgrade, with $0.4 \times 0.4 \times 3 \text{ mm}^3$ resolution in TA 4:52 min. Image (5B) was acquired for the same indication after the upgrade using CS 3D SPACE with $0.4 \times 0.4 \times 0.5 \text{ mm}^3$ and TA 4:10 min.

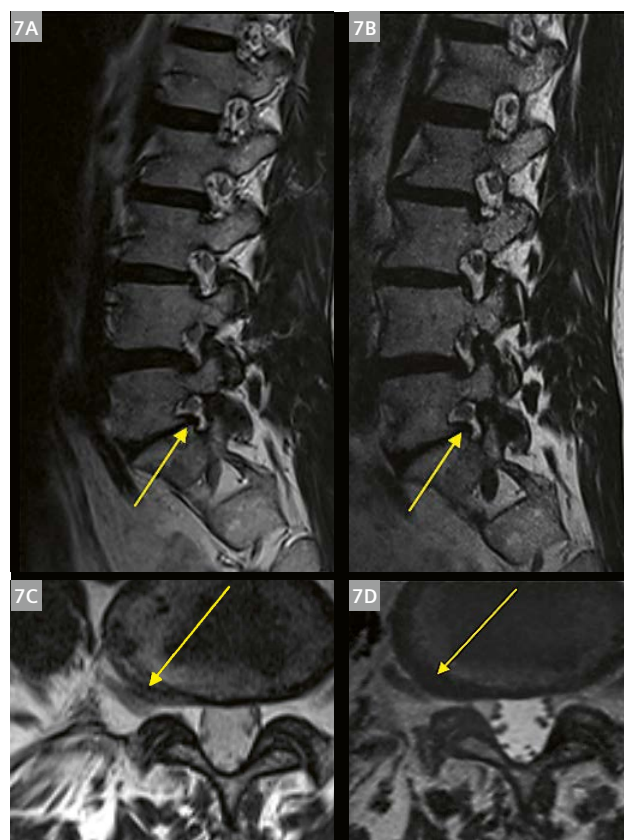


6 Comparison of FLAIR scans before and after upgrade: Image **(6A)** was acquired using a 2D FLAIR with $0.7 \times 0.7 \times 5 \text{ mm}^3$ in TA 4:32 min.; **(6B)** and **(6C)** are from one 3D SPACE FLAIR exam with 0.6 mm iso in TA 4:00 min.

With the BioMatrix upgrade, our head and neck patients now benefit greatly from the new tiltable head and neck coil. Some patients didn't fit in the head coil we used before, but now they can have an MRI exam thanks to the head tilt. Furthermore, we constantly use the coil in the 9° position, which gives all our patients more comfort and reduces motion artifacts.

3. Spine examinations

We have also reduced scan times in spine examinations by shifting to 3D SPACE instead of 2D gradient echo sequences for most indications. The following examples show two L-spine examinations in the same patient with neuroforaminal disc protrusion and discoradicular conflict, before and after the upgrade (Fig. 7). Images 7A and 7C are T2 TSE images acquired on our MAGNETOM Aera before the upgrade with an acquisition time of 3 minutes each. Images 7B and 7D were acquired with one 3D T2 SPACE sequence in 5:43 minutes on our MAGNETOM Sola Fit using Compressed Sensing.



7 L-spine examinations in the same patient with neuroforaminal disc protrusion and discoradicular conflict: **(7A)** and **(7C)** are T2 TSE images acquired before the upgrade in TA 2:57 min and 3:05 min respectively, and at a resolution of $0.7 \times 0.7 \times 3 \text{ mm}^3$; **(7B)** and **(7D)** are 2 mm MPRs from a Compressed Sensing 3D T2 SPACE sequence acquired on MAGNETOM Sola Fit in TA 5:43 min with a resolution of $0.4 \times 0.4 \times 0.45 \text{ mm}^3$.

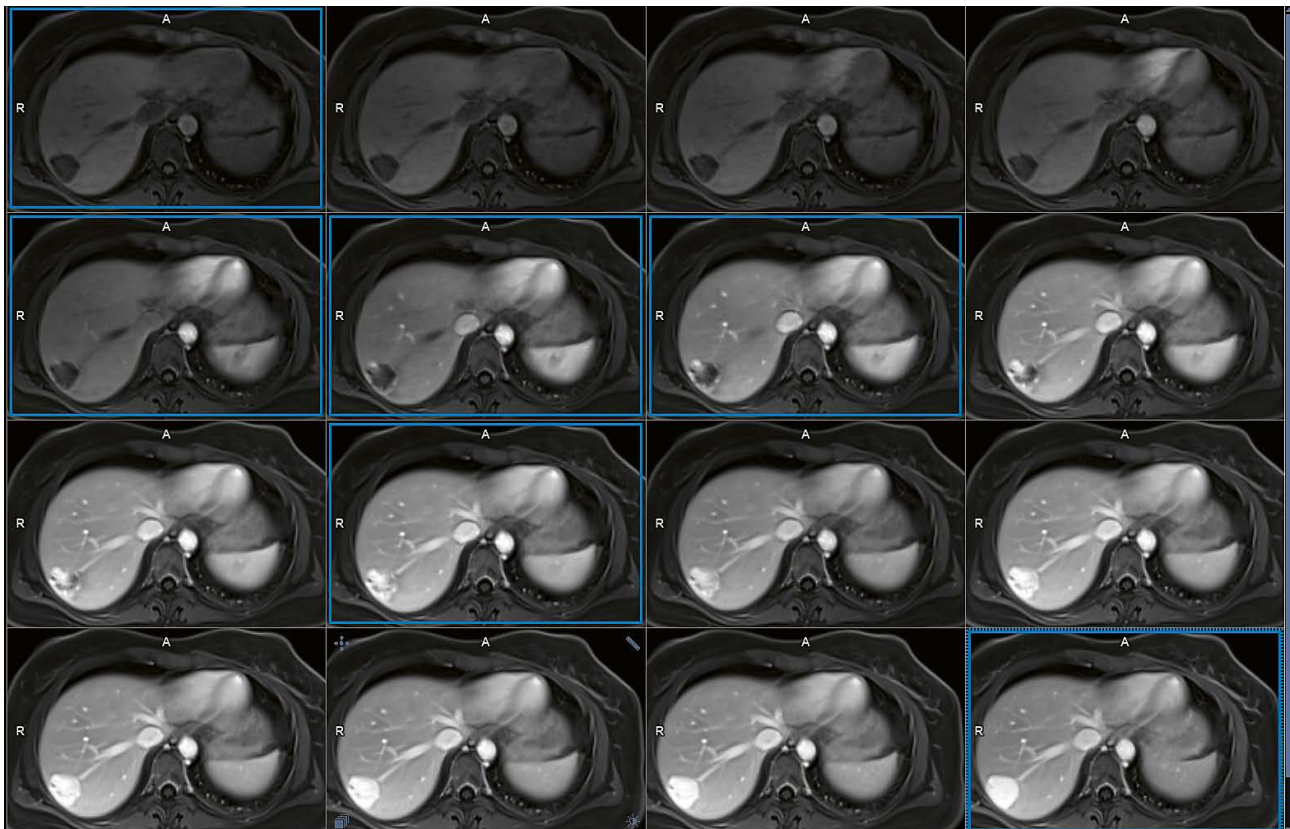
4. Abdominal examinations

For abdominal imaging, we particularly feel the benefits of the BioMatrix respiratory sensor during our MRCP examinations. Technicians no longer have to place the PACE navigator on the liver dome. This results in an easier workflow and faster acquisitions overall. The following example of a respiratory-triggered coronal T2 SPACE MRCP was acquired in 42 seconds using the built-in respiratory sensor (Fig. 8). The main pancreatic duct is dilated, with multiple cystic dilatations of the side branches (= mixed type IPMT).

Nearly all abdominal examinations are now performed under free breathing using the Compressed Sensing GRASP-VIBE technique. As well as being a great relief to many patients who struggle to hold their breath or follow breath-hold commands, it also increases our diagnostic confidence as we have more dynamic phases. In the images of a patient with liver hemangioma (Fig. 9) the high temporal resolution of GRASP-VIBE allows to visualize the gradual centripetal, nodular filling of the lesion in the liver (classical enhancement pattern of a hemangioma). Images with a blue frame are the automatically preselected phases identified by the GRASP-VIBE algorithm: one pre-arterial, three arterial, one portal-venous, and one late phase.



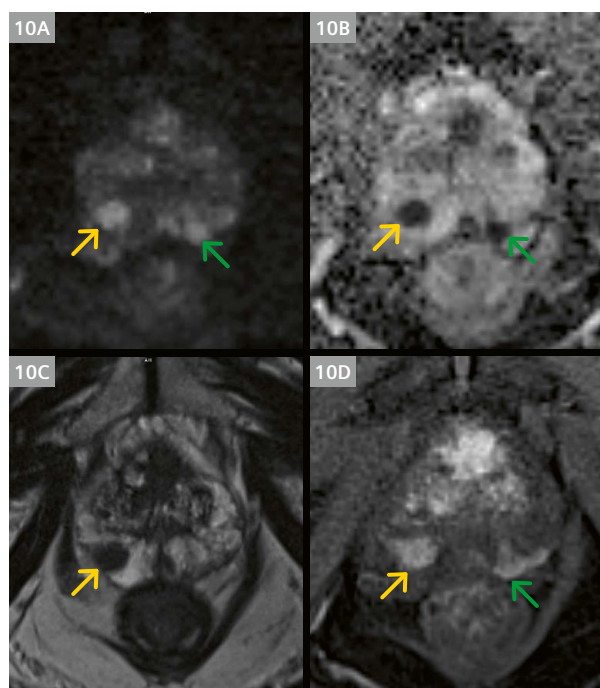
8 Coronal respiratory-triggered T2 SPACE MRCP acquired in 42 s with CAIPIRINHA 4 acceleration and using the built-in respiratory sensor as the triggering device.



9 Liver dynamics of a hemangioma using Compressed Sensing GRASP-VIBE with a temporal resolution of 8.6 s, acquired under free breathing.

5. Prostate examinations

After the upgrade, all routine prostate examinations now have an average examination time of 23 minutes. In our standard prostate protocol, we are now using the GRASP-VIBE technique for our dynamics and have incorporated high-resolution multi-shot diffusion – known as the RESOLVE technique. In this image example (Fig. 10) of a PI-RADS 4 lesion in the right peripheral zone (yellow arrow), a marked focal hyperintensity is seen at high b -value and a corresponding hypointensity is seen on ADC. In particular, the hyperintensity on the high b -value image of this proven malignant lesion is better appreciated on our DWI-RESOLVE sequence than on our DWI images before the upgrade. Also, a smaller PI-RADS 3 lesion is clearly depicted in the left peripheral zone on the same images (green arrow).

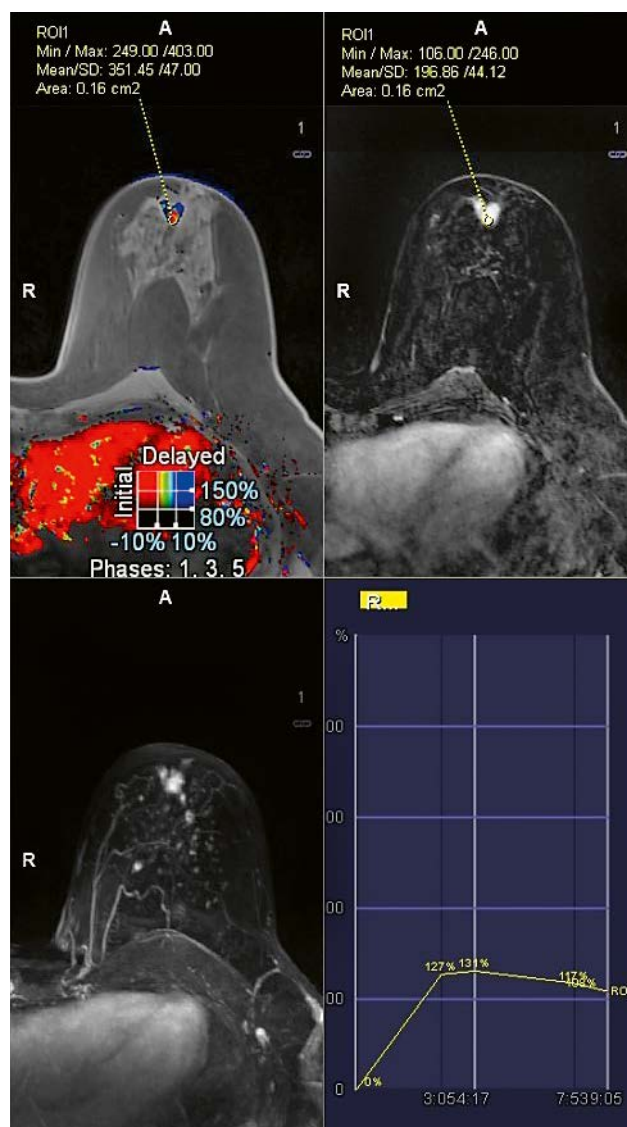


10 PI-RADS 4 lesion in the right peripheral zone and a smaller lesion in the left peripheral zone of the prostate in RESOLVE diffusion with $b=1000 \text{ s/mm}^2$ (10A), ADC image (10B), T2 TSE (10C), and Prostate GRASP-VIBE (10D) with high temporal resolution (during initial contrast uptake) of 1.8 s per frame.

6. Breast examinations

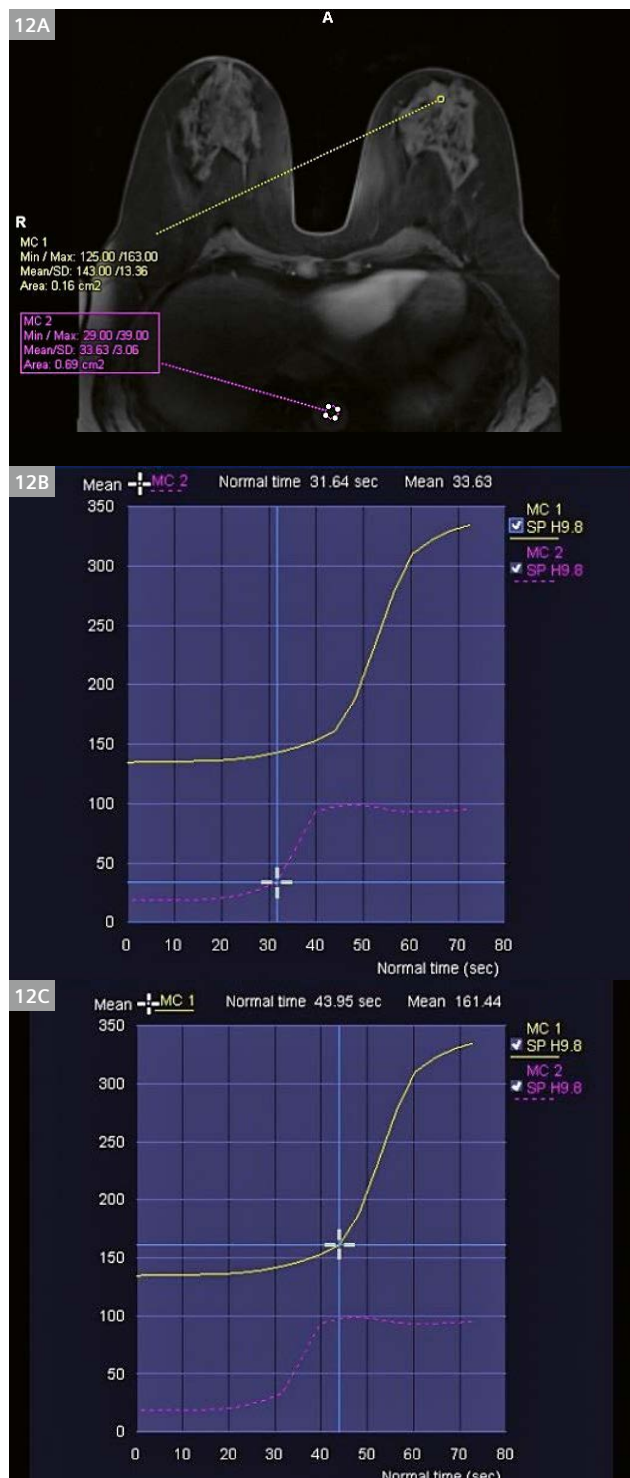
We adjusted our protocol for breast examinations. After contrast media injection, the first dynamic sequence has been replaced by a 1 minute Compressed Sensing GRASP-VIBE acquisition as a supplement in order to compare the outcome of GRASP-VIBE to conventional dynamic analysis. This has been especially useful for proving the benign characteristics of enhancing small lesions (using time-to-enhancement relative to the aorta).

In the following example, the lesion in the retro-areolar region of the left breast showed morphologic features suspicious for malignancy. On conventional dynamic analysis (T1 f13D FS), this lesion shows a type 2–3 time intensity curve, not entirely convincing for malignancy (Fig. 11).



11 Conventional dynamic analysis based on T1 f13D FS, not entirely convincing for malignancy.

The GRASP-VIBE sequence shows that the time difference between the start of enhancement in the lesion and in the aorta is 12.3 seconds, which is indicative of malignancy



12 GRASP-VIBE dynamics show a time difference of 12.3 s between the start of enhancement in the aorta (**12B**) and in the lesion (**12C**) below the malignancy threshold [1].

based on the 12.96 second threshold established by Mus et al. in Eur J Radiol. 2017 [1] (Fig. 12). This finding added diagnostic confidence, and pathologically this lesion proved to be malignant. There is another, smaller lesion located deeper and more laterally in the same breast, which has more or less the same morphologic characteristics (Fig. 13). The GRASP-VIBE sequence clearly shows the slower enhancement and a different type of enhancement curve compared to the bigger lesion, so we could state that this smaller lesion was probably benign. Anatomopathology of the smaller lesion proved it was benign (a fibro-adenoma).

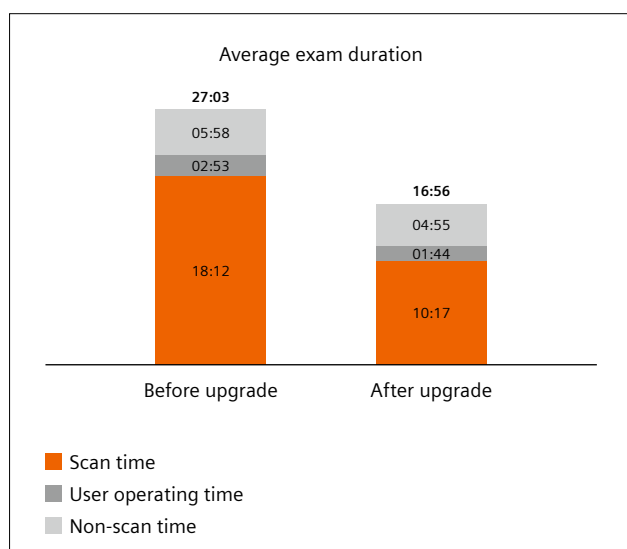


13 A smaller lesion located deeper and more laterally: a GRASP-VIBE sequence with slower enhancement and different enhancement curve led to the conclusion that the lesion was benign.

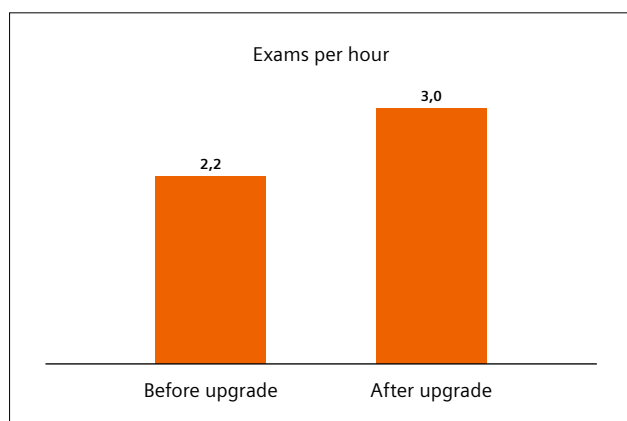
Increasing our productivity

In most of the body areas, we achieved much shorter examination times while maintaining our image quality. This is thanks to new sequence technologies that reduce our average exam duration by 37% (Fig. 14). Additionally, we reduced the patient changeover times from 5:58 minutes on average for all types of examinations to 4:55 minutes. This was thanks to the new patient positioning with the intelligent one-touch positioning that comes with the new system.

Thanks to all of this, we have significantly increased the number of patients that can be scanned per hour. Depending on the type of examination, we can scan up to 4 patients in an hour, which is a 30% increase on average (Fig. 15).



14 Comparison of average examination times.



15 Average number of exams per hour on MAGNETOM Aera (Jun – Jul 2019) and on MAGNETOM Sola Fit (Oct 19 – Nov 2019).

Conclusion

The installation of the Sola Fit upgrade went smoothly and quickly. Throughout the whole process, both I and our technicians could rely on the 24/7 support from the application specialists at Siemens Healthineers. The main benefits of the Sola Fit upgrade for our MRI unit are the accelerated acquisition times, increased patient throughput, and continuing high image quality. The new coils, especially the comfortable and tiltable head/neck coil, are also a major advantage. We see many clinical benefits, especially increased diagnostic confidence in prostate and mammography exams (GRASP VIBE, better diffusion images), abdominal exams (GRASP VIBE for liver lesions, MRCP with free breathing thanks to the respiratory sensors), and MSK exams (e.g., high-resolution 3D images of meniscal tears). Overall, we are glad to have upgraded to MAGNETOM Sola Fit.

Reference

- 1 Mus RD, Borelli C, Bult P, Weiland E, Karssemeijer N, Barentsz JO, et al. Time to enhancement derived from ultrafast breast MRI as a novel parameter to discriminate benign from malignant breast lesions. *Eur J Radiol.* 2017;89: 90–96.



Contact

Philip Chappel, M.D.
Head of MRI Unit
ZNA Jan Palfijn Hospital
Lange Bremstraat 70
2170 Merksem
Belgium
philip.chappel@zna.be
<https://www.zna.be/nl/zna-jan-palfijn>

Improving Productivity in MRI – Clinical Experience in a Multisite Outpatient Practice Setting

Mike Notohamiprodjo, M.D., MHBA; Gerwin Schmidt, M.D.

DIE RADIOLOGIE, Munich, Germany

Introduction

Magnetic resonance imaging (MRI) is one of the most commonly performed procedures and the financial backbone of diagnostic imaging. Since the populations of industrial countries are continuously aging and average morbidity is therefore increasing, demand for diagnostic procedures is growing. Labor and operating costs, however, are rising while reimbursement for medical procedures is declining. This makes efficient exploitation of the available resources of pivotal importance in an increasingly competitive healthcare market.

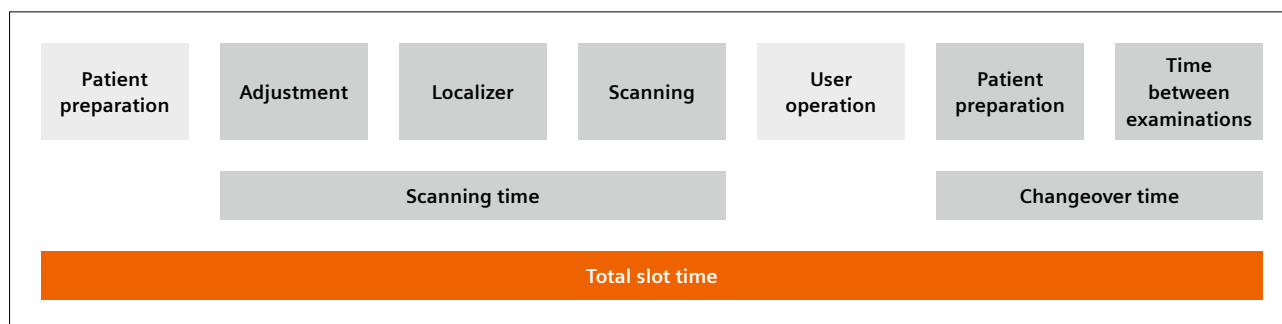
Expanding the number of examined patients per MR scanner will help to meet the growing clinical demand and reliably improve profitability [1].

For this reason, an efficient and productive workflow with short patient changeover and acquisition times is essential. MR protocols should be sufficiently short, without losing time for planning and setting up the examinations. At the same time, high image quality has to be maintained to ensure diagnostic relevance. Investing in new acceleration techniques and workflow solutions will help to achieve these goals and bring forward the break-even point.

The recently introduced BioMatrix Technology and syngo MR XA software provide several methods to streamline the daily workflow of MR technologists. In order to

shorten patient changeover times, automated selection and positioning of coils have been integrated, as has automation of image acquisition using Dot engines. In addition to established parallel imaging techniques such as GRAPPA and CAIPIRINHA, advanced acceleration methods have been integrated into the clinical protocols: Simultaneous Multi-slice (SMS) imaging employs complex RF pulses to simultaneously acquire several sections along the z-axis, allowing a significant reduction in the image acquisition time by shortening the required TR time with little SNR penalty [2], while Compressed Sensing (CS) rapidly accelerates MR imaging by reconstructing sparse data from a highly undersampled *k*-space [3].

DIE RADIOLOGIE, a large radiology network in the Munich area, recently installed a 1.5T MAGNETOM Sola scanner equipped with BioMatrix Technology and the newest acceleration techniques, as provided by the syngo MR XA20 software. Recent studies have shown that these methods can shorten individual sequences and entire examinations. However, we were interested to know whether the integrated technology is also effective in daily clinical routine and whether it could potentially increase the profitability of an MR scanner.



1 Definition of the components of an examination slot.

To study the effects of these novel techniques on patient throughput and subsequently on profitability, we performed a retrospective study that compared a 1.5T MAGNETOM Sola scanner with its predecessor, the 1.5T MAGNETOM Aera, in daily clinical routine.

Material and methods

MR scanners

DIE RADIOLOGIE is one of Germany's largest diagnostic imaging service providers with currently 13 outpatient practice sites in and around the Munich area. It operates 15 MR scanners, performing over 150,000 examinations per year. Over 250 healthcare professionals working as physicians, technologists, front-desk and administrative staff ensure that diagnostic and interventional procedures are performed to a high level.

The MAGNETOM Sola and MAGNETOM Aera (both Siemens Healthcare, Erlangen, Germany) are operated at different but similar sites in Munich. At each of these sites, another 1.5T scanner is operated in an adjacent suite.

The MAGNETOM Sola (software version *syngo* MR XA20; XJ gradients with 33 mT/m at 125 T/m/s, 32 channels) was installed mid-2019 and is equipped with a full coil set (20-channel tiltable head-neck-coil, 24-channel spine coil, 12-channel body coil, 16-channel Shoulder Shape coil, 18-channel Tx/Rx knee coil, 18-channel UltraFlex coil, 16-channel hand/wrist-coil, and 16 channel foot/ankle-coil), as well as the Turbo Suites Essential (iPAT, tPAT, PAT², CAIPIRINHA VIBE, CAIPIRINHA SPACE) and Excelerate (SMS EPI for DWI / DTI / BOLD, SMS TSE, CS TOF, CS SPACE), so that, in particular, Simultaneous Multislice imaging for DWI and TSE sequences and Compressed Sensing for MRCP and 3D time-of-flight sequences can now be integrated into clinical protocols. Furthermore, automated coil selection and patient positioning was applied.

The MAGNETOM Aera (software version *syngo* MR D13D, XQ gradients with 45 mT/m at 200 T/m/s, 48 channels) has been in operation since 2013, and features a similar coil set to the MAGNETOM Sola (20-channel head-neck coil, 32-channel spine coil, 18-channel body coil, 16-channel shoulder large/small, 15-channel Tx/Rx knee coil, 4-channel flex coil, 16-channel hand/wrist-coil and 16-channel foot/ankle coil). The most recent acceleration techniques, SMS and CS, are not available on this scanner.

Core examination times were between 8 a.m. and 6 p.m. on both systems. During core times, both scanners are usually operated by two technologists. The standard examination slot is 20 minutes long, so that three patients are examined per hour on average.

Usually, several examination slots are grouped by body region to minimize coil setup and examination

times. There is no scheduled break during the day.

The standard examination schedule for both scanners mainly consists of musculoskeletal and body imaging slots.

Prior to the study, internal and external application specialists matched the image quality of the MAGNETOM Sola to the MAGNETOM Aera, applying available acceleration techniques to shorten examination times. Image quality was approved by the authors of the study.

Data collection

Capacity utilization of the scanners was monitored using the cloud-based service teamplay (Siemens Healthcare, Erlangen, Germany) from August to October 2019.

The extracted data comprised the body region examined, the coils used, the timepoints of patient registration, and all acquired sequences, including localizers and completion of the examination.

Using this data, parameters such as average patient preparation time before examination, average scanning time, average user operating time, average patient preparation time after examination, average time between examinations, and changeover time (sum of the last two items) could be derived (Fig. 1).

Only data collected during the core time between 8 a.m. and 6 p.m. was included. Days on which scanners were out of operation for more than one hour due to maintenance, for example, were excluded from the analysis.

Statistical analysis

Scanner operating times were found to exhibit normal distribution based on visual evaluation and were therefore summarized as mean values. To investigate differences between scanner operating times, one-tailed *t*-tests were performed on two independent samples with null hypotheses of time differences that equal zero and alternative hypotheses of greater time values for the MAGNETOM Aera than for the MAGNETOM Sola. Due to multiple testing, a *p*-value of < 0.001 (Bonferroni-corrected) was considered statistically significant. Time savings as a percentage were calculated as a time difference in relation to the operating times of the MAGNETOM Aera. Statistical analyses were conducted using Stata 16.1 (Stata Corporation, College Station, TX, USA).

Results

Examination mix

The most commonly performed examination on both scanners was MRI of the knee (Sola vs. Aera; 23% vs. 18%), of the lumbar spine (15% vs. 18%), of the cervical spine (12% vs. 16%), and of the shoulder (11% vs. 10%). Significantly more brain MRIs were performed on the MAGNETOM Aera than on the MAGNETOM Sola (6% vs. < 1%) (Fig. 2).

Clinical throughput

The average number of patients examined during the core time was significantly higher ($p < 0.001$) for the MAGNETOM Sola, $n = 30$ as opposed to $n = 26$ for the MAGNETOM Aera. This is a difference of 16%. On the busiest day, the number of examined patients was $n = 33$ for the MAGNETOM Sola and $n = 29$ for the MAGNETOM Aera.

The highest reduction in total slot time was achieved for MRI of the thoracic spine (21:55 vs. 28:09 minutes), lumbar spine (18:49 vs. 22:46 minutes), and the abdomen (22:23 vs. 26:57 minutes). The highest reduction in the average scan time was achieved for MRI of the knee (10:56 vs. 13:31 minutes), abdomen (14:20 vs. 17:34 minutes), and thoracic spine (14:41 vs. 17:18 minutes). The average slot time length was significantly shorter ($p < 0.001$), with 19:58 minutes for the MAGNETOM Sola and 22:35 minutes for the MAGNETOM Aera. The total slot time for the most commonly performed regions knee, lumbar and cervical spine, shoulder and ankle was reduced by between 10% and 17% on the MAGNETOM Sola (Fig. 3).

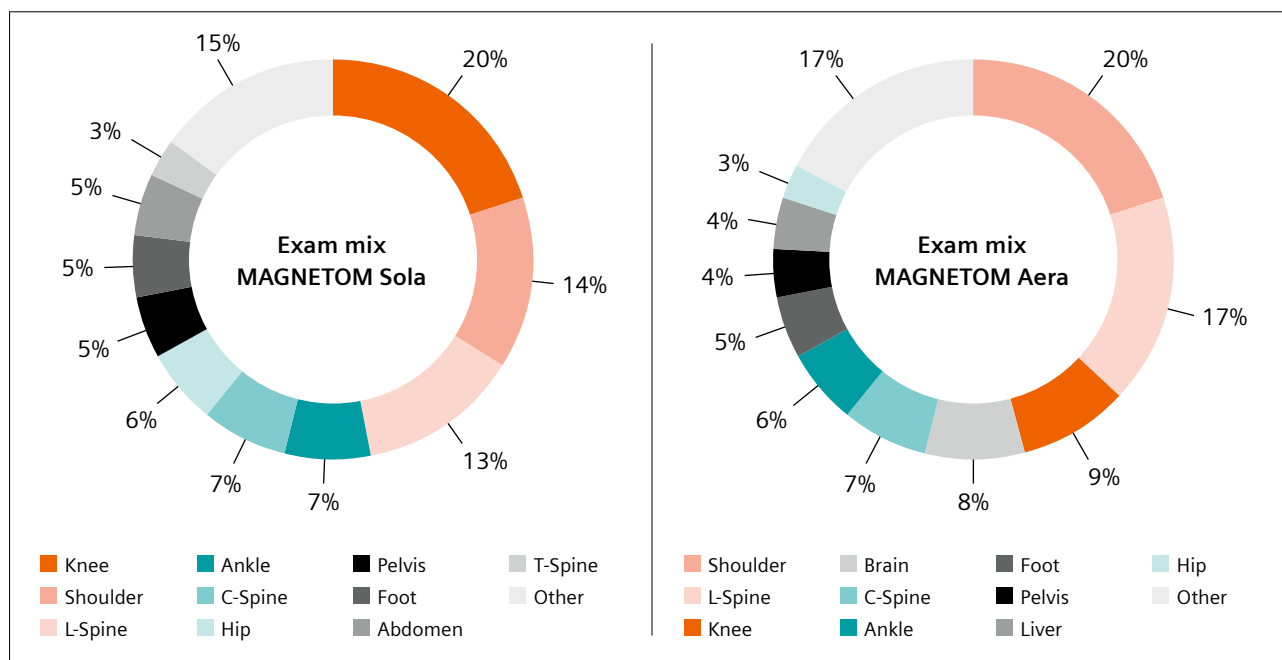
The overall average scanning time (adjustment, localizers, and measurement) on the MAGNETOM Sola was significantly, that is 12%, shorter ($p < 0.001$) than on the MAGNETOM Aera (12 minutes vs. 15 minutes). The average operating time (time for planning, patient communication during measurement) was also significantly, that is 22%, shorter ($p < 0.001$) for the MAGNETOM Sola (1:45 minutes vs. 2:15 minutes). The average changeover time (patient preparation after examination and time

between examinations) was 3:42 minutes for the MAGNETOM Sola and 3:54 for the MAGNETOM Aera (Fig. 4), and therefore not significantly different.

Discussion

Our clinical productivity study shows that clinical throughput was significantly higher on the MAGNETOM Sola when compared with a similarly equipped MAGNETOM Aera. The average examination slot time was shortened by 2.5 minutes, which can be largely attributed to a shorter scanning time. The most frequently performed MR procedures were shortened by 11–17%, while maintaining similar image quality. These findings are of interest because the MAGNETOM Aera features stronger gradients and a higher number of channels while the MAGNETOM Sola is equipped with more recent accelerated acquisition techniques and coils.

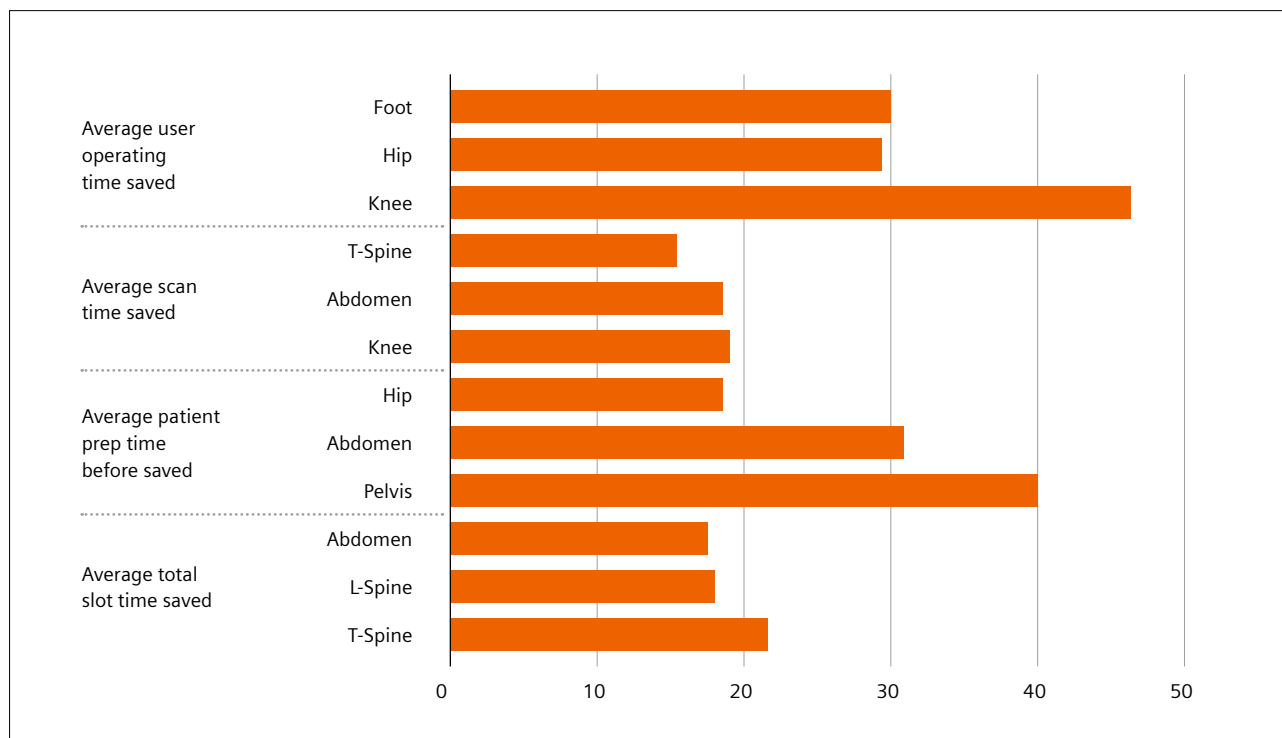
The results of this study are significant because diagnostic imaging providers are also financial units, which are expected to achieve a certain profitability to meet the economic agenda of their respective shareholders. DIE RADIOLOGIE is still privately owned by its associate physicians, so that medical aspects such as high-quality examinations and precise diagnostic tests, an appropriate working environment, and comfortable patient experience still take precedence over purely financial aspects. In principle, a further shortening of the protocols is still potentially possible if necessitated by financial circumstances. However, for the time being we have decided against further accelerating MR protocols.



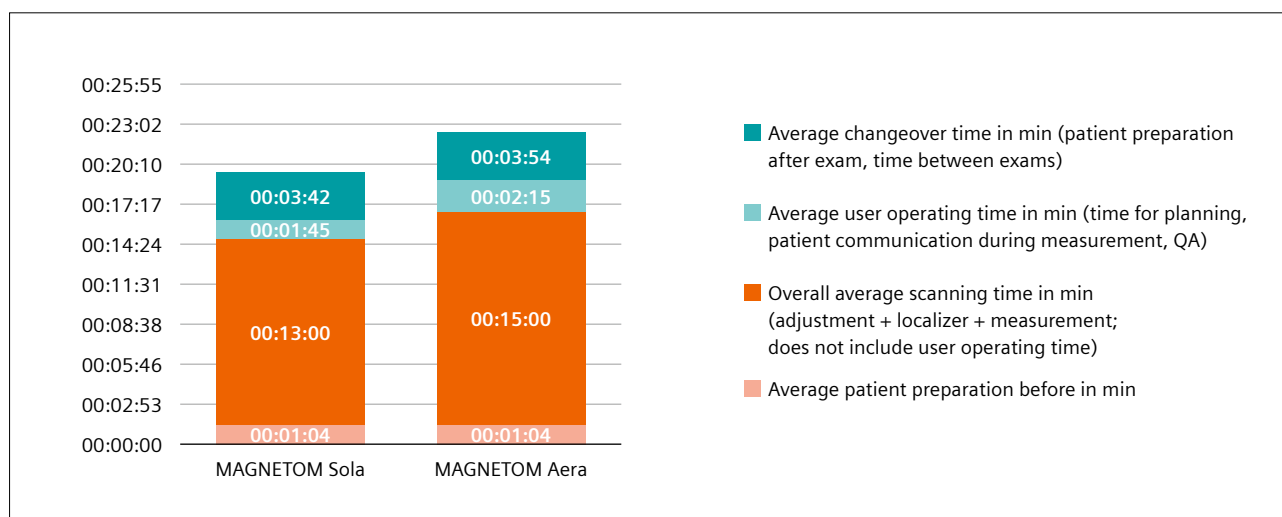
2 Exam mix of the MAGNETOM Sola and Aera.

With increasing patient throughput, a reduction in patient scanning time is one of the key components for shortening the examination slot time. While parallel imaging, usually with a GRAPPA acceleration factor of $R = 2$, is applied to most acquisition sequences, we have also integrated SMS acceleration into our clinical routine protocols on the MAGNETOM Sola to allow for a four-fold acceleration (achieved by combining GRAPPA $R = 2$ and SMS = 2). We have found that SMS acquisition is particular-

ly helpful in examinations in which several slices are acquired, such as transversal sections of extremities or pelvic MR examinations. These findings corroborate previous studies, showing a significant reduction in the examination time when using this respective technique for rapid musculoskeletal imaging [4, 5] or diffusion-weighted imaging, particularly of abdominal organs [2, 6] and the prostate [7].



3 Top three savings in % by time category.



4 Time allocation comparison.

Alternatively, sequences accelerated with Compressed Sensing may lead to a significant reduction in acquisition time, such as for musculoskeletal imaging [1, 8, 9] or body imaging [3, 10, 11]. In our study, Compressed Sensing was applied for the acquisition of MRCP sequences in one breath-hold [3], providing excellent image quality in a considerably shortened acquisition time compared with the lengthy standard navigator-triggered acquisition technique, which is also susceptible to respiratory motion. The significantly shorter acquisition time of MRCP sequences most likely contributed considerably to the reduction in scan time for abdominal MRI on the MAGNETOM Sola.

Another important factor when attempting to accelerate patient throughput is shortening the non-scanning time, which consists of the changeover time and the operating time. The average changeover time was slightly shorter for the MAGNETOM Sola, which features automated coil detection and positioning. The operating

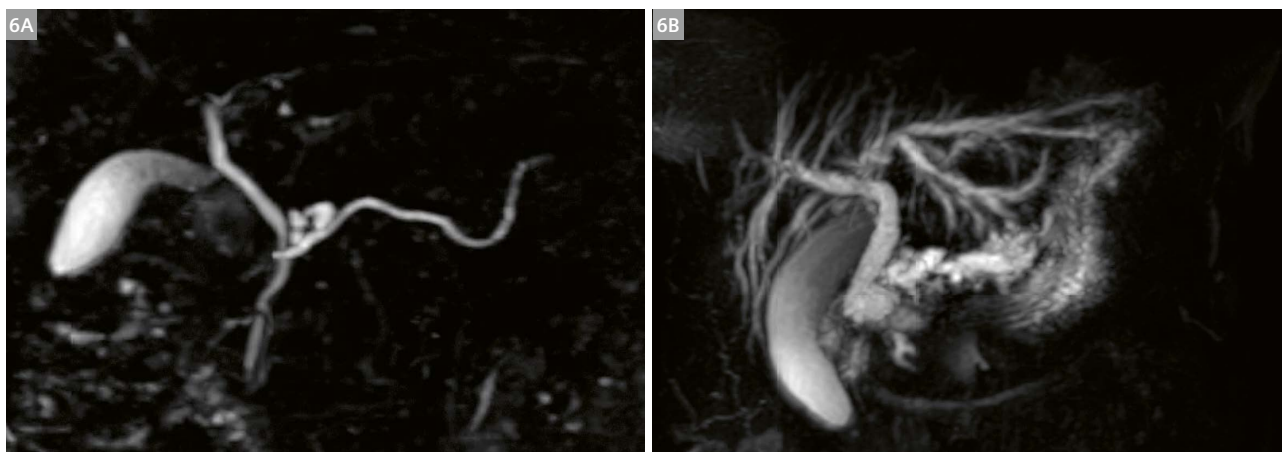
time was shortened by 22%, presumably by exploiting the automated positioning of sequences in spine and knee examinations.

On average, the MAGNETOM Sola permitted the examination of four additional patients during the core scanning time. If we extrapolate the results of this study, we can expect to scan approximately one thousand additional patients each year, or save more than 300 hours of labor time. Both scenarios mean a significant increase in profitability of the scanner with a quick return on investment, while diagnostic image quality is maintained. It should be noted, however, that the additional examinations cause additional workload for the radiologists, so that any further acceleration of complex examinations would require the assistance of artificial intelligence to support quick and reliable diagnosis [12].

This study has its limitations. First, the study was performed three months after installation of the



5 Example MRI of the knee acquired with the MAGNETOM Sola: Fat-saturated PD-weighted images in three planes (matrix 384 / slice thickness 3 mm / scan time 2 minutes approx. each / GRAPPA 2 / SMS2) and sagittal T1-weighted sequence (matrix 448 / slice thickness 3 mm / scan time 1:30 minutes / GRAPPA 2). Total scan time was approximately nine minutes including localizers / shimming / user operation.



6 Example MRCP accelerated with CS acquired with the MAGNETOM Sola: **(6A)** Examination of a 56-year-old male patient with a branch duct type intraductal papillary mucinous neoplasia. **(6B)** Examination of a 62-year-old female patient with a papillary mass obstructing the common bile duct and pancreatic duct. Scan time was 18 seconds each.

MAGNETOM Sola, which was compared with a system that had been in operation for seven years, so further refinement of protocols and therefore acceleration is to be expected. Second, each scanner was operated by a different team of technologists, so that changeover and operating times, for example, could also be dependent on the individual speed of the technologist. However, the reduction in slot duration was largely achieved by adjusting the scanning time. Thirdly, we did not factor in repetition of sequences, for example, due to motion artifacts, or canceled examinations, which resulted in an increased time between examinations.

In summary, the advanced acceleration techniques of the MAGNETOM Sola allowed for a significant reduction in examination time, leading to a higher throughput during clinical routine and therefore dramatically increasing profitability of the scanner.

Acknowledgments

We would like to thank Dr. Roberto Lorbeer from Ludwig-Maximilians-University (LMU) Munich for advice on the statistical analysis.

References

- 1 Bratke G, Rau R, Weiss K, Kabbasch C, Sircar K, Morelli JN, et al. Accelerated MRI of the Lumbar Spine Using Compressed Sensing: Quality and Efficiency. *J Magn Reson Imaging*. 2019;49(7):e164-e75.
- 2 Taron J, Martirosian P, Schwenzer NF, Erb M, Kuestner T, Weiss J, et al. Scan time minimization in hepatic diffusion-weighted imaging: evaluation of the simultaneous multislice acceleration technique with different acceleration factors and gradient preparation schemes. *MAGMA*. 2016;29(5):739-49.
- 3 Taron J, Weiss J, Notohamiprodjo M, Kuestner T, Bamberg F, Weiland E, et al. Acceleration of Magnetic Resonance Cholangiopancreatography Using Compressed Sensing at 1.5 and 3 T: A Clinical Feasibility Study. *Invest Radiol*. 2018;53(11):681-8.
- 4 Fritz J, Fritz B, Zhang J, Thawait GK, Joshi DH, Pan L, et al. Simultaneous Multislice Accelerated Turbo Spin Echo Magnetic Resonance Imaging: Comparison and Combination With In-Plane Parallel Imaging Acceleration for High-Resolution Magnetic Resonance Imaging of the Knee. *Invest Radiol*. 2017;52(9):529-37.
- 5 Kaller S, Rullmann M, Patt M, Becker GA, Luthardt J, Girbardt J, et al. Test-retest measurements of dopamine D1-type receptors using simultaneous PET/MRI imaging. *Eur J Nucl Med Mol Imaging*. 2017;44(6):1025-32.
- 6 Taron J, Weiss J, Martirosian P, Seith F, Stemmer A, Bamberg F, et al. Clinical Robustness of Accelerated and Optimized Abdominal Diffusion-Weighted Imaging. *Invest Radiol*. 2017;52(10):590-5.
- 7 Weiss J, Martirosian P, Taron J, Othman AE, Kuestner T, Erb M, et al. Feasibility of accelerated simultaneous multislice diffusion-weighted MRI of the prostate. *J Magn Reson Imaging*. 2017;46(5):1507-15.
- 8 Fritz J, Fritz B, Thawait GK, Raithel E, Gilson WD, Nittka M, et al. Advanced metal artifact reduction MRI of metal-on-metal hip resurfacing arthroplasty implants: compressed sensing acceleration enables the time-neutral use of SEMAC. *Skeletal Radiol*. 2016;45(10):1345-56.
- 9 Fritz J, Raithel E, Thawait GK, Gilson W, Papp DF. Six-Fold Acceleration of High-Spatial Resolution 3D SPACE MRI of the Knee Through Incoherent k-Space Undersampling and Iterative Reconstruction-First Experience. *Invest Radiol*. 2016;51(6):400-9.
- 10 Weiss J, Notohamiprodjo M, Taron J, Martirosian P, Nickel D, Bamberg F, et al. Continuous Hepatic Arterial Multiphase Magnetic Resonance Imaging During Free-Breathing. *Invest Radiol*. 2018;53(10):596-601.
- 11 Weiss J, Notohamiprodjo M, Martirosian P, Taron J, Nickel MD, Kolb M, et al. Self-gated 4D-MRI of the liver: Initial clinical results of continuous multiphase imaging of hepatic enhancement. *J Magn Reson Imaging*. 2018;47(2):459-67.
- 12 Rueckel J, Kunz WG, Hoppe BF, Patzig M, Notohamiprodjo M, Meinel FG, et al. Artificial Intelligence Algorithm Detecting Lung Infection in Supine Chest Radiographs of Critically Ill Patients With a Diagnostic Accuracy Similar to Board-Certified Radiologists. *Crit Care Med*. 2020.



Gerwin Schmidt



Mike Notohamiprodjo

Contact

Prof. Mike Notohamiprodjo
Deputy Managing Partner
DIE RADIOLOGIE
Sonnenstr. 17
80331 München
Germany
Phone: +49 (89) 550596-0
Mike.Notohamiprodjo@die-radiologie.de

Utilizing Blended Learning for Customer Support During the COVID-19 Pandemic: An Experience from the UK and Ireland

Chris Kasap, MRI Clinical Expert Applications Specialist

With thanks to Karen Hackling-Searle, Head of MRI, Cobalt Health

Introduction

The coronavirus (SARS-CoV-2) pandemic continues to spread, confronting MRI staff around the world with unprecedented clinical and operational challenges [1]. As radiographers and radiologists innovate to deal with this extraordinary situation, they must also continue to care for their patients [2].

The urgency and complexity of the current situation allows us to provide support using the existing training portfolio of blended learning [3]. Beginning MRI scanning with a new vendor is already challenging, but in the current context of lockdown, self-isolation, and staff sickness, the benefits of blended learning and remote support really come to the fore [4].

Globally, governments are implementing self-isolation, social distancing, and working from home whenever possible in order to reduce the spread of the disease and to minimize morbidity and mortality rates and demands on healthcare resources including the National Health Service & Health Service Executive (HSE) Ireland public hospitals [5]. The objective is to reduce the R (reproduction number) of coronavirus (SARS-CoV-2) and thus reduce its spread [6]. The R value is the average number of people that one infected person will pass the virus on to [7]. At Siemens Healthineers, we are aware of the urgency and complexity of the current situation, and we are working hard to use digital services to provide the best possible support to healthcare providers during COVID-19.

Blended Learning

With the aim of minimizing on-site attendance to that which is absolutely essential, the UK & Ireland Customer Services Applications & Education team escalated and intensified the provision of Blended Learning packages for customer training to help providers meet the challenge of the coronavirus pandemic [4].

The key was and is to successfully plan and manage a bespoke training package that enables the delivery of a viable remote training solution for our customers.

The customer

Cobalt Health (Cobalt) is a medical charity, primarily supporting people affected by cancer and dementia. They deliver exceptional quality diagnostic MRI, CT, and PET/CT services for over 75,000 patients each year at their imaging centre in Cheltenham and research imaging centre



1 MRI clinical leads Jono Humphris and Zoe Wray practicing social distancing in front of 1.5T MAGNETOM Solo.

Birmingham and through a modern fleet of mobile MRI and CT scanners that travel throughout the UK. They fund and participate in and support research on a local, national, and international level and provide unique education events for medical professionals on a national and international basis. They work collaboratively with the NHS and other carefully selected and respected industry partners to pioneer significant advancements for the benefit of patients now and into the future.

As a charity, Cobalt believes that everyone should have access to the best medical imaging for their diagnosis, supporting clinicians to make a clear diagnosis and produce appropriate and personalized treatment plans for precision medicine [8, 9]. This focus on precision medicine is consistent with the aims of Siemens Healthineers.

At the imaging center in Cheltenham, a 1.5T MAGNETOM Sola with syngo MR XA20 software has just been installed to help the facility stay at the forefront of diagnostic imaging. The Institute of Translational Medicine Imaging Centre in Birmingham houses a 3T MAGNETOM Skyra pTX, and the staff also have access to a relocatable 1.5T MAGNETOM Aera.

The challenge

The COVID-19 situation poses unprecedented challenges for customer training. Many hospitals are restricting access for any external personnel, including staff from Siemens Healthineers, unless absolutely essential. On March 3, the UK government warned that a fifth of the national workforce could be absent from work during the

SARS-CoV-2 peak [10], which has implications for both the customer workforce and the MRI applications workforce. As we confront these new challenges, both personal and professional, we must not lose sight of the fact that our customers are facing even bigger challenges and obstacles.

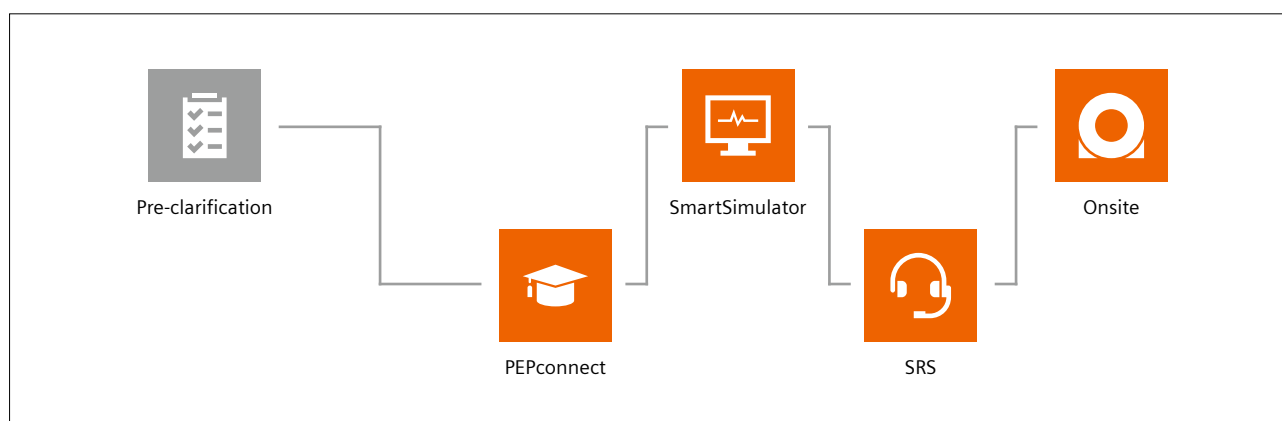
Recent travel restrictions, containment measures, and redeployment of imaging staff to other modalities such as CT have resulted in customers cancelling the majority of onsite visits and training for MRI applications. In addition, the UK Siemens Healthineers Academy has also been closed for classroom courses. Though this may pose great difficulties, it does not negate the need to continuously support our customers. Now more than ever, we must find new and innovative ways to deliver on our promise of outstanding customer support and education.

The need for transitioning from onsite to online training has never been higher or more crucial. Remote training allows us to be more flexible and, most importantly, to more easily adapt to the ever-changing needs of our customers during the pandemic.

With this goal in mind, the Customer Services MR Education & Applications team began offering a COVID-19 Blended Learning package to help successfully plan, manage, and execute a remote training package for customers.

Blended Learning consists of four pillars

Blended Learning is an evolutionary approach to applications training that consists of four pillars (shown in Figure 2), which are based on a pre-clarification meeting.



2 The four pillars of Blended Learning: PEPconnect, SmartSimulator, Siemens Remote Service (SRS), and Onsite support.

3

Customer and site information

Person completing this questionnaire

Date and time

Preferred training dates

Customer site

Site name

Full address

ex. Henkestr.127, 91052 Erlangen (Germany)

Customer hours of operation

ex. Mo-Fr 8-18:30, Sa 9-12:15

Type of customer

Further details on customer profile

Number of customer sites

This customer facility (choose)

☐ Works as stand-alone facility
 ☐ Serves as centralized reference/primary facility for other satellites.
 ☐ Serves as a satellite for centralized reference/primary facility? Which one(s)?
☐ Works in conjunction with another facility. Which one?

Department/site using/receiving images from this system

Details/contact person in the department/site (include details in customer participants list)

◀
▶

Customer & Site

Department Focus

Participants

MR System purchased

Clinical Usage

Environment & Operators

Customer Expectation

Restricted © Siemens Healthcare GmbH, 2019

The pre-clarification meeting

This was undertaken using a piloted standardized customer questionnaire (Fig. 3).

Further questions enabled stratification of Cobalt Health specialties and workflow requirements (Fig. 4).

This in-depth discussion took place on Christmas Eve, before SARS-CoV-2 was first reported by UK media. Following discussions with her team, Head of MRI Karen Hackling-Searle highlighted the following key areas for customer training:

- BioMatrix Technologies
- Protocol building
- Parallel imaging techniques
- Multiparametric prostate dynamic contrast imaging
- Image optimization – parameter changes and how this compares to current vendor
- Simultaneous Multi-Slice (SMS) and Compressed Sensing (CS)

4

Department focus

What is the focus of the department?

☐ General Radiology
 ☐ Neuroradiology
 ☐ Cardiology
 ☐ Men's Health (e.g. Prostate)
 ☐ Women's Health (e.g. Breast, Cervix)
 ☐ Oncology
 ☐ Pediatrics
 ☐ Orthopedics
 ☐ Other: (specify)

The Cobalt radiographers were very experienced in MRI but many had not used equipment from Siemens Healthineers before. The Blended Learning package therefore included classroom places at the UK Siemens Healthineers Academy [11]. However, due to the distance from Cobalt Health and for customer operational capacity, the initial plan – prior to SARS-CoV-2 – was to deliver this using the Mobile Imaging Academy and implementing SmartSimulators in the customer's education room.

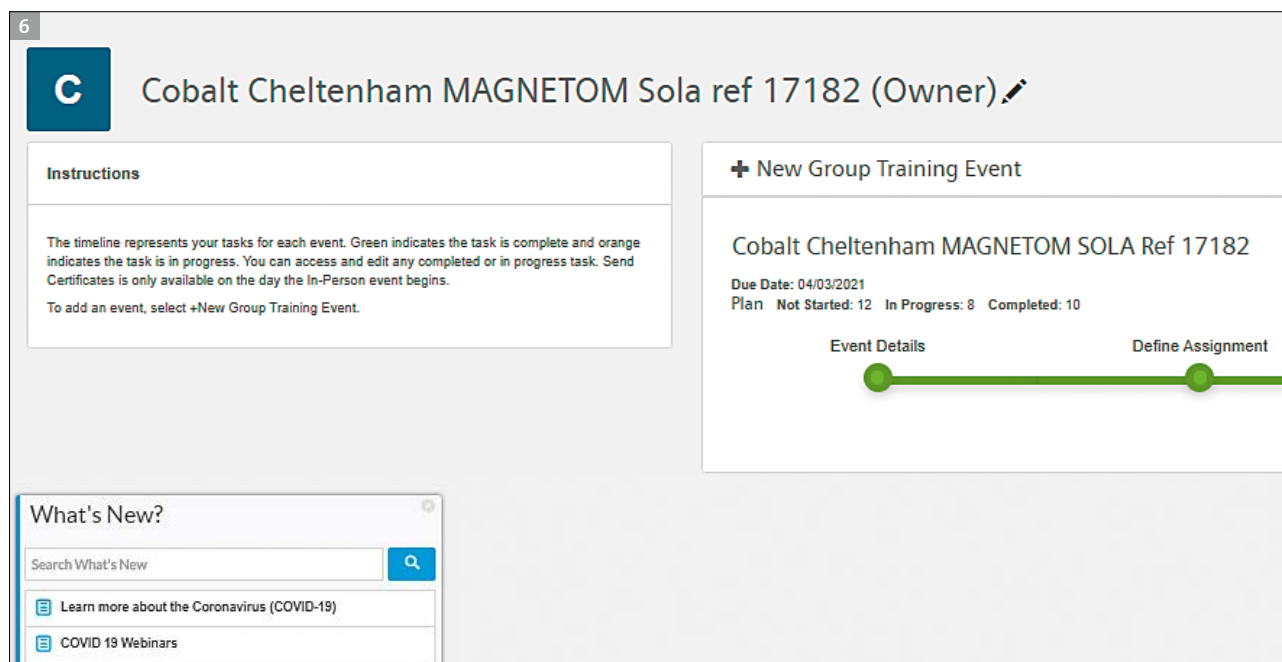
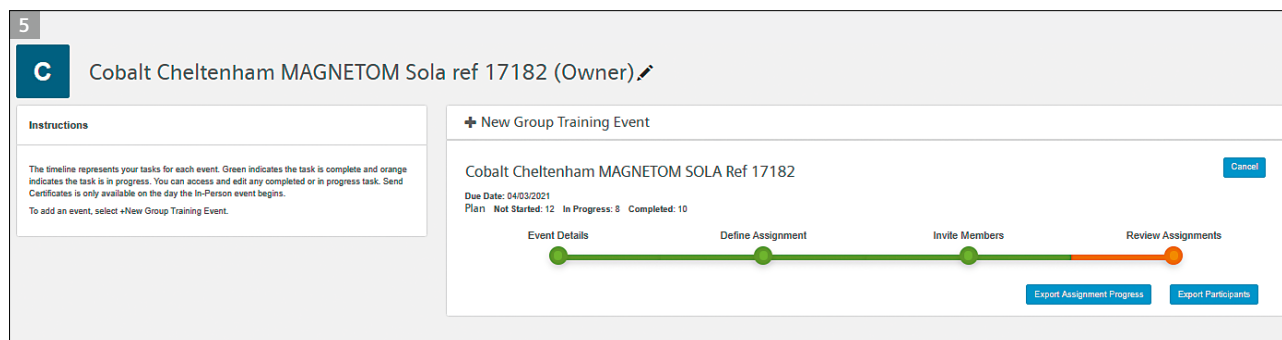
The first pillar: PEPconnect

PEPconnect provides access to extensive online material in a customer online training platform, which is free of charge. This was helpful, for example, in demonstrating the aim of Biomatrix Technologies before onsite training. It also helped the participants learn about the objectives of parallel imaging techniques, Simultaneous Multi-Slice (SMS), and Compressed Sensing. The training is self-paced and can be undertaken at any time and wherever there is an internet connection. The learning material can be repeated as often as needed, and can also be shared with colleagues. For the customer, a bespoke PEPconnect group

was created with educational content that focused on MAGNETOM Sola and XA20 software so that Karen could manage the learning of her large team of 30 MRI radiographers. Figure 5 shows early adoption and use of the PEPconnect group by staff in early January.

In addition, the availability and reminders of new COVID-19 information on PEPconnect provided critical information for online education (Fig. 6).

The Cobalt Health PEPconnect group enables the team to look at imaging protocols/techniques and examination workflows to help them become operational as quickly as possible.



The UK began its lockdown on March 23, and Ireland phased its lockdown in between March 12 and 27 [12]. For staff who were self-isolating at home and therefore unable to visit the imaging centre, PEPconnect allowed them to continue their professional development by learning about COVID-19 and the use of their own MRI systems (Fig. 7).

➤ <https://pep.siemens-info.com/en-us/coronavirus-covid-19>

This was crucial at the time of an upcoming new system installation. In addition, the customer could specifically access decontamination documents via the UK version of the page “The role of Siemens Healthineers in the COVID-19 pandemic” (Fig. 8). This was cascaded to staff by one of the MRI team leads at Cobalt.

➤ https://www.siemens-healthineers.com/en-uk/press-room/press-features/pf-covid-19.html#07105259_EN_GB

In addition, the Cobalt team had access to the MR user community at Siemens Healthineers, MAGNETOM World ➤ www.siemens.com/magnetom-world. This included the information in the Clinical Corner for planning and considering alternative clinical approaches, e.g., for their objective of multiparametric prostate dynamic contrast imaging. They were also able to download protocols from this worldwide community of MAGNETOM users in preparation for the new system [13]. In summary, the PEPconnect group videos and guides facilitated an easier transition to using the SmartSimulators in Pillar 2 by providing familiarity.

7

SIEMENS Healthineers

PEPconnect

Explore: Search Content and Groups

Coronavirus (COVID-19)

General Resources Healthcare Provider Resources

General Resources

- Coronavirus (COVID-19) Information EN
- Health & Wellness EN
- Infection Prevention and Control EN
- Patient Experience EN

TOP ^

Healthcare Provider Resources

- Blood Gas EN
- Computed Tomography EN
- Hematology/Hemostasis EN
- Immunoassay/Chemistry EN
- Molecular Diagnostics EN
- Ultrasound EN

8

System Decontamination Documents

Magnetic Resonance

- ↓ [MAGNETOM Vida/Sola 0.3 MB](#)
- ↓ [MAGNETOM Avanto/Verio 0.2 MB](#)
- ↓ [MAGNETOM Altea/Lumina 0.9 MB](#)
- ↓ [MAGNETOM Aera/Skyra/Prisma/Avanto 1.1 MB](#)
- ↓ [MAGNETOM Amira 1.0 MB](#)
- ↓ [MAGNETOM Terra 0.9 MB](#)
- ↓ [MAGNETOM Avanto/Espreo/Verio/Spectra 0.1 MB](#)
- ↓ [MAGNETOM coil cleaning instructions 0.8 MB](#)
- ↓ [Biograph mMR 1.1 MB](#)

The second pillar: SmartSimulator

SmartSimulators running XA platform software were used on February 11 and 12 to deliver classroom training in the customer's education room (Fig. 9). This was just five days after the third case of SARS-CoV-2 infection was confirmed in the UK [14]. The UK Siemens Healthineers Academy course introducing MAGNETOM Sola was delivered for the first time with a cloud-based SmartSimulator (Fig. 10) to the four key users on the Cobalt team.

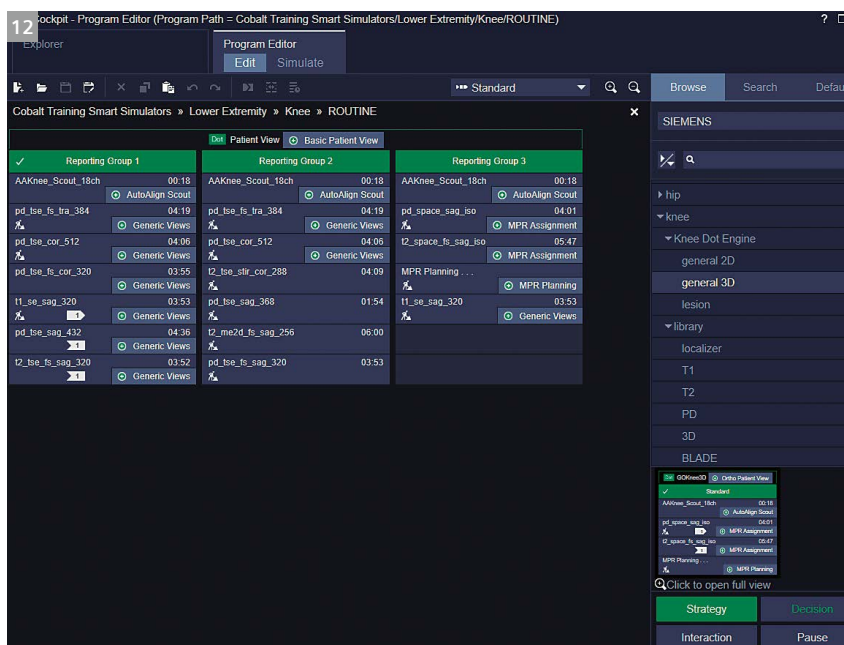
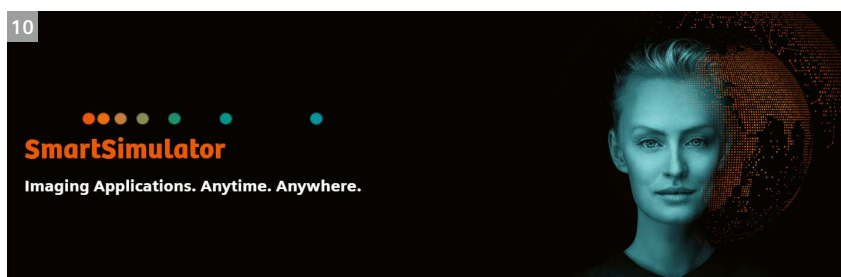
Changing from onsite to remote training delivery

There were extensive discussions between Karen at Cobalt Health and Siemens Healthineers throughout the day of March 16. The topic was whether the planned second part of pre-application training using SmartSimulators scheduled for March 17 and 18 would go ahead as planned with an applications specialist on-site. A decision was made with the customer to deliver the training remotely using the SmartSimulators and a PowerPoint presentation given via Microsoft Teams. A training plan

was disseminated and instructions were sent to the customer explaining the remote course delivery with Microsoft Teams and the SmartSimulators.

The decision to transfer the training to a remote format rather than on-site proved to have been the right one: On the evening of March 16, the UK government advised everyone in the UK to avoid "non-essential travel and contact with others, to curb coronavirus, as well as to work from home if possible" [15]. The two-day remote virtual training using SmartSimulators allowed

1. delivery of the Academy classroom course XA DotCockpit (Fig. 11);
2. hands-on, targeted, and bespoke exercises to meet customer workflows (Fig. 12);
3. Dot Engine simulator suites to see workflows in the scan queue;
4. free time to gain familiarity and confidence using the software.



The general format involved the following:

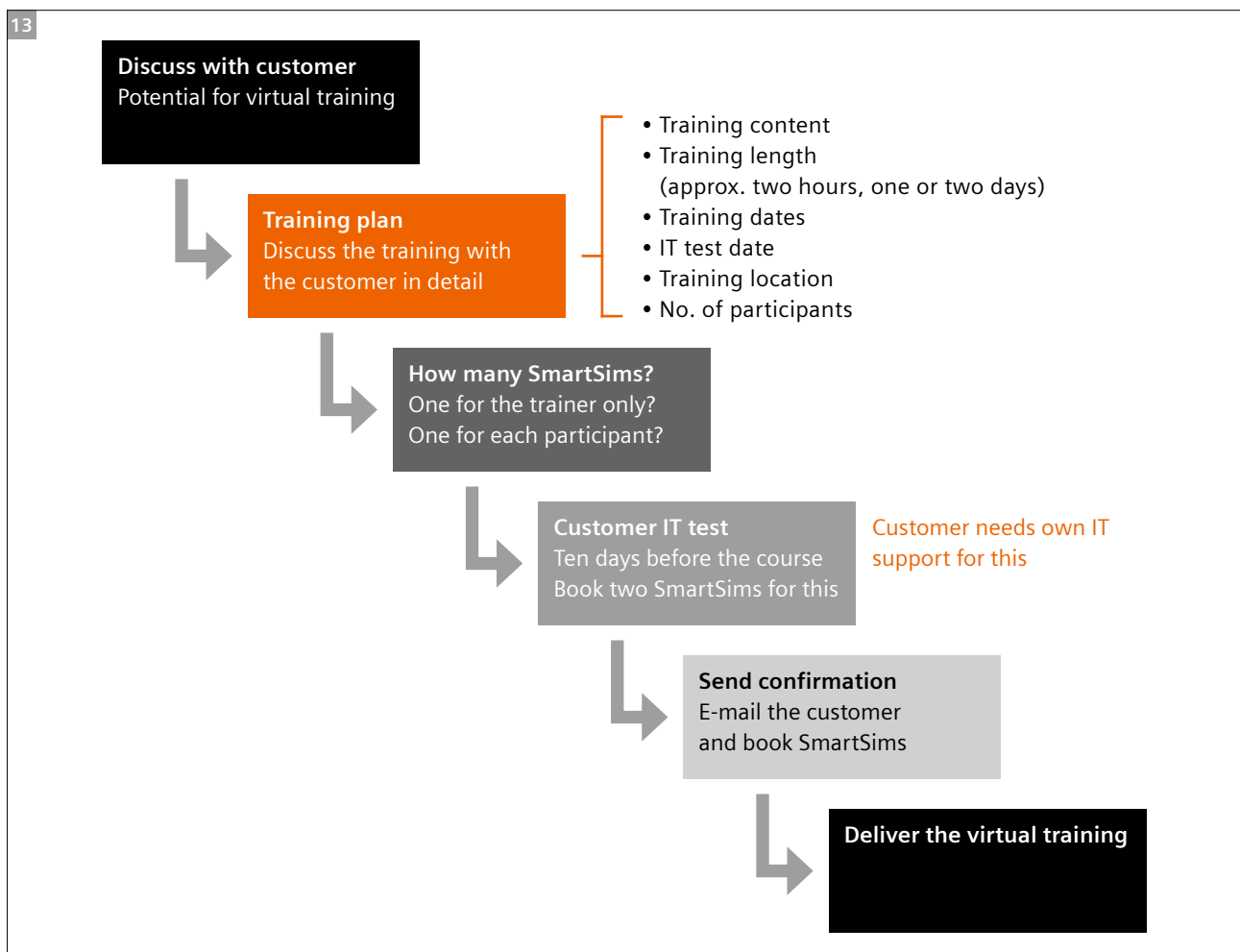
1. Presentation of the theory using PowerPoint via MS Teams
2. Provision of a guided demonstration via SmartSimulators
3. Hands-on customer session on using SmartSimulators, with exercises; trainer could provide guidance and answer questions by viewing the participants' SmartSimulators
4. A Q&A session

Potential challenges for virtual remote training

Working with Karen and the team, we identified the following potential challenges:

- Internet connection – needs to be checked in advance via a customer IT check session
- Microsoft Teams connectivity – needs to be checked in advance via a customer IT check session
- SmartSimulator – needs to be checked in advance via a customer IT check session with two SmartSimulators for the trainer and a trainee; during training, the technical support team is available but may need time to resolve
- Monitor / headset / microphone / speaker setup – needs testing and familiarization within IT check session

This led to the development of the following structure (Fig. 13).



Feedback

The SmartSimulators were very well received for the way they allowed users to build protocols and then see how strategies and decisions would behave when scanning (Fig. 14). For example, participants could see how strategies could be used for different reporting groups nationally. The customer was able to compare the session with the onsite training that used SmartSimulators in February and was very pleased with the remote training solution provided at short notice. It was felt that the training was of the same quality.

"The virtual training worked really well. I don't think anything was lost without face to face. It is important to ask for help if you don't follow. If the instructor was in the room, I think they would spot if someone was struggling very quickly, but this could be missed in the virtual world. The trainer was very good at waiting for a response from everyone to say they were happy before moving on the next topic."

Ruth Pearson, Cobalt Health MRI Clinical Lead

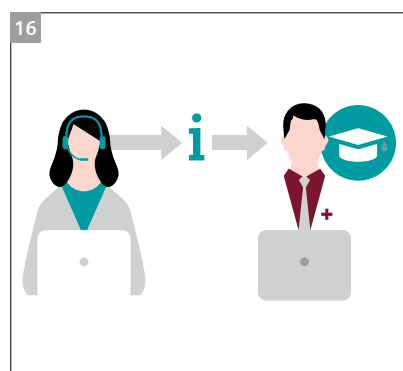
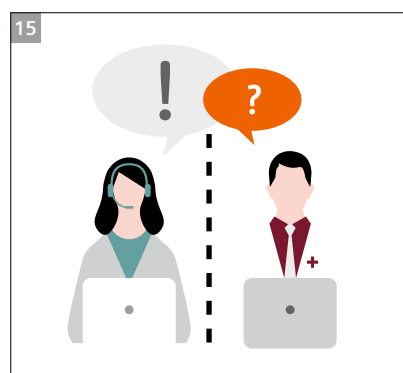
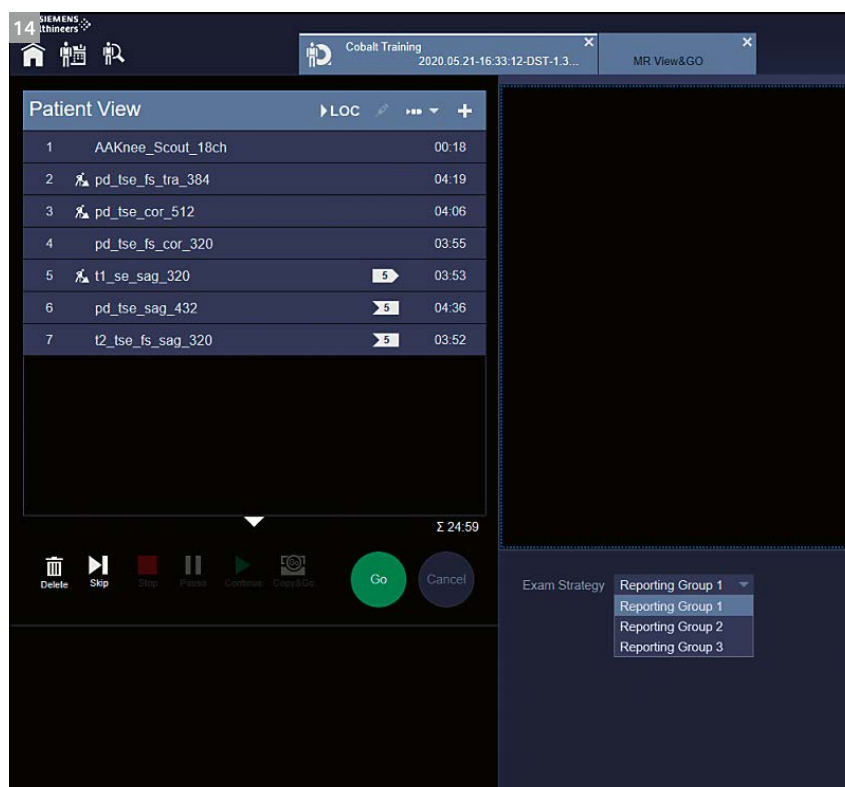
"I think the simulator was excellent, and it was good to get some hands on practice. The simulator was a really good way of introducing the Dot Cockpit concept and had an excellent opportunity to think and practice how we would like to set up protocols. I think a blended approach to

learning is good to ensure that all learning styles are catered for. After the training we received I did feel well prepared for the on-site applications training."

Liz Loele, Cobalt Health MRI Clinical Lead

"From my perspective as the Head of the department, it was easy to set up the training and liaise with the Siemens team. The team were open to our needs and flexible, particularly as Coronavirus developed into a pandemic at the same time the training program was to be delivered. Remote training was a perfect solution to this and enabled the continuation of the training without cancellation, whilst at the same time we were able to ensure staff and Siemens colleagues were safe and socially distanced and non-essential travel guidance adhered to! With a little tweaking to smooth out some of the communications challenges, remote training is a serious contender to bring teams together for training and collaboration. It is so much more efficient, time and cost saving."

Karen Hackling-Searle, Head of MRI, Cobalt Health



The third pillar: Smart Remote Service (SRS)

SRS is a proven way of delivering both Remote Assist for real-time interaction between clinical staff and clinical application experts (Fig. 15), and Remote Trainer allows for a more structured remote education performed on customer equipment (Fig. 16) [16].

In the context of COVID-19, remote scanning assistance can minimize the number of onsite training days to help reduce the R number and conserve valuable resources of personal protective equipment (PPE) needed for front-line staff. In addition, MR protocols can be prebuilt or sent to the customer and directly imported into the scanner if required to reduce initial set-up time. Cobalt's key national role in providing COVID-19 CT services for NHS England and the Nightingale field hospitals has meant that many MRI staff have been redeployed. Consequently, a plan for SRS training has been provided to support the customer in prebuilding protocols before the start of the clinical service and has been made easier through training for Pillar 1 (PEPconnect) and Pillar 2 (SmartSimulator).

The fourth pillar: Onsite training

The customer's local risk assessment of the small control room in the context of SARS-CoV-2 and social distancing meant that on-site applications had to be postponed until the 8th of June. In addition, the specialist MRI radiographers were still being redeployed to cover self-isolation and the increased capacity needed for COVID-19 CT scans. With the first three pillars, we provided a solid foundation that will allow the staff at Cobalt Health to start on-site training with MAGNETOM Sola (Fig.17) with increased knowledge and experience that can be cascaded to their colleagues.

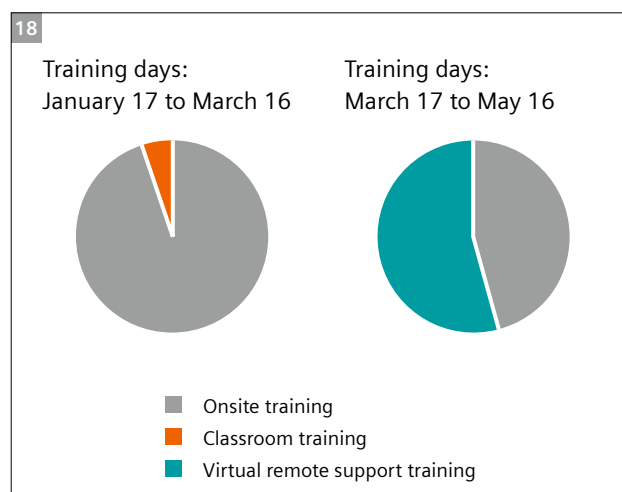
Summary

The aspiration to drive innovations forward so that people can live healthier and longer lives is more valid today than ever before. By stepping up our remote offerings earlier and as a partner to support Cobalt Health, we have enabled flexibility for the benefit of its patients.

The pie charts (Fig. 18) show a paradigm shift in how MRI training was delivered in the UK and Ireland as a result of SARS-CoV-2. They reflect the two months before restrictions began, and the two months directly after.

The four pillars of Blended Learning lead to an automatic repetition of the material – and, as we know, repetition is the key to learning. By covering the theory and basics (buttonology) with the first two pillars, SRS and Onsite training can concentrate on deepening the knowledge and customizing the workflows or scan protocols to the needs of the customer. Onsite training can be continually supported by PEPconnect, SmartSimulator, and SRS. This learning approach shifts parts of the training into a different form, which has added value for the customer. For example, further SmartSimulator training could be provided to customers working from home.

There are also sociological benefits of providing remote applications support and training. If one application specialist travels to the site, they might interact with many people – for instance, at gas stations, train stations, or airports; on public transport or on flights; in hotels or restaurants; and of course during staff interactions on a hospital visit [5]. These situations all have the potential for virus transmission, and could therefore significantly increase the R value [7]. Blended Learning can potentially reduce local R values [7]. In addition, using PEPconnect and SmartSimulators for staff in self isolation can further reduce the R value. Therefore, training at home through these solutions will become even more valuable as the UK and Ireland begin to ease their lockdown.



References

- 1 WHO. Country & Technical Guidance – Coronavirus disease (COVID-19) [Internet]. Geneva: World Health Organization; © 2020 [cited March 27, 2020]. Available from: <https://www.who.int/emergencies/diseases/novel-coronavirus-2019>
- 2 The Royal College of Radiologists. RCR advice on non-urgent and cancer imaging during the coronavirus pandemic [Internet]. London: RCR; March 30, 2020 [cited May 12, 2020]. Available from: <https://www.rcr.ac.uk/college/coronavirus-covid-19-what-rcr-doing/clinical-information/rcr-advice-non-urgent-and-cancer>
- 3 Siemens Healthineers. MR Conferences & Training: Benefit the most from your MR scanner and its software application [Internet]. Frimley, Camberley, UK: Siemens Healthcare Limited; © 2020 [cited May 10, 2020]. Available from: <https://www.siemens-healthineers.com/en-uk/magnetic-resonance-imaging/magnetom-world/training>
- 4 Siemens Healthineers. Education & Training [Internet]. Frimley, Camberley, UK: Siemens Healthcare Limited; © 2020 [cited May 20, 2020]. Available from: <https://www.siemens-healthineers.com/en-uk/education>
- 5 WHO. Coronavirus disease (COVID-19) technical guidance: Maintaining Essential Health Services and Systems [Internet]. Geneva: World Health Organization; © 2020 [cited May 12, 2020]. Available from: <https://www.who.int/emergencies/diseases/novel-coronavirus-2019/technical-guidance/maintaining-essential-health-services-and-systems>
- 6 Public Health England. Stay at home: guidance for households with possible or confirmed coronavirus (COVID-19) infection [Internet]. London: Public Health England; updated May 28, 2020 [cited May 18, 2020]. Available from: <https://www.gov.uk/government/publications/covid-19-stay-at-home-guidance/stay-at-home-guidance-for-households-with-possible-coronavirus-covid-19-infection>
- 7 Huilan Tu, Sheng Tu, Shiqi Gao, Anwen Shao, Jifang Sheng. The epidemiological and clinical features of COVID-19 and lessons from this global infectious public health event. J Infect. 2020; doi: 10.1016/j.jinf.2020.04.011 [Epub ahead of print].
- 8 Harvard Business Review Analytic Services. Expanding Precision Medicine: The Path to Higher-Value Care [white paper on the Internet]. Boston, Massachusetts: Harvard Business School Publishing; © 2018 [cited May 19, 2020]. Available from: [hbr_whitepaper_expanding-precision-medicine-06057346.pdf](https://www.hbr.org/whitepaper/06057346-expanding-precision-medicine)
- 9 Lasalvia L, Merges R. Expanding Precision Medicine [article on the Internet]. Fishers, Indiana, U.S.: The Journal of Precision Medicine; August 2019 [cited April 27, 2020]. Available from: <https://www.thejournalofprecisionmedicine.com/wp-content/uploads/2019/09/jpm319-Merges.pdf>
- 10 BBC. Coronavirus: Up to fifth of UK workers 'could be off sick at same time' [Internet]. London: BBC; March 3, 2020 [cited March 16, 2020]. Available from: <https://www.bbc.co.uk/news/uk-51718917>
- 11 Siemens Healthineers. Magnetic Resonance Imaging: Courses and registration [Internet]. Frimley, Camberley, UK: Siemens Healthcare Limited; © 2020 [cited May 12, 2020]. Available from: <https://www.siemens-healthineers.com/en-uk/education/siemens-healthineers-academy/medical-imaging/magnetic-resonance-imaging>
- 12 BBC. Coronavirus: The world in lockdown in maps and charts [Internet]. London: BBC; April 7, 2020 [cited April 7, 2020]. Available from: <https://www.bbc.co.uk/news/world-52103747>
- 13 Siemens Healthineers. MAGNETOM World: Welcome to your Siemens MR User Community [Internet]. Frimley, Camberley, UK: Siemens Healthcare Limited; © 2020 [cited March 17, 2020]. Available from: <https://www.siemens-healthineers.com/en-uk/magnetic-resonance-imaging/magnetom-world>
- 14 BBC. Coronavirus: Third UK patient 'caught coronavirus in Singapore' [Internet]. London: BBC; February 6, 2020 [cited March 16, 2020]. Available from: <https://www.bbc.co.uk/news/uk-51398039>
- 15 legislation.gov.uk. The Health Protection (Coronavirus, Restrictions) (England) Regulations 2020, UK Statutory Instruments 2020 No. 350 [Internet]. Kew, Richmond, Surrey, UK: legislation.gov.uk; March 26, 2020 [cited April 27, 2020]. <http://www.legislation.gov.uk/uk/si/2020/350/contents/made/data.htm>
- 16 Smith G. Using Remote Assist to Expand Your Expertise. MAGNETOM Flash. 2015;63(3): RSNA Edition, 87–89.
- 17 <https://www.cobalthhealth.co.uk/>



Left to right: Jono Humphris (MRI clinical lead), Zoe Wray (MRI clinical lead), Karen Hackling-Searle (Head of MRI), and Adrian Lowe (MRI Applications Specialist Siemens Healthineers)

Contact

Chris Kasap
 Siemens Healthcare Limited
 SHS EMEA GBI CS BD AM MR
 United Kingdom
 Tel.: +44 7808 825264
 Mobile: +44 7808 825264
christopher.kasap@siemens-healthineers.com

Embrace human nature

siemens-healthineers.com/BioMatrix-Upgrades



The clinical overlay is not that of the individual pictured.
It was modified for better visualization.



Upgrade to BioMatrix Technology

The increasing number of exams, complexity, and cost-pressure are placing challenges on MRI. MRI needs to better handle patient variability, deliver fast and robust results for all patient types, and become more cost-effective. With an upgrade of your MR scanner to BioMatrix Technology, you can master the challenges facing MRI today, helping you to expand your services and make the most of your initial investment while keeping your investment costs low.

*Still under development and not commercially available yet.
Its future availability cannot be ensured.*

Turn your MAGNETOM Aera or
MAGNETOM Skyra to MAGNETOM Sola Fit
or MAGNETOM Vida Fit and

- Embrace consistency for fewer rescans,
higher diagnostic confidence:
With BioMatrix technology
- Embrace efficiency with up to 50% faster exams:
With GO technologies and Turbo Suite
- Embrace new clinical capabilities and financial
opportunities:
With an upgrade into the future

The entire editorial staff at Siemens Healthineers extends their appreciation to all the radiologists, technologists, physicists, experts, and scholars who donate their time and energy – without payment – in order to share their expertise with the readers of MAGNETOM Flash.

MAGNETOM Flash – Imprint

© 2020 by Siemens Healthcare GmbH,
All Rights Reserved

Publisher:

Siemens Healthcare GmbH
Magnetic Resonance,
Karl-Schall-Str. 6, D-91052 Erlangen, Germany

Editor-in-chief:

Antje Hellwich
(antje.hellwich@siemens-healthineers.com)

Editorial Board:

Rebecca Ramb, Ph.D.; Sunil Kumar S. L., M.D.;
Wellesley Were; Jane Kilkenny; Nadine Leclair, M.D.

Review Board:

André Fischer, Ph.D.; Daniel Fischer;
Christian Geppert, Ph.D.; Giulia Ginami, Ph.D.;
Heiko Meyer, Ph.D.; Gregor Thörmer, Ph.D.

Copy Editing:

Sheila Regan, Jen Metcalf, UNIWORKS,
www.uni-works.org
(with special thanks to Kylie Martin)

Layout:

Agentur Baumgärtner,
Friedrichstr. 4, D-90762 Fürth, Germany

Production:

Norbert Moser,
Siemens Healthcare GmbH

Printer:

G. Peschke Druckerei GmbH,
Taxenstr. 4, D-85599 Parsdorf b. Munich, Germany

Note in accordance with § 33 Para.1 of the German Federal Data Protection Law: Despatch is made using an address file which is maintained with the aid of an automated data processing system.

MAGNETOM Flash is sent free of charge to Siemens Healthineers MR customers, qualified physicians, technologists, physicists and radiology departments throughout the world. It includes reports in the English language on magnetic resonance: diagnostic and therapeutic methods and their application as well as results and experience gained with corresponding systems and solutions. It introduces from case to case new principles and procedures and discusses their clinical potential. The statements and views of the authors in the individual contributions do not necessarily reflect the opinion of the publisher.

The information presented in these articles and case reports is for illustration only and is not intended to be relied upon by the reader for instruction as to the practice of medicine. Any health care practitioner reading this information is reminded that they must use their own learning, training and expertise in dealing with their individual patients. This material does not substitute for that duty and is not intended by Siemens Healthcare to be used for any purpose in that regard. The drugs and doses mentioned herein are consistent with the approval labeling for uses and/or indications of the drug. The treating physician bears the sole responsibility for the diagnosis and treatment of patients, including drugs and doses prescribed in connection with such use. The Operating Instructions must always be strictly followed when operating the MR system. The sources for the technical data are the corresponding data sheets. Results may vary.

Partial reproduction in printed form of individual contributions is permitted, provided the customary bibliographical data such as author's name and title of the contribution as well as year, issue number and pages of MAGNETOM Flash are named, but the editors request that two copies be sent to them. The written consent of the authors and publisher is required for the complete reprinting of an article.

We welcome your questions and comments about the editorial content of MAGNETOM Flash. Please contact us at
magnetomworld.team@siemens-healthineers.com

Manuscripts as well as suggestions, proposals and information are always welcome; they are carefully examined and submitted to the editorial board for attention. MAGNETOM Flash is not responsible for loss, damage, or any other injury to unsolicited manuscripts or other materials. We reserve the right to edit for clarity, accuracy, and space. Include your name, address, and phone number and send to the editors, address above.

MAGNETOM Flash is also available online:

www.siemens.com/magnetom-world

Not for distribution in the US

On account of certain regional limitations of sales rights and service availability, we cannot guarantee that all products included in this brochure are available through the Siemens sales organization worldwide. Availability and packaging may vary by country and is subject to change without prior notice. Some/All of the features and products described herein may not be available in the United States.

The information in this document contains general technical descriptions of specifications and options as well as standard and optional features which do not always have to be present in individual cases, and which may not be commercially available in all countries.

Due to regulatory reasons their future availability cannot be guaranteed. Please contact your local Siemens organization for further details.

Siemens reserves the right to modify the design, packaging, specifications, and options described herein without prior notice. Please contact your local Siemens sales representative for the most current information.

Note: Any technical data contained in this document may vary within defined tolerances. Original images always lose a certain amount of detail when reproduced.

Siemens Healthineers Headquarters

Siemens Healthcare GmbH
Henkestr. 127
91052 Erlangen, Germany
Phone: +49 9131 84-0
siemens-healthineers.com